Studies on hydrothermal liquefaction of lignocellulosic biomass using zero-valent iron

Miyata, Yoshinori

(Degree)
博士（工学）

(Date of Degree)
2019-09-25

(Date of Publication)
2020-09-01

(Resource Type)
doctoral thesis

(Report Number)
甲第7608号

(URL)
https://hdl.handle.net/20.500.14094/D1007608

Doctoral Dissertation

Studies on hydrothermal liquefaction of lignocellulosic biomass using zero-valent iron

0 価鉄を用いたリグノセルロース系バイオマスの水熱液化反応に関する研究

July 2019

Graduate School of Engineering

Kobe University

Yoshinori Miyata

Contents

General Introduction

Climate change: a product of the rapid growth of world population and development of global economics

The global population reached 7.5 billion in 2017 and is still increasing at an annual rate of 1.1% (an increase of 83 million annually). Although this growth rate has been modest for the past 10 years, the world's population is predicted to reach 8.6 billion in 2030, exceed 9.8 billion in 2050, and reach 11.2 billion in 2100. [1]

In addition to the population growth, as a result of the exponential growth in economic activity since the industrial revolution, a global consumerist society focused on utilization of resources and energy has developed. Global energy consumption has increased at an average annual rate of 2.6% from 3.7 billion tons of oil equivalents in 1965 to 13.1 billion tons in 2015. In the Asia–Pacific region in particular, consumption growth rates have increased in the past two decades, driven primarily by emerging economies.[2] At present, the primary energy demands are largely covered by fossil fuel resources such as oil and coal. However, these are limited resources, and there are growing concerns about global climate change caused by emission of greenhouse gases, including carbon dioxide, which are primarily produced by consumption of fossil resources.

The United Nations Framework Convention on Climate Change (UNFCCC) in 1992 in Rio de Janeiro, Brazil, established an international framework to tackle the issue of global warming, which has guided global efforts for the reduction of emissions of greenhouse gases.[3] In 2015, the Paris Agreement was adopted at the 2015 United Nations Climate Change Conference (COP 21), which determined that global average

temperature rise must be limited to less than 2 °C compared to pre-industrial temperatures.[4] To-date, the global average temperature has already risen by 1 °C. Consequently it is necessary to take immediate further actions to limit future increases in temperature.

In terms of CO_2 emission ratios by sector, the largest emission source is the industrial sector, which exceeds emissions from the transport sector. Direct CO_2 emissions alone represent 21% of the total, and this rises to 32% (equivalent to 17 Gt-CO_2 annual emissions) when indirect emissions from electricity and heat production are included.[5] Consequently it is a significant challenge to reduce energy consumption in the industrial sector and to convert energy use to renewables in order to reduce greenhouse gas emissions. Within the various industrial sectors, the chemical, steel, and cement industries are the major source of CO_2 release. The chemical sector alone is estimated to emit 3.1 Gt-CO_2 annually,[6] and its potential for future reductions is considered to be significant.

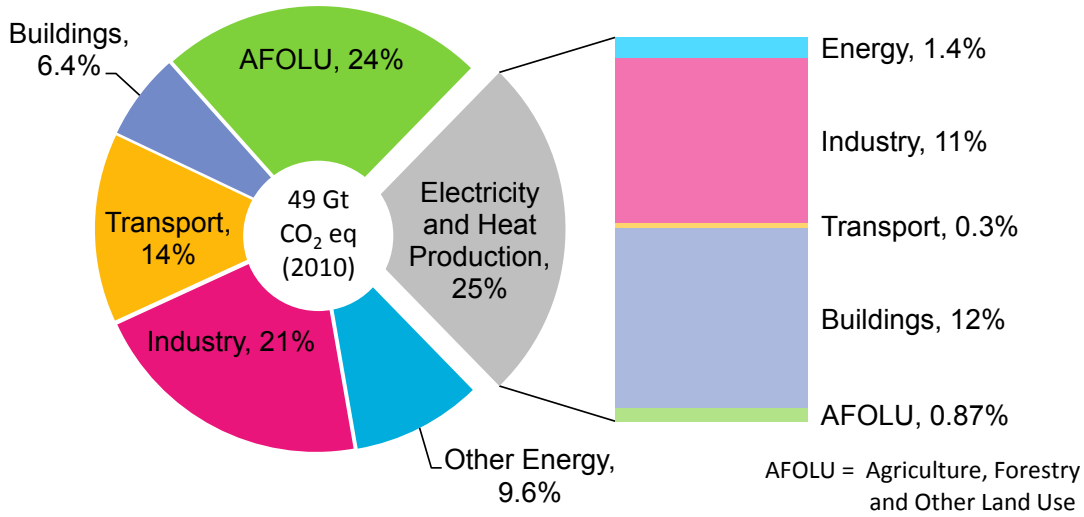

Figure 1. Greenhouse Gas Emissions by Economic Sectors.[5]

Petrochemical industry

Today, our lives are supported by a number of industrial products. Organic chemical products derived from petroleum are one key example. A wide variety of products, from bulk chemicals such as plastics and rubber, to fine chemicals such as pharmaceuticals, are manufactured from petroleum, which are essential for living in a modern society. The main petrochemical starting material is naphtha, which is composed of unsaturated hydrocarbons, including lower olefins (ethylene, propylene, and butylene) as well as benzene, toluene, and xylene (BTX). By making full use of various catalytic reactions and organic synthetic reactions, everything from commonly available chemicals to complex highly refined chemicals, can be synthesized (Scheme 1). For example, polyethylene and polypropylene are commonly used plastics produced by polymerizing ethylene and propylene, respectively. Ethylene can also be converted into other monomers, including ethylene oxide, ethylene glycol, vinyl acetate, vinyl chloride and styrene, while propylene is oxidized to acrylic acid by catalytic oxidation or converted to acrylonitrile through ammoxidation. These are used as raw materials for paints, fibers, and adhesives. Moreover, the sodium salt of polyacrylic acid is important as a raw material of super absorbent polymer. BTX are also converted to monomers, including styrene and terephthalic acid, and also as feedstocks for the production of basic chemicals such as phenol and phthalic anhydride. Furthermore, these basic commodity chemicals are combined to make complex pharmaceutical intermediates and functional polymers. Therefore, despite the simplicity of these raw materials, the petrochemical industry has built very complex supply chains and there are significant numbers of diverse products. The annual production of lower olefins and BTX is over 300 Mt,[7] equivalent to 1 Gt-CO_2 when converted to CO_2. If it were possible to establish

a technology to produce olefins and BTXs from non-fossil resources, it would represent a major contribution to mitigation of climate change.

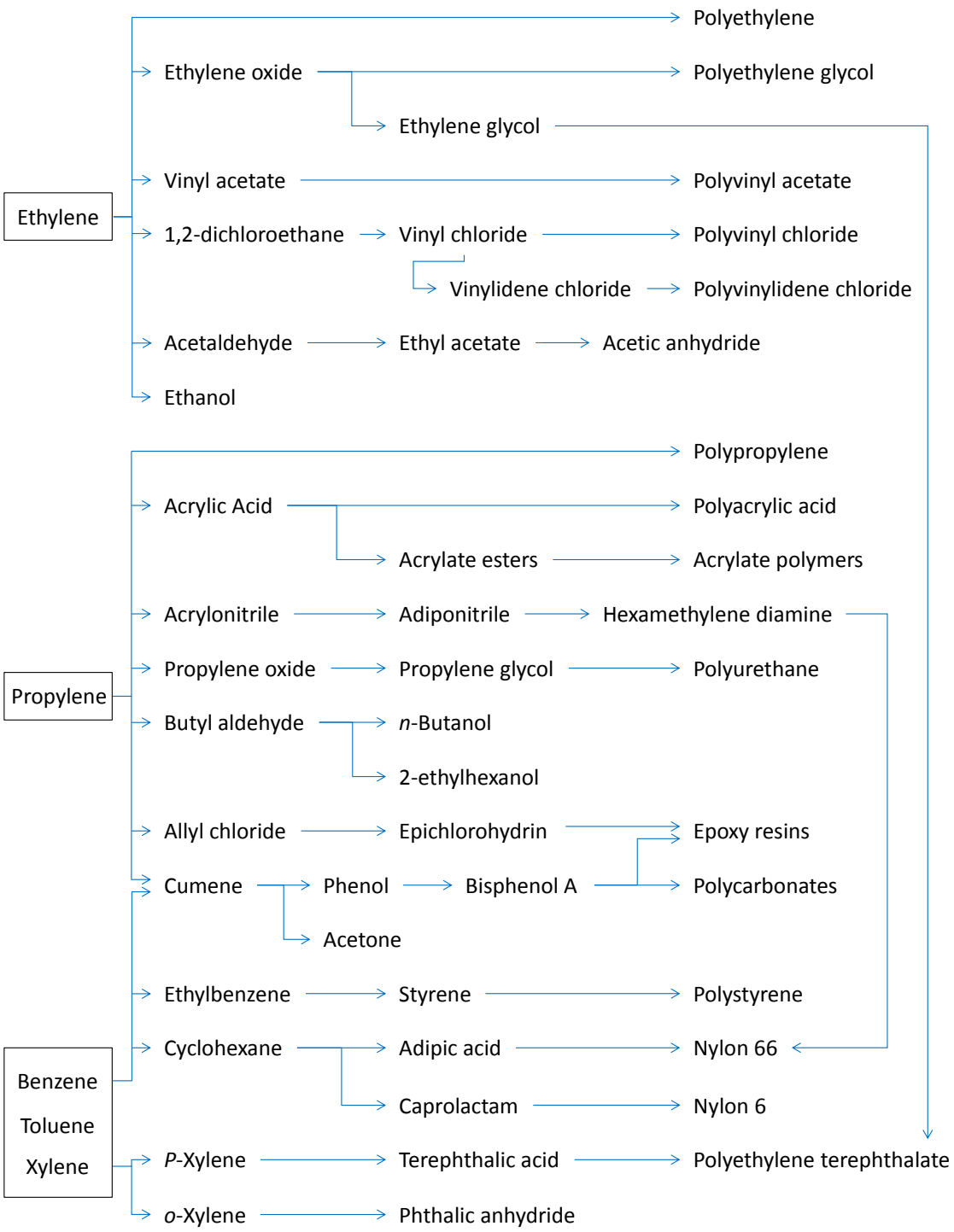

Scheme 1. Examples of derivertives from ethylene, propylene and BTX.

Biomass

Biomass is a renewable, biogenic organic resource and the term excludes fossil resources.[8] It originates from organic matter synthesized from water and carbon dioxide (CO_2) in the atmosphere by photosynthesis, a process undertaken by phototrophs. Biomass can be continuously regenerated as long as sunlight, water, atmospheric CO_2 and phototrophs (also called autotrophs) are available. Unlike CO_2 derived from fossil resources, CO_2 emitted by burning biomass does not contribute to a net increase in atmospheric CO_2 concentration, because the CO_2 released during combustion was originally fixed by photosynthesis of an organism prior to combustion. That is, biomass is considered to be "carbon neutral" and biomass utilization for the production of chemical resources and energy is expected to be an effective measure for causing a reduction of CO_2 emissions. Basic and applied research by industry-academia-government has progressed significantly in recent decades, achieving remarkable progress.

Biomass can be classified into three groups, according to source: (1) waste biomass, as represented by animal manure and sewage sludge; (2) agricultural residues, including rice straw, wheat straw and oil palm wastes; and (3) crops such as corn, sugar cane and switchgrass.[8] In addition, biomass can be categorized into edible biomass and non-edible biomass. Edible crops, including corn and sugar cane, were used at an early stage. Fermentation processes using the sugars easily obtained from these crops have been developed and put into practical use in order to obtain ethanol for use as a fuel. However, as a result of increased demand for bio-fuel, competition between bio-fuels and food has emerged.[9] A World Bank report on biofuels has concluded that the generation of biofuels from food crops was the most important factor in causing large

increases in food prices in 2008.[10] Since the global demand for food is expected to increase with growth in the world's population, the large-scale conversion of food resources into fuel must be avoided.

Because of the need to minimize competition between food and biofuel production, the development of technologies to allow utilization of "second generation biomass," which uses non-edible sources of biomass, is receiving increased attention as a solution. Most waste biomass and unutilized biomass are non-edible resources, and globally they are abundantly available. Bentsen and co-workers estimated that the total amount of residues generated from six major crops (barley, corn, rice, soybeans, sugar cane, wheat) in 227 countries is 3.7 Gt/y (dry weight).[11] This is about the same order of magnitude as the production volume of chemicals and shows that agricultural residues are a promising potential source of chemical feedstocks. Agricultural residues have a high potential as a resource in terms of cost since they are inexpensive. The use of second generation biomass is considered to have the potential to contribute to the creation of a sustainable society, and practical technologies for its use should be developed as soon as possible.

Most non-edible biomass contains lignocellulose as the main component. Lignocellulose is mainly composed of cellulose, hemicellulose, and lignin.[12] Cellulose is a linear polymer in which glucose is polymerized by β-1,4 linkages and accounts for 20–50% of the mass of biomass. Multiple polymer chains interact by hydrogen bonding, forming crystalline structures with high chemical stability and physical strength. Hemicellulose is a polysaccharide, comprising 20–40% of the mass of biomass. Unlike cellulose, hemicellulose consists of a mixture of a five-carbon sugar, such as xylose and arabinose, and a six-carbon sugar, such as galactose, glucose, and mannose.

Hemicellulose has a branched structure and is amorphous. Lignin constitutes 15–30% of the mass of biomass. It has a highly polymerized and branched structure and is composed of up to three different phenyl propane monomers. Lignocellulose is formed by complex higher-order structures of these three components (lignin, cellulose, and hemicellulose), which strengthens the cell walls of the biomass. In order to utilize biomass, it is necessary to fractionate lignocellulose into each component and to further decompose it into monomeric units efficiently. However, the complex and strong structure of lignocellulose makes this difficult.

Conversion of lignocellulosic biomass

The methods available for utilization of lignocellulosic biomass are classified into three processes (Scheme 2).[12] The first is a process in which biomass is thermochemically decomposed at high temperature and converted to a synthetic gas consisting predominantly of carbon monoxide (CO) and hydrogen, called syngas. Syngas can be chemically converted into various products using a catalyst.[13] For example, syngas can be converted to alkanes through Fischer–Tropsch synthesis using cobalt or iron catalyst, and its use as a diesel fuel or gasoline feedstock is also being investigated. In addition, it can be converted not only into methanol using a Cu/ZnO catalyst but also hydrogen by the water gas shift reaction.

The second method available for the use of biomass is the process in which biomass is used as a fermentation feedstock and converting it to various chemicals, especially ethanol.[14] In this process, lignin is generally removed from the raw lignocellulose by treatment with an acid, alkali, or high-pressure steam. Fractionated cellulose and hemicellulose are hydrolyzed by two enzymes, cellulase and

hemicellulase, to produce fermentable sugars. In order to further develop low-cost and efficient methods, improvements to pretreatment conditions and development of saccharifying enzymes and fermentation strains are being investigated.

The third method available for the use of biomass is a thermochemical process in which biomass is decomposed by a thermochemical reaction such as fast pyrolysis or hydrothermal liquefaction (HTL).[15-16] The liquefied product, i.e., bio-oil, is used as a fuel or chemical feedstock. Fast pyrolysis is a process used to obtain bio-oil by heating biomass at a high temperature (about 500 °C) for a short time in the absence of air.[17] Fast pyrolysis has the benefit that biomass is converted directly into a liquid product. It is important to ensure a rapid elevation of temperature and cooling in this fast pyrolysis process. In order to improve the conduction of heat, the raw materials need to be sufficiently dried and pulverized. In contrast, HTL is a process used to obtain bio-oil by treating biomass in subcritical or supercritical water.[18] HTL uses water, which is an eco-friendly solvent, as a reaction medium and requires relatively low temperature (280–370 °C) compared with fast pyrolysis. Because wet biomass can be used without drying, it can be applied to a wide range of biomass resources, including residues of crops with high water content, algae, and sludge. Consequently, HTL is attracting attention as a promising method for biomass conversion, and extensive research on this process has been made.

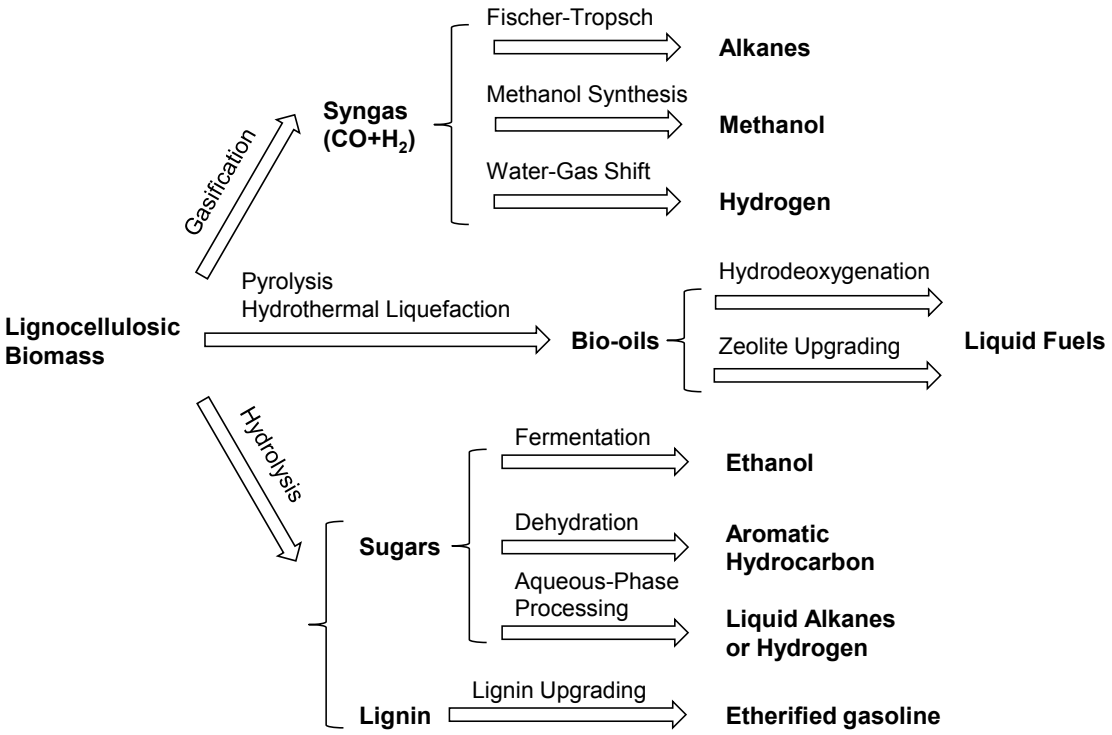

Scheme 2. Strategies for production of fuels from lignocellulosic biomass.[12]

Challenges of hydrothermal liquefaction

In HTL, four fractions are obtained as products, including two oil fractions (water-soluble oil and water-insoluble oil), a solid residue (char) and gas. The suppression of char formation is one of the challenges of HTL. Char is formed by repolymerization and carbonization of the degradation products of biomass. In order to suppress the formation of char, the definition of suitable reaction conditions and effective catalysis are required and these requirements are being explored. Progress has been made in these areas. For example, alkaline catalysts, including Na_2CO_3, K_2CO_3, KOH, $Ca(OH)_2$, $Ba(OH)_2$, RbOH, and CsOH have been widely investigated in HTL to enhance the yield of liquid products and to suppress char formation.[19-21] Nazari and co-workers screened the activities of several homogeneous and heterogeneous catalysts,

including KOH, $FeSO_4 \cdot 7H_2O$, K_2CO_3, and MgO in HTL of birch wood sawdust at 300 °C with a 30 min residence time.[22] The yield of liquid products without catalysts was reported to be as low as 49.3%; by using K_2CO_3 as a catalyst the liquid product yield increased to 78.0%.

An additional problem for HTL is the low quality of the oil products. The composition of bio-oil obtained by the usual HTL is largely different from that of fossil resources, especially in terms of elemental composition. The van Krevelen diagram (Figure 2) is a very practical means of portraying the compositions of various fuel resources, in which the atomic H/C ratio *versus* the atomic O/C ratio are plotted.[23] A plot of HTL bio-oil (water-insoluble) reveals that HTL water-insoluble bio-oil is altered compared with raw biomass, but the O/C ratio is still high compared with fossil resources. The high content of oxygen is owing to the presence of a number of oxygenated compounds, including alcohols, ketones, aldehydes, carboxylic acids, sugars, furans, and phenols, which affects the heating value, acidity, stability, and viscosity of the bio-oil. Further, because of the presence of polar oxygenated compounds (especially alcohols, aldehydes, and carboxylic acids), bio-oil contains a large amount of water. High moisture content and the presence of oxygenated compounds results in a low calorific value of the bio-oil. Owing to the presence of acids and phenols, bio-oil is corrosive to equipment used for storage, transport, and processing. Bio-oil contains highly unstable compounds, including aldehydes and ketones, which rapidly undergo repolymerization in storage. During storage, the average molecular weight and viscosity of bio-oil increases, and the quality of the oil declines. These properties make the direct use of bio-oil in oil refineries impossible.

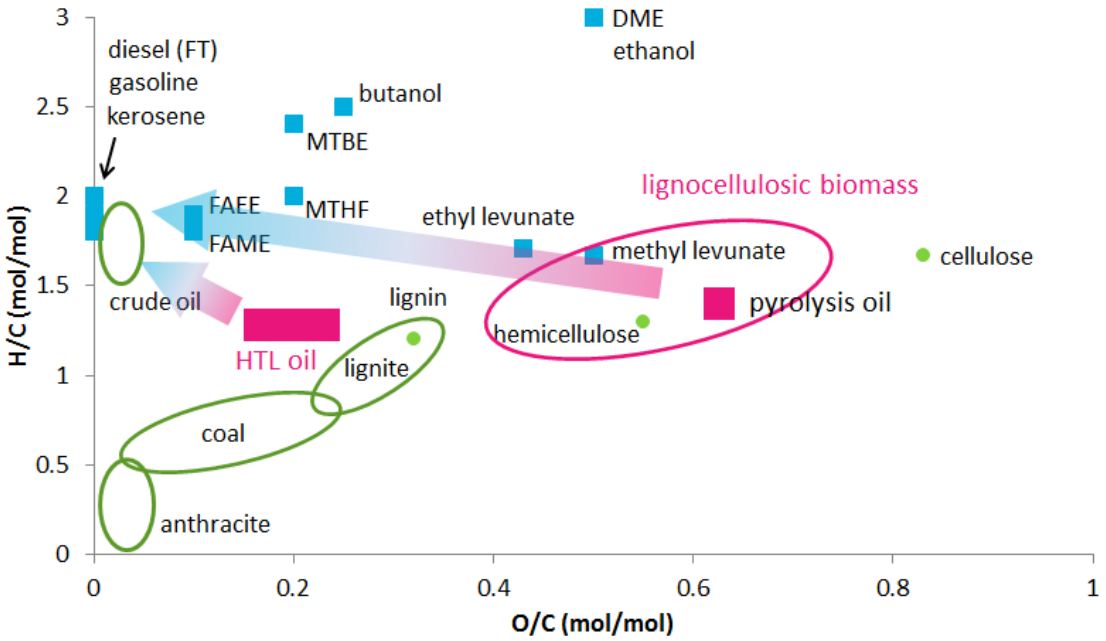

Figure 2. van Krevelen diagram.[23]

In order to improve the properties of bio-oil, hydrodeoxygenation using high pressure hydrogen in the presence of a heterogeneous metal catalyst has been developed. In this process, metal supported catalysts using Pt, Ru, Pd, Rh, Ni-MoS_2, or Co-MoS_2 have been employed and hydrodeoxygenation is conducted at a temperature of 250–450 °C, with a hydrogen pressure of 7.5–30 MPa.[24] By hydrogenating and deoxygenating oxygenated compounds in bio-oil, the energy content and stability of the oil is significantly improved. However, since hydrogen is very explosive, it is necessary to construct a large number of dedicated facilities for hydrogen production, storage, and transportation, which contributes to an increase in capital costs of this process.[25] Furthermore, at present, hydrogen is mainly produced using fossil resources as a feedstock, and consequently a large amount of CO_2 is emitted as a byproduct. Although the development of renewable hydrogen production by electrolysis of water, using electricity generated from renewable energy sources such as solar and wind power, are

progressing, mainly in Europe, this process is yet to replace fossil-derived hydrogen.[26]

Metal reductants in organic synthesis and applications for bio-oil upgrading

In the field of organic synthesis, various reductive reactions are made possible by utilizing zero-valent metals. For example, the Bouveault–Blanc reduction uses sodium to convert a carbonyl compound to an alcohol and the Birch reduction uses lithium to hydrogenate an aromatic compound.[27-28] Other than reactions using a highly reactive alkali metal, such as sodium, stable metals can be used for reductive reaction. Reaction of alkyl halides and carbonyl compounds in the presence of magnesium or zinc (the Barbier reaction) is an example of reactions using a metal reductant.[29] Iron, which is stable, abundant, and cheap, can also be used as the reducing agent for dehalogenation of haloalkenes,[30] amination of nitro compounds,[31] and hydrogenation of carbonyl compounds.[32]

Recently, some groups have demonstrated utilization of these zero-valent metals for upgrading bio-oil. In 2012, Liu and co-worker demonstrated that bio-oil was upgraded following treatment of the fast pyrolysis oil of rice husk with zero-valent zinc at room temperature.[33] In this study, carbonyl compounds, which are the principal cause of instability of bio-oils, were hydrogenated and reduced, and acidic compounds, which cause corrosiveness, decreased and the pH value was higher than raw bio-oil. In 2014, Hargus and co-workers conducted experiments to feed acetic acid to a fixed bed flow reactor filled with zinc or zinc oxide powder under high temperature conditions and demonstrated that zinc exhibited better selectivity than zinc oxide.[34] In 2017, Cheng and co-workers obtained upgraded oil by treating fast pyrolysis bio-oil of pine sawdust in the presence of metallic zinc under hydrothermal conditions (250–400 °C).[35] It was

suggested that higher temperatures yielded better hydrodeoxygenation activity and that a large proportion of the water-insoluble oil was reduced to hydrocarbon at 400 °C.

Zero-valent metals can be easily regenerated using renewable resources. Hargus and co-workers have proposed a concept of recycling metal oxides that are exhausted after bio-oil upgrading by reducing them in a high-temperature solar thermal reactor.[34] In the area of steel making process, use of a biomass-derived reducing agent as a substitute for coal coke has been investigated.[36] If these regeneration processes can be combined, zero-valent metals can be used as an ideal renewable reductant for bio-oil, and it will be possible that an eco-friendly and high quality bio-oil production process can be constructed.

Catalytic cracking of bio-oil

Bio-oils produced by fast pyrolysis or HTL can be upgraded by cracking using solid acid catalysts, including zeolite, silica-alumina, and molecular sieves.[37] Catalytic cracking is a complex process involving many reactions, including cracking, decarboxylation, decarbonylation, hydrodeoxygenation, hydrocracking, hydrogenation, and repolymerization;[16] C_2-C_4 olefins and BTX are obtained as the main products. These products can be used as naphtha and can be the basic raw materials of the petrochemical industry. Thus, biomass-derived olefin and BTX (green olefin and BTX) can be directly fed to current oil refineries, enabling most petroleum-derived products to become carbon-neutral.

Catalytic cracking is, however, subject to many challenges, including the need for a suppression of the formation of coke, which causes catalyst deactivation and reduced yield of the product. Efforts to improve catalyst selectivity and optimize

reaction conditions have been made in recent years. In addition, it has been found that the quality of the bio-oil fed into the cracking process affect the performance of that process. Vispute and co-workers demonstrated an integrated process of hydrodeoxygenation of water extracts of bio-oil obtained by fast pyrolysis and catalytic cracking.[38] Thqey showed that the two-stage hydrogenation reaction with Ru and Pt not only improved the yield of olefin and BTX, but also suppressed coke formation. They have conducted cracking reactions using various biomass-derived model substrates and have confirmed that the elemental composition (C/H/O) of the substrates correlates with cracking performance.[39]

Present work

As previously discussed, the production of green olefin/BTX by a combination of HTL of biomass and catalytic cracking is a promising candidate for innovative biomass conversion and will enable carbon neutral chemical production. In the present study, the author focused on the HTL process and developed a new reaction system using zero-valent metallic iron as an additive. HTL using zero-valent iron as an additive was performed for the purpose of simultaneously liquefying and upgrading lignocellulosic biomass, and efficiently obtaining a high quality liquefied product suitable as a feedstock for cracking. The effect of addition of zero-valent iron was confirmed from the profiles and detailed analysis of products and on through determination of the applicability of liquefied products to cracking. In addition, the reaction pathway of Fe-assisted HTL of lignocellulosic biomass was elucidated, and optimization of the process was studied. The experimental contents of this thesis are presented in four chapters, which are now briefly described.

In chapter 1, the author demonstrates the development of a novel biomass HTL process using inexpensive and renewable iron as a reducing agent. HTL of palm empty fruit bunches (EFB) was examined using metallic iron as an additive, which exhibited high yields of the water-soluble (WS) and water-insoluble (WI) fractions and the suppression of char formation, compared with conventional HTL. The quality of the WS fraction obtained by Fe-assisted HTL was confirmed by catalytic cracking of the WS fraction using zeolite catalyst. The recyclability of iron was also investigated and it was demonstrated that iron can be repeatedly used for HTL.

In chapter 2, comprehensive analysis for clarifying the composition of the WS fraction is provided by combining various analyses including gas chromatography–mass spectrometry (GC–MS), gas chromatography–flame ionization detection (GC–FID), elemental analysis, gel–permeation chromatography (GPC), and Fourier-transform infrared spectroscopy (FT-IR). Volatile compounds and the heavy components in the WS fraction were analyzed separately and the effect of the addition of iron was quantitatively evaluated.

In chapter 3, the reactivity of each component of lignocellulosic biomass (cellulose, hemicellulose, and lignin) is discussed in order to clarify the mechanisms underlying the increase of the WS fraction and upgrading of products, by iron. Commercially available hydrocarbons and enzymatically isolated lignin were used as model substrates and the contribution of each substrate to the formation of HTL products were clarified both in the presence and absence of iron. On the basis of the reactivity of each component, the overall reaction pathway was proposed.

In chapter 4, the author focused on the improvement of reaction conditions of Fe-assisted HTL. In order to maximize the rate of utilization of the reducing capacity of

iron, the addition of a hydrogenation catalyst was investigated. The effect of the supported metal catalyst was evaluated by analysis and catalytic cracking of the WS fraction.

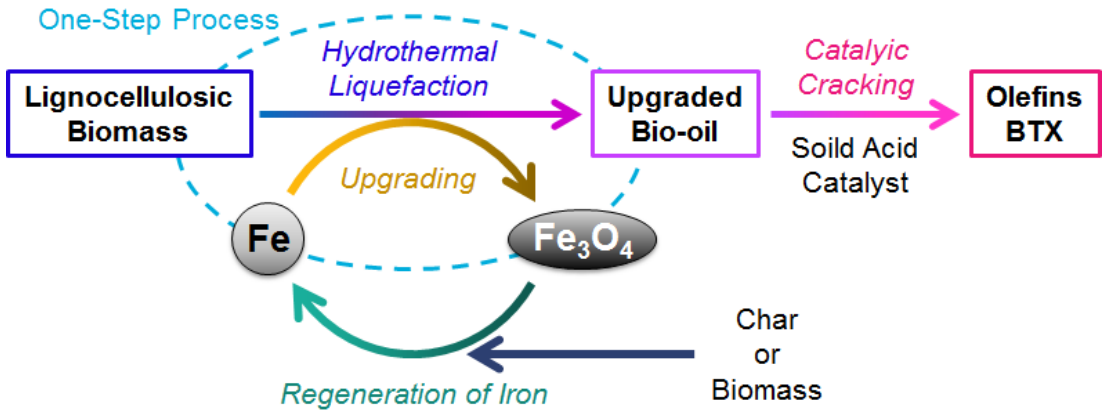

Scheme 3. Schematic of biomass utilization system using iron reductant.

References

1. *World Population Prospects: The 2017 Revision, Key Findings and Advance Tables*; ESA/P/WP/248; United Nations, Department of Economic and Social Affairs, Population Division: 2017.
2. *Japan's Energy White Paper 2017*, Ministry of Economy,Trade and Industry 2017, 199, https://www.enecho.meti.go.jp/about/whitepaper/2017pdf/whitepaper2017pdf_2_2.pdf.
3. *United Nations Framework Convntion on Climate Change*, United Nations, 1992.
4. *The Paris Agreement*, United Nations, 2015.
5. Edenhofer, O.; Pichs-Madruga, R.; Sokona, Y.; Farahani, E.; Kadner, S.; Seyboth, K.; Adler, A.; Baum, I.; Brunner, S.; Eickemeier, P.; Kriemann, B.; Savolainen, J.;

Schlömer, S.; von Stechow, C.; Zwickel, T.; Minx, J. C., Eds., *Climate Change 2014: Mitigation of Climate Change. Contribution of Working Group Iii to the Fifth Assessment Report of the Intergovernmental Panel on Climate Change*; Summary for Policymakers, The Intergovernmental Panel on Climate Change: 2014.

6. Bajželj, B.; Allwood, J. M.; Cullen, J. M., Designing Climate Change Mitigation Plans That Add Up. *Environ. Sci. Technol.* **2013,** *47* (14), 8062–8069.
7. *Forecast of Global Supply and Demand Trends for Petrochemical Products*, Ministry of Economy, Trade and Industry, 2017, https://www.meti.go.jp/policy/mono_info_service/mono/chemistry/downloadfiles/teikihapyousiryou/170718sekaijyukyudoko.pdf.
8. Fujimoto, K., Biomass Nippon Strategy. *Waste Manage. Res.* **2004,** *15* (2), 53–59.
9. Inderwildi, O. R.; King, D. A., Quo Vadis Biofuels? *Energy Environ. Sci.* **2009,** *2* (4), 343–346.
10. Mitchell, D. *A Note on Rising Food Prices*; Policy Research Working Paper, 4682; World Bank: 2008.
11. Bentsen, N. S.; Felby, C.; Thorsen, B. J., Agricultural Residue Production and Potentials for Energy and Materials Services. *Prog. Energy Combust. Sci.* **2014,** *40*, 59–73.
12. Huber, G. W.; Iborra, S.; Corma, A., Synthesis of Transportation Fuels from Biomass: Chemistry, Catalysts, and Engineering. *Chem. Rev.* **2006,** *106* (9), 4044–4098.
13. Rauch, R.; Hrbek, J.; Hofbauer, H., Biomass Gasification for Synthesis Gas Production and Applications of the Syngas. *WIREs Energy Environ.* **2014,** *3* (4),

343–362.

14. Menon, V.; Rao, M., Trends in Bioconversion of Lignocellulose: Biofuels, Platform Chemicals & biorefinery Concept. *Prog. Energy Combust. Sci.* **2012,** *38* (4), 522–550.

15. Xiu, S.; Shahbazi, A., Bio-Oil Production and Upgrading Research: A Review. *Renew. Sust. Energy Rev.* **2012,** *16* (7), 4406–4414.

16. Baloch, H. A.; Nizamuddin, S.; Siddiqui, M. T. H.; Riaz, S.; Jatoi, A. S.; Dumbre, D. K.; Mubarak, N. M.; Srinivasan, M. P.; Griffin, G. J., Recent Advances in Production and Upgrading of Bio-Oil from Biomass: A Critical Overview. *J. Environ. Chem. Eng.* **2018,** *6* (4), 5101–5118.

17. Bridgwater, A. V.; Peacocke, G. V. C., Fast Pyrolysis Processes for Biomass. *Renew. Sust. Energy Rev.* **2000,** *4* (1), 1–73.

18. Toor, S. S.; Rosendahl, L.; Rudolf, A., Hydrothermal Liquefaction of Biomass: A Review of Subcritical Water Technologies. *Energy* **2011,** *36* (5), 2328–2342.

19. Li, H.; Hurley, S.; Xu, C., Liquefactions of Peat in Supercritical Water with a Novel Iron Catalyst. *Fuel* **2011,** *90* (1), 412–420.

20. Wang, Y.; Wang, H.; Lin, H.; Zheng, Y.; Zhao, J.; Pelletier, A.; Li, K., Effects of Solvents and Catalysts in Liquefaction of Pinewood Sawdust for the Production of Bio-Oils. *Biomass Bioenergy* **2013,** *59*, 158–167.

21. Xu, C.; Etcheverry, T., Hydro-Liquefaction of Woody Biomass in Sub- and Super-Critical Ethanol with Iron-Based Catalysts. *Fuel* **2008,** *87* (3), 335–345.

22. Nazari, L.; Yuan, Z.; Souzanchi, S.; Ray, M. B.; Xu, C., Hydrothermal Liquefaction of Woody Biomass in Hot-Compressed Water: Catalyst Screening and Comprehensive Characterization of Bio-Crude Oils. *Fuel* **2015,** *162*, 74–83.

23. O'Connor, P., Chapter 1 - a General Introduction to Biomass Utilization Possibilities. In *The Role of Catalysis for the Sustainable Production of Bio-Fuels and Bio-Chemicals*, Triantafyllidis, K. S.; Lappas, A. A.; Stöcker, M., Eds. Elsevier: Amsterdam, 2013; pp 1–25.

24. Mortensen, P. M.; Grunwaldt, J. D.; Jensen, P. A.; Knudsen, K. G.; Jensen, A. D., A Review of Catalytic Upgrading of Bio-Oil to Engine Fuels. *Appl. Catal., A* **2011,** *407* (1-2), 1–19.

25. Padró, C. E. G.; Putsche, V. *Survey of the Economics of Hydrogen Technologies*; NREL/TP-570-27079; National Renewable Energy Laboratory: 1999.

26. Parkinson, B.; Balcombe, P.; Speirs, J. F.; Hawkes, A. D.; Hellgardt, K., Levelized Cost of Co2 Mitigation from Hydrogen Production Routes. *Energy Environ. Sci.* **2019,** *12* (1), 19–40.

27. Birch, A. J., 117. Reduction by Dissolving Metals. Part I. *J. Chem. Soc.* **1944,** (0), 430–436.

28. Bouveault, L.; Blanc, G., Préparation Des Alcools Primaires Au Moyen Des Acides Correspondants. *Compt. Rend.* **1903,** *136*, 1676–1678.

29. Barbier, P., Synthèse Du Diéthylhepténol. *Compt. Rend.* **1899,** *128*, 110–111.

30. Roberts, A. L.; Totten, L. A.; Arnold, W. A.; Burris, D. R.; Campbell, T. J., Reductive Elimination of Chlorinated Ethylenes by Zero Valent Metals. *Environ. Sci. Technol.* **1996,** *30* (8), 2654–2659.

31. Kadam, H. K.; Tilve, S. G., Advancement in Methodologies for Reduction of Nitroarenes. *RSC Adv.* **2015,** *5* (101), 83391–83407.

32. Clarke, H. T.; Dreger, E. E., N-Heptyl Alcohol. *Org. Synth.* **1926,** *6*, 52–53.

33. Liu, W.-J.; Zhang, X.-S.; Qv, Y.-C.; Jiang, H.; Yu, H.-Q., Bio-Oil Upgrading at

Ambient Pressure and Temperature Using Zero Valent Metals. *Green Chem.* **2012,** *14* (8), 2226–2233.

34. Hargus, C.; Michalsky, R.; Peterson, A. A., Looped-Oxide Catalysis: A Solar Thermal Approach to Bio-Oil Deoxygenation. *Energy Environ. Sci.* **2014,** *7* (10), 3122–3134.

35. Cheng, S.; Wei, L.; Julson, J.; Muthukumarappan, K.; Kharel, P. R.; Cao, Y.; Boakye, E.; Raynie, D.; Gu, Z., Hydrodeoxygenation Upgrading of Pine Sawdust Bio-Oil Using Zinc Metal with Zero Valency. *J. Taiwan Inst. Chem. Eng.* **2017,** *74*, 146–153.

36. Wei, R.; Zhang, L.; Cang, D.; Li, J.; Li, X.; Xu, C. C., Current Status and Potential of Biomass Utilization in Ferrous Metallurgical Industry. *Renew. Sust. Energy Rev.* **2017,** *68*, 511-524.

37. Rezaei, P. S.; Shafaghat, H.; Daud, W. M. A. W., Production of Green Aromatics and Olefins by Catalytic Cracking of Oxygenate Compounds Derived from Biomass Pyrolysis: A Review. *Appl. Catal., A* **2014,** *469*, 490–511.

38. Vispute, T. P.; Zhang, H. Y.; Sanna, A.; Xiao, R.; Huber, G. W., Renewable Chemical Commodity Feedstocks from Integrated Catalytic Processing of Pyrolysis Oils. *Science* **2010,** *330* (6008), 1222–1227.

39. Zhang, H.; Cheng, Y.-T.; Vispute, T. P.; Xiao, R.; Huber, G. W., Catalytic Conversion of Biomass-Derived Feedstocks into Olefins and Aromatics with ZSM-5: The Hydrogen to Carbon Effective Ratio. *Energy Environ. Sci.* **2011,** *4* (6), 2297–2307.

Chapter 1. Fe-assisted hydrothermal liquefaction of lignocellulosic biomass for producing high-grade bio-oil

1.1. Introduction

Growing concerns over the environmental impact of fossil fuels and their inevitable depletion, as well as climate change caused by greenhouse gas emissions, have led to extensive research on the development of alternative energy sources. In this regard, biomass as a possible renewable resource for energy fuels and chemicals has received significant attention.[1-3] Various researchers have investigated biomass-to-liquid (BTL) conversion as a possible method for utilizing biomass.[4]

Bio-oil produced by thermochemical processes, such as pyrolysis or hydrothermal liquefaction of biomass, is being investigated widely. It can be upgraded to transportation fuels and industrial chemicals.[5-11] Hydrothermal liquefaction, in which biomass is decomposed under subcritical or supercritical water, is a promising candidate for producing bio-oil.[7-11] Contrary to pyrolysis, hydrothermal liquefaction has the advantage of not requiring pre-drying the biomass feedstock, which originally contains water.[3, 6] Several groups have made significant efforts to enhance the yield of liquid products in this process and suppress the formation of char.[8,10,11]

However, compared to fossil oil, bio-oil contains significantly higher amounts of water and oxygen. Hence, in terms of fuel property, it exhibits a low calorific value.[12] Because of the presence of oxygen-rich compounds, bio-oil is both chemically and thermally unstable, which hinders its direct application in the current infrastructure of oil refinery. Hence, the high oxygen content must be reduced by upgrading technologies such as hydrotreating and catalytic cracking.[13-15] Vispute and co-workers have reported

an integrated catalytic approach combining hydroprocessing with zeolite catalysis for the conversion of bio-oils into light olefins (C_2–C_4 olefins), as well as benzenes, toluene, and xylenes (BTX), which are industrial commodity chemical feedstock.[15] The upgraded bio-oil after two-step hydrogenation exhibited higher selectivity of light olefins and BTX than the crude oil. For the hydrogenation process, the cost of hydrogen would be a key factor of the economic efficiency for utilizing bio-oil as a chemical feedstock. Although renewable production of hydrogen has been developed, its cost is still high, mainly due to the high capital investment and delivery cost.[16-20]

In this context, the author developed a method to produce high-quality oil directly from biomass, without requiring the necessary expensive equipment. The author investigated the effect of metal Fe on the hydrothermal reaction of biomass to afford high-quality bio-oil, which involves the generation of hydrogen in situ from the reaction between metal and water. This system promotes the decomposition of biomass while simultaneously performing hydrogenation (shown in Scheme 1). Char byproduct produced during the reaction can be used as a reductant for regenerating the oxidized metal. Therefore, this process as a whole is carbon neutral and environmentally friendly. The author reports the reactivity of oil palm empty fruit bunch (EFB) in hydrothermal liquefaction, the effect of Fe as the hydrogen-generating agent, and the regeneration of oxidized Fe. In addition, the author shows the conversion of the water-soluble fraction into C_2–C_4 olefins and aromatics over an HZSM-5 zeolite catalyst.

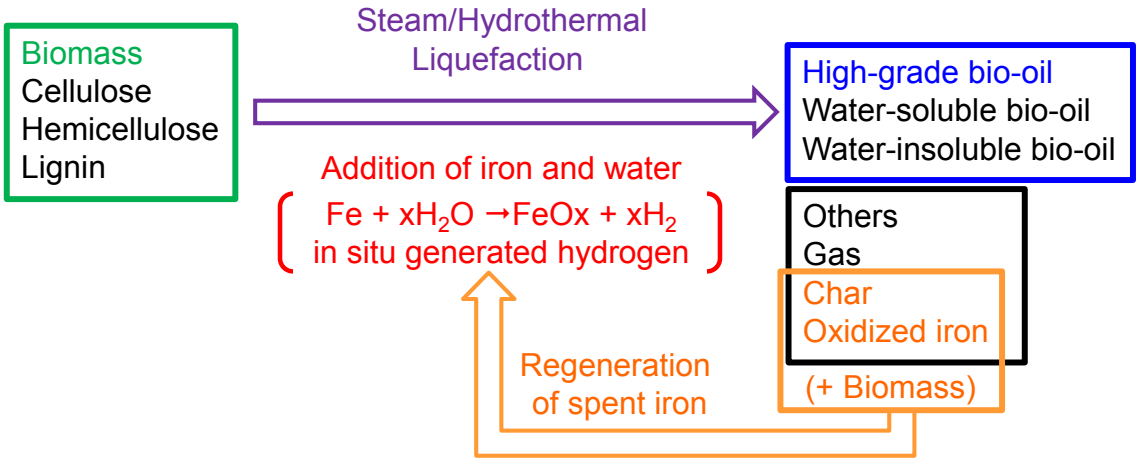

Scheme 1. Overview of the liquefaction of biomass using hydrogen generated in situ from Fe and H_2O.

1.2. Experimental

1.2.1. Materials

Oil palm empty fruit bunch (EFB) from Indonesia was supplied from Nippon Shokubai Co., Ltd. (Japan), and it was used as the lignocellulosic biomass feedstock. EFB was dried at 25 °C and crushed into particles with a size of less than 300 μm. Table 1 shows the EFB composition.[21] Moisture and ash content were determined by thermogravimetry at 120 °C and 1000 °C (EXSTAR TG/DTA 7200, Hitachi High-Tech Science Corporation). Fe powder (99.9%, NM-0029-UP) was purchased from Ionic Liquids Technologies GmbH (Germany). HZSM-5 zeolite with a Si/Al ratio of 24:1 was supplied by Nippon Shokubai Co., Ltd. (Japan). All other chemicals were commercially obtained: cellulose (Avicel® PH-101, Sigma-Aldrich), xylan from corn core (Tokyo Chemical Industry Co., Ltd.), D-(+)-glucose (100%, Wako Pure Chemical Industries, Ltd.), D-(+)-xylose (99.7%, Wako Pure Chemical Industries, Ltd.), dihydroxyacetone

dimer (99.8%, Wako Pure Chemical Industries, Ltd.), pyruvaldehyde solution (38.4%, Wako Pure Chemical Industries, Ltd.), hydroxyacetone (99.2%, Wako Pure Chemical Industries, Ltd.), and copper powder (99.9%, Ionic Liquids Technologies GmbH).

Table 1. Composition of oil palm empty fruit bunch (EFB)

Composition[a] (wt%)			Composition (wt%)		Composition[b] (wt%)			
Cellulose	Hemicellulose	Lignin	Moisture	Ash	C	H	N	O[c]
37.9	35.0	24.0	6.7	4.6	46.5	5.6	0.7	42.6

[a] See reference 21. [b] Percent weight on dry basis. [c] Calculated by difference.

Fe was oxidized by the following procedure. First, Fe powder (3.5 g) and H_2O (2.238 g) were introduced into a 100 mL Hastelloy C high-pressure reactor (OM Lab-Tech., MMJ-100), and the reactor was purged four times with nitrogen. Second, the reactor was heated to 300 °C, and this temperature was maintained for 10 min. Finally, after cooling the reactor to 25 °C, the oxidized Fe samples were separated by filtration, followed by drying overnight under vacuum at 70 °C.

1.2.2. Liquefaction and separation

All EFB liquefaction experiments were conducted in the batch mode using the Hastelloy C high-pressure reactor. First, EFB (1.0 g), Fe powder (0 or 1.564 g), and H_2O (0, 1, 3, 5, 10, or 40 g) were introduced into the reactor, which was purged four times with nitrogen. Second, the initial pressure was set to 1.0 MPa with nitrogen, and the stirring rate was adjusted to 700 rpm. Next, the reactor was heated to 300 °C and maintained constant at that temperature for 10 min. Upon reaction completion, the reactor was rapidly cooled to 25 °C using ice water.

Bio-oil, gas, and char products were separated following a previously published method.[22] The gaseous products were collected in a gas sampling bag, and the water-soluble products were filtered and designated as "WS." Then, the reactor wall was washed with acetone, and the resulting acetone solution with the residue was filtered. The residue was rinsed with acetone repeatedly until the eluent became colorless. The final acetone solution was evaporated at 30 °C under reduced pressure, and the temperature was increased to 60 °C to remove water. The resulting residues were designated as "water-insoluble" fractions (WI). In addition, the residue from the filter paper was dried overnight at 70 °C under reduced pressure, affording the solid residue (SR).

1.2.3. Catalytic cracking of bio-oil

A fixed-bed continuous flow reactor was utilized for the production of light olefins from WS by catalytic cracking. This reaction system consisted of a stainless steel tube reactor, gas feeding system, liquid feeding pump, heating system, gas wash bottle with ice-cold water, and gas sampling system (Figure 1). HZSM-5 zeolite (0.85–1.7 mm, 6 mL) was added into the reactor, followed by adding stainless steel beads for vaporizing the liquid feedstock. The catalyst was flushed with nitrogen (50 mL/min) for 1 h at 25 °C, followed by heating to 600 °C under nitrogen (50 mL/min). The aqueous WS solution was fed into the reactor using a plunger pump at a weight hourly space velocity of 1.1 h^{-1}. During the reaction, the condensed products were collected using the gas wash bottle with either water or acetone. All gaseous products were collected in a gas sampling bottle. Finally, the HZSM-5 catalyst was removed and crushed in a mortar for coke analysis.

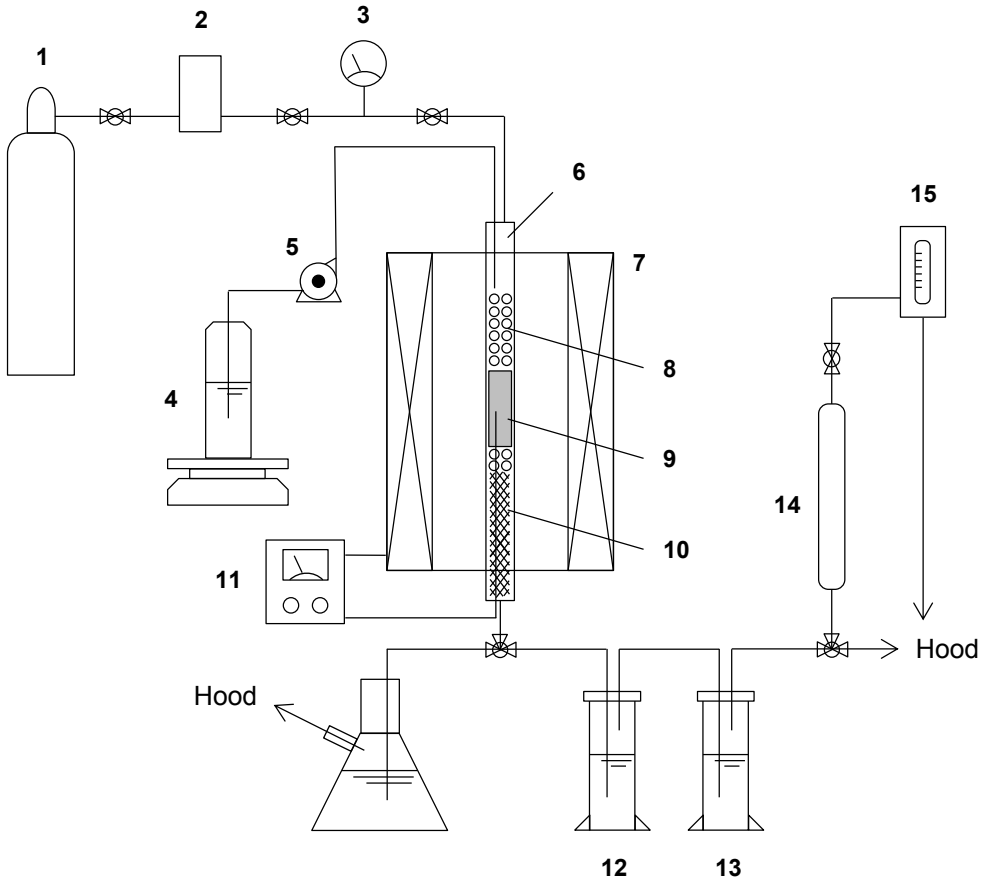

Figure 1. The fixed-bed continuous flow reactor for catalytically cracking the WS fraction into olefin and aromatics. **1**: N_2 gas cylinder, **2**: flow control, **3**: pressure gauge, **4**: aqueous solution of WS fraction, **5**: plunger pump, **6**: stainless steel tube reactor, **7**: tubular furnace, **8**: stainless steel beads, **9**: catalyst, **10**: stainless steel mesh, **11**: temperature control, **12**, **13**: gas wash bottles with water or acetone, **14**: gas sampling bottle, and **15**: soap film flowmeter.

1.2.4. Product analysis

The organic carbon content of WS was measured using a total organic carbon analyzer (Shimadzu, TOC-$L_{CSH/CSN}$). The WS solution was analyzed by

high-performance liquid chromatography (Shimadzu, Prominence) using Aminex® HPX-87P and HPX-87H columns (Bio-Rad, 300 mm × 7.8 mm ID) equipped with a refractive index detector. In addition, the sample was diluted with acetone (1:1 by volume) and analyzed with a gas chromatography system (Shimadzu, GC-2010) using a capillary column (Restek, Stabilwax®, 30 m × 0.25 mm ID × 0.25 μm film thickness) and a flame ionization detector. The gas chromatography–mass spectrometry (GC–MS) analysis was performed using a Shimadzu QP-2010 system equipped with a capillary column (GL Sciences, Inert-cap® WAX-HT, 30 m × 0.25 mm ID × 0.25 μm film thickness). Elemental analysis (CHN) of the EFB, WI, and SR samples was performed using an elemental analyzer (Elementar Vario EL cube) using sulfanilamide as the calibration standard. The oxygen mass content was calculated by the difference. The yields of hydrothermal liquefaction and catalytic cracking were calculated as follows:

$$\text{Yield of hydrothermal liquefaction (\%)} = \frac{\text{Moles of carbon in product}}{\text{Moles of carbon in raw material}} \times 100 \quad (1)$$

$$\text{Yield of catalytic cracking (\%)} = \frac{\text{Moles of carbon in product}}{\text{Moles of carbon in WS fraction fed in}} \times 100 \quad (2)$$

Quantitative ^{13}C NMR spectra of the WS and WI samples were recorded on a Varian VNMRS 600 MHz spectrometer using an inverse-gated decoupling pulse sequence, a pulse angle of 90°, and a relaxation delay of 8 s.[23] Dimethyl sulfoxide (DMSO)-d_6 was used as the solvent. The molar distribution of carbon in the WS and WI fractions was determined as follows:

$$\text{Molar distribution of carbon (\%)} = Y_{WS\ or\ WI} \times \frac{A_{\ each\ chemical\ shift\ region}}{A_{all\ chemical\ shift\ regions}} \quad (3)$$

Here, $Y_{WS\ or\ WI}$ represents the carbon yield of the WS or WI fraction, $A_{each\ chemical\ shift\ region}$ represents the total peak area of each chemical shift, and $A_{all\ chemical\ shift\ regions}$ represents the total peak area of all chemical shifts (0–230 ppm). Gaseous products were analyzed using two gas chromatography systems: Shimadzu GC-8A equipped with silica gel (Shinwa Chemical Industries, ZS-74) and molecular sieve 5A (Shinwa Chemical Industries, ZM-1) columns with a thermal conductivity detector for CO_2 and CO, and Shimadzu GC-2014 equipped with a Sunpak-A column (Shinwa Chemical Industries, ZS-72) with a flame ionization detector for hydrocarbons.

1.2.5. Regeneration of Fe

The fixed-bed continuous flow reactor was utilized for the regeneration of the used Fe sample, i.e., reduction of oxidized Fe. First, char-containing oxidized Fe (3.85 g) was mixed with EFB (1.93 g) using a mortar for 10 min. Second, the resulting mixture was added into a quartz reactor and heated to 1000 °C at a heating rate of 10 °C/min under nitrogen (100 mL/min), and the final temperature was maintained for 2 h. Third, the reactor was cooled to 25 °C, and the resulting Fe sample was reused for the liquefaction of EFB. The crystalline phase of the regenerated sample was determined using a Rigaku SmartLab diffractometer with CuKα radiation. Finally, in situ high-temperature X-ray diffraction (HT-XRD) measurements of the oxidized Fe and EFB mixture were performed on a Rigaku RINT TTR3 diffractometer under nitrogen (500 mL/min) using CuKα radiation.

1.3. Results and Discussion

1.3.1. Effect of H_2O/EFB weight ratio on the liquefaction of EFB in the absence or presence of Fe

The hydrothermal liquefaction of EFB with and without Fe was performed at varying H_2O/EFB weight ratios between 0:1 and 40:1. The amount of saturated water vapor in the reaction system at 300 °C was ~3.5 g. As such, all H_2O existed as steam at H_2O/EFB ≤ 3:1, while a portion of the H_2O also existed in the condensed phase at H_2O/EFB ≥ 5:1. Figure 2 shows the effect of water content on the hydrothermal liquefaction of EFB. As shown in Figure 2(a), in the absence of Fe, the yield of bio-oil (WS + WI) gradually increased from 20% to 29% with increasing H_2O/EFB ratio from 0:1 to 5:1; at a H_2O/EFB ratio of 40:1, the yield of bio-oil further increased to 82%. On the other hand, with increasing H_2O/EFB ratio, the SR yield consistently decreased. As shown in Figure 2(b), in the presence of Fe, the yield of bio-oil drastically increased from 25% to 79% with increasing H_2O/EFB ratio from 0:1 to 5:1, while the yield of SR decreased. At a H_2O/EFB ratio of 40:1, the corresponding yield of bio-oil increased to 84%. Thus, although the yield of bio-oil increased with the H_2O/EFB ratio both in the presence and absence of Fe, Fe exhibits a more pronounced effect at low H_2O/EFB ratios. As the solvent can dilute the degradation products and suppress polymerization,[24-25] the increase in the yield of bio-oil with increasing H_2O/EFB ratio is tentatively attributed to the inhibition of re-polymerization and the formation of carbonized products by dilution with H_2O. Similar yields for CO and CO_2 (~10%) were observed for all systems.

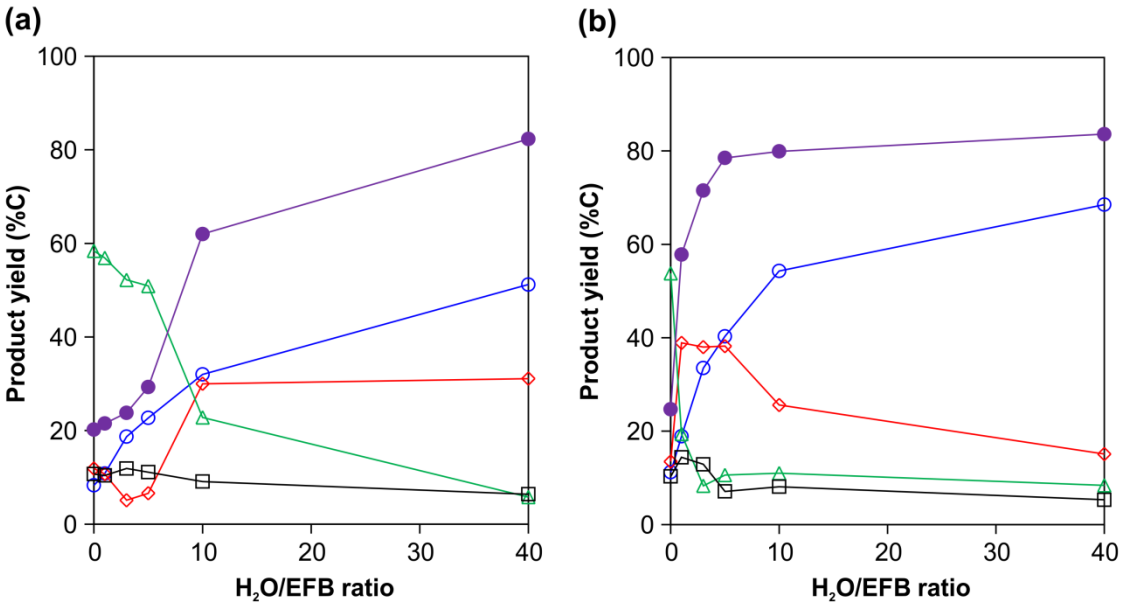

Figure 2. Yields of carbon products obtained from the liquefaction of EFB as a function of the H_2O/EFB weight ratio in the (a) absence and (b) presence of Fe. (●) WS + WI, (○) WS, (◊) WI, (□) gas, and (Δ) SR. Reaction conditions: EFB = 1.0 g, Fe = 1.564 g, H_2O = 0–40 g, P_{N2} = 1.0 MPa, temperature = 300 °C, time = 10 min.

1.3.2. Promotion of EFB liquefaction by Fe

1.3.2.1. H_2O/EFB weight ratio = 1:1

As discussed above, the yield of bio-oil from the liquefaction of EFB was enhanced by Fe at any given H_2O content. The generation of hydrogen from the reaction between Fe and H_2O ($3Fe + 4H_2O \rightarrow Fe_3O_4 + 4H_2$) is a key reaction in the H_2O/EFB/Fe system. As summarized in Table 2, H_2 was both produced and consumed during the liquefaction of EFB.

Table 2. Production and consumption of H_2 from the reaction between Fe and H_2O at 300 °C

H_2O content (mL)	H_2 in the reactor (mmol)		Utilization rate of H_2 (%)
	without EFB[a]	with EFB[b]	
1	13	9	31
3	24	9	63
5	25	10	60
10	22	13	41
40	20	13	35

Reaction conditions: [a] H_2O = 1–40 g, Fe = 1.564 g, P_{N2} = 1.0 MPa, temperature = 300 °C, time = 10 min. [b] EFB = 1 g, H_2O = 1–40 g, Fe = 1.564 g, P_{N2} = 1.0 MPa, temperature = 300 °C, time = 10 min.

To confirm the effect of H_2 produced from Fe and H_2O, control experiments were conducted at a H_2O/EFB ratio of 1:1, as summarized in Table 3. In the presence of oxidized Fe or Cu, both of which produce no hydrogen, only marginal variation was observed with respect to the yield of bio-oil. Cu exhibits high thermal conductivity; however it did not affect the yield of bio-oil. Thus, the increased yield of bio-oil in the presence of Fe is not due to the thermal conductivity of Fe. Furthermore, the H_2O/EFB system had similar yield of bio-oil with or without 1 MPa of added H_2 gas. These results indicate that hydrogen generated from Fe and H_2O in situ apparently is responsible for the increased of bio-oil yields.

Table 3. Effect of the addition of Fe on the liquefaction of EFB at a H_2O/EFB weight ratio = 1:1

Reaction system	Carbon yield (%C)				Carbon balance (%)
	WS	WI	Gas	SR	
H_2O/EFB	11	11	10	57	89
H_2O/EFB/Fe[a]	19	39	14	19	91
H_2O/EFB/Oxidized Fe[b, d]	13	18	12	49	92
H_2O/EFB/Cu[c]	11	11	11	55	88
H_2O/EFB[e]	12	16	7	53	88

Reaction conditions: EFB = 1 g, H_2O = 1 g, [a] Fe = 1.564 g, [b] Oxidized Fe = 2.161 g, [c] Cu = 1.779 g, P_{N2} = 1.0 MPa, temperature = 300 °C, time = 10 min. [d] Oxidized Fe was prepared by the treatment of Fe powder with H_2O at 300 °C for 10 min (see experimental section) [e] 1.0 MPa N_2 + 1.0 MPa H_2.

Figure 3 shows the molar distribution of carbon in the WS and WI fractions as determined by their ^{13}C NMR spectra. The presence of aliphatic carbon (0–55 ppm); alcohols, ethers, and carbohydrates moieties (55–95 ppm); aromatics and olefins (95–165 ppm); esters and carboxylic acids (165–180 ppm); and ketones and aldehydes (180–215 ppm) was confirmed. With a H_2O/EFB ratio of 1:1 (Figure 3(a)), the main carbon signals were attributed to aliphatics, aromatics, and olefins, with the appearance of a few oxygenated carbon resonances. The addition of Fe resulted in the significant increase of aliphatics, aromatics, and olefins, suggesting that it increases the yield of bio-oil without increasing the oxygen content.

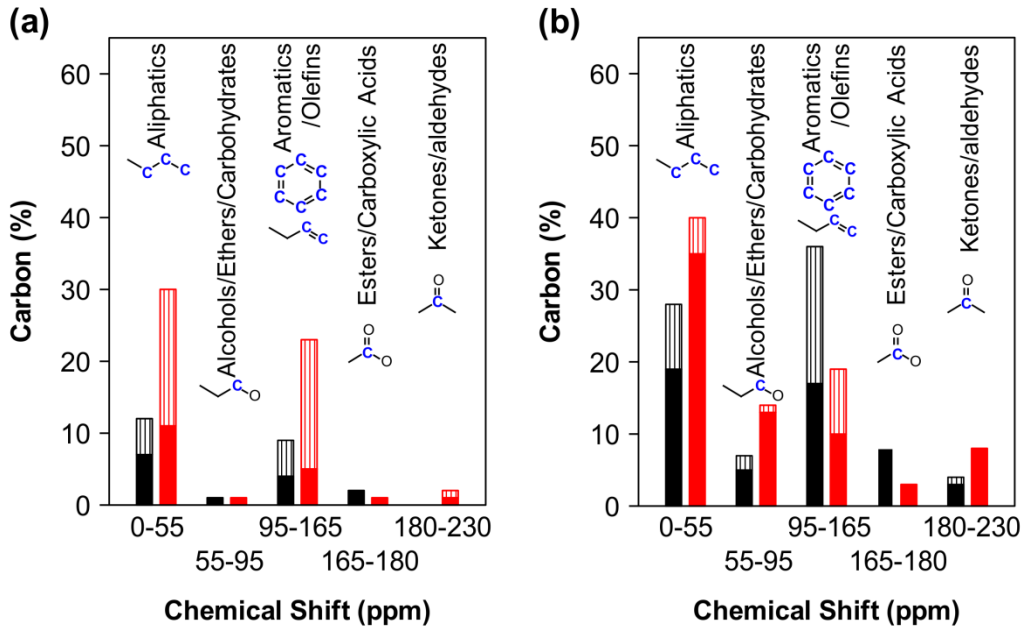

Figure 3. ^{13}C NMR spectral distribution of functional groups in the bio-oil obtained at H_2O/EFB weight ratios of (a) 1:1 and (b) 40:1, and in the absence (black bar) or presence (red bar) of Fe (Plain: WS / Striped: WI).

Fe and H_2O promote the degradation of polymeric chain of the biomass components (cellulose, hemicellulose, and/or lignin), which serve as precursors for the liquid products. Hydrogen inhibits the condensation, cyclization, and re-polymerization of the intermediates and liquid products, which in turn results in reduced char formation.[8] From the above results, the increased bio-oil yield with Fe is therefore attributed to the stabilization of the EFB degradation products by the hydrogen generated in situ, resulting in reduced char formation.

1.3.2.2. H_2O/EFB weight ratio = 40:1

In addition, the effect of Fe addition was investigated at a H_2O/EFB weight ratio of 40:1, which resulted in the more selective production of the WS fraction, albeit with a relatively constant yield of bio-oil (WS + WI). As shown in Table 4, the distribution of products in both the H_2O/EFB and H_2O/EFB/Oxidized Fe systems was similar regardless of the presence of hydrogen gas, indicating that in this case the hydrogen generated by reacting Fe and H_2O results in the selective production of the WS fraction. From the ^{13}C NMR results shown in Figure 3(b), as compared with those from the H_2O/EFB system, the liquefied products obtained from the H_2O/EFB/Fe system mainly consisted of aliphatics, albeit with a higher amount of oxygenated functional groups and a lower amount of aromatic compounds. Interestingly, the addition of Fe suppressed the formation of carboxylic compounds, indicating that formyl groups of degraded compounds are converted into alcohols instead of carboxylic acids. These results indicate that the increased yield of WS by the addition of Fe is attributed to the suppression of the aromatization of degraded compounds, and the retention of aliphatic compounds bearing oxygen-containing functional groups.

Table 4. Effect of the addition of Fe on the liquefaction of EFB with a H_2O/EFB weight ratio = 40:1

Reaction system	Atmosphere	Carbon yield (%C)						Carbon balance (%)
		WS			WI	Gas	SR	
		WS	HA[e]	HB[f]				
H_2O/EFB	N_2	51	5	−	31	6	6	94
H_2O/EFB/Fe[a]	N_2	69	20	7	15	5	8	97
H_2O/EFB/Oxidized Fe[b, d]	N_2	53	5	1	29	7	8	97
H_2O/EFB	N_2+H_2[c]	57	5	−	35	8	6	106
H_2O/EFB/Fe[a]	N_2+H_2[c]	67	19	7	19	4	9	99
H_2O/EFB/Oxidized Fe[b, d]	N_2+H_2[c]	55	3	2	30	9	5	99

Reaction conditions: EFB = 1 g, H_2O = 40 g, [a] Fe = 1.564 g, [b] Oxidized Fe = 2.161 g, atmosphere = 1.0 MPa (N_2), [c] 1.0 MPa N_2 + 1.0 MPa H_2, temperature = 300 °C, time = 10 min. [d] Oxidized Fe was prepared by the treatment of Fe powder with H_2O at 300 °C for 10 min (see experimental section). [e] Hydroxyacetone and [f] 3-hydroxy-2-butanone.

The WS fractions obtained both in the presence and absence of Fe were characterized by GC–MS, as summarized in Table 5 (chromatograms are shown in Figure 4). Both systems were predominantly composed of acids, ketones, acyclic and cyclic aliphatic compounds, alcohols, aldehydes, esters, and aromatic compounds. Nevertheless, in both cases, small peak areas were observed for aromatic and olefinic compounds, suggesting that a majority of aromatic and olefinic compounds are present as oligomers, which did not vaporize in the GC inlet. With the addition of Fe, the WS fraction contained significantly higher quantities of hydroxyketones than that obtained without Fe, which was in agreement with the NMR results (Figure 3), indicating that the addition of Fe increased the formation of aliphatic and oxygenated products. Previously, Hirano and co-workers have reported that hydroxyacetone and 3-hydroxy-2-butanone

are produced by the hydrogenation of degradation products from glucose, and the presence of Fe_3O_4 and/or dissolved Fe promotes the isomerization and retro-aldol condensation of sugars.[26] The aforementioned result indicates that the iron species in this novel system possibly functions as a catalyst for generating such precursors in the WS fraction. In addition, as shown in Table 4, a significantly higher yield of hydroxyketones was observed for the H_2O/EFB/Fe system, compared to the H_2O/EFB and H_2O/EFB/Oxidized Fe systems with or without added hydrogen. Furthermore, in the H_2O/EFB/Fe system, comparable yields of hydroxyketones were observed in the presence and absence of hydrogen, suggesting that metallic Fe acts as a highly active reductant under hydrothermal condition and contributes to the formation of hydroxyketone components in the WS fraction.

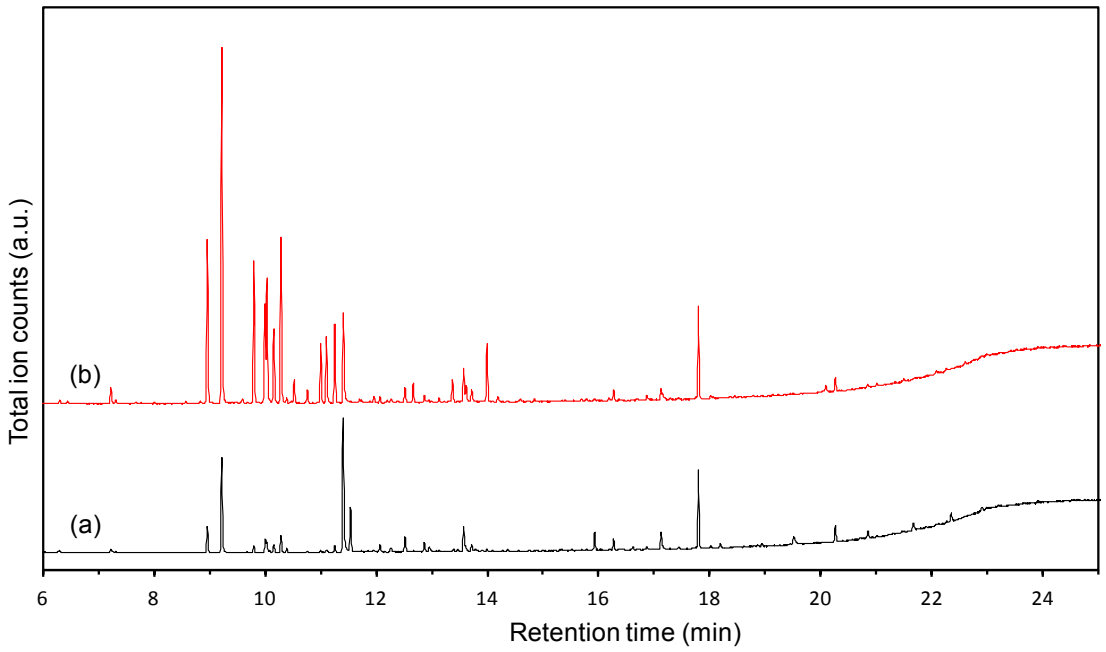

Figure 4. GC/MS spectra of the WS fraction obtained by the liquefaction of EFB at a H_2O/EFB weight ratio of 40:1 in the (a) absence and (b) presence of Fe.

Table 5. GC–MS analysis of the WS fraction obtained at a H_2O/EFB weight ratio = 40:1 both in the presence and absence of Fe

	RT (min)	Compound	Area %		Group[a]
			No Fe	Fe	
1	7.22	Cyclopentanone	0.3	0.8	A-2
2	8.96	3-Hydroxy-2-butanone	3.2	8.1	A-1,2
3	9.22	Hydroxyacetone	11.5	17.6	A-1,2
4	9.59	3-Methyl-2-cyclopentene-1-one	0.0	0.3	A-2
5	9.80	1,2-Butanediol	0.8	6.7	A-1
6	9.99	4-Heptanone	1.7	5.2	A-2
7	10.03	2-Hydroxy-3-pentanone	1.2	6.2	A-1,2
8	10.15	2-Methyl-2-pentene-1-one	1.0	3.9	A-2
9	10.28	1-Hydroxy-2-butanone	2.0	8.2	A-1,2
10	10.38	Tetradecane	0.4	0.2	A
11	10.52	Tetrahydro-6-methyl-2H-pyran-2-one	0.0	1.1	A-4
12	10.76	4-Hydroxy-3-hexanone	0.1	0.6	A-1,2
13	11.00	2-Pentyl methoxyacetate	0.2	2.7	A-4,5
14	11.10	4-Heptanol	0.4	3.2	A-1
15	11.25	1-Hydroxy-2-pentanone	0.8	3.9	A-1,2
16	11.41	Acetic acid	19.3	5.2	A-3
17	11.54	Furfural	5.4	0.0	B-6
18	11.96	5-Hydroxy-4-octanone	0.3	0.3	A-1,2
19	12.06	2,5-Hexanedione	0.8	0.3	A-2
20	12.52	Propanoic acid	2.0	0.8	A-3
21	12.66	Methyl 3-methyl-2-oxopentanoate	0.1	0.9	A-2,4
22	12.87	2-Methylpropanoic acid	1.2	0.3	A-3
23	13.37	2-Hydroxycyclohexanone	0.0	1.1	A-1,2
24	13.58	Ethylene glycol	3.8	1.7	A-1
25	13.62	4-Methyl-4-hexene-3-one	0.0	0.8	A-2
26	13.72	4-Butyrolactone	0.9	0.7	A-4
27	13.99	Di(3-methylbutyl)amine	0.3	2.9	A-7
28	15.93	Cyclooctane	2.2	0.1	A
29	16.28	Guaiacol	1.3	0.5	C-5,8
30	17.13	2-Ethylhexanoic acid	2.3	0.5	A-3
31	17.80	Phenol	9.6	4.5	C-8
32	19.52	2-Hydroxy-4-butyrolactone	1.8	0.0	A-1,4
33	20.26	Syringol	1.9	0.7	C-5,8
34	20.85	4-Oxopentanoic acid	1.0	0.2	A-2,3
35	21.67	3-Pyridinol	1.4	0.0	C-7,8
36	22.36	5-Hydroxymethyl-2-furaldehyde	1.1	0.0	B-1,6
Total			80.2	90.5	

1.3.2.3. Reactivities of degradation products

For examining the degradation characteristics and hydrothermal stability of the degradation products of EFB, possible intermediate compounds were tested under hydrothermal conditions, as summarized in Table 6. When saccharides such as cellulose, xylan, glucose, and xylose were used as substrates, the yield of the WS fraction was improved by the addition of Fe. Dihydroxyacetone and pyruvaldehyde, which are intermediates in the degradation of saccharides,[27] furnished similar results despite the fact that these aldehydes are known to form water-insoluble long chain molecules via aldol condensation under hydrothermal conditions. On the other hand, all substrates formed significant amounts of hydroxyacetone in the presence of Fe. Hydroxyacetone exhibited high hydrothermal stability both in the presence and absence of Fe. Thus, unstable aldehydes generated by the degradation of EFB are apparently converted into stable compounds such as hydroxyketones in the Fe/H_2O system, contributing to the high WS yield.

Based on these results, the positive effects of the H_2O/EFB/Fe system on the steam and hydrothermal liquefaction of EFB were investigated. In this system, Fe_3O_4 and active hydrogen were produced from the reaction between Fe and H_2O in both the steam and hydrothermal systems. Fe_3O_4 catalyzed the retro-aldol reaction of sugars under hydrothermal conditions, while the active hydrogen efficiently converted the highly reactive products into stable compounds. The stable compounds could not undergo successive condensation, cyclization, re-polymerization, and carbonization, thus reducing char formation.

Table 6. Yields of carbon products obtained from the hydrothermal treatment of model substrates in EFB degradation

Substrate	Additive	Product yield (%C)						Carbon balance (%)
		WS			WI	Gas	SR	
		WS	HA[a]	HB[b]				
Cellulose	Fe	93	27	7	2	6	2	103
Cellulose	none	58	2	−	23	7	8	96
Xylan	Fe	80	19	3	4	7	3	94
Xylan	none	64	2	1	18	5	7	94
Glucose	Fe	74	22	3	8	9	4	95
Glucose	none	53	5	3	26	6	10	95
Xylose	Fe	80	20	3	5	8	4	97
Xylose	none	64	2	1	19	5	6	94
Dihydroxyacetone	Fe	72	21	−	18	8	5	103
Dihydroxyacetone	none	41	2	−	31	8	17	97
Pyruvaldehyde	Fe	61	24	−	20	5	4	90
Pyruvaldehyde	none	35	2	−	27	6	17	85
Hydroxyacetone	Fe	96	81	−	−	3	−	99
Hydroxyacetone	none	95	103	−	−	3	−	98

Reaction conditions: Substrate = 1 g, H_2O = 40 g, Fe = 1.564 g, P_{N2} = 1.0 MPa, temperature = 300 °C, and time = 10 min. [a] Hydroxyacetone and [b] 3-hydroxy-2-butanone.

1.3.3. Regeneration and reuse of Fe

Iron oxide can be reduced to metallic iron using biomass char[28] or biomass waste, such as sugar pine sawdust,[29] rice husk,[30] and palm kernel shells.[31] Since biomass wastes are renewable resources and CO_2 neutral, they are not only cost-effective, but also eco-friendly as a reductant source. The author recycled the oxidized Fe by using char and biomass. Figure 5 shows the XRD patterns of the EFB/SR mixture obtained at different temperatures. Signals observed at 30.2°, 35.5°, 37.2°, and 43.1° were attributed to Fe_3O_4 (Joint Committee on Powder Diffraction Standards (JCPDS) file No. 19−629), while a weak signal observed at 44.8° was attributed to α-Fe (JCPDS file No. 6−0696).

By heating the mixture to 800 °C, Fe_3O_4 was transformed into FeO, and at 900 °C, the formation of Fe (43.0°, γ phase (JCPDS file No. 31−619) and 44.2°, α phase) was observed. At 1000 °C, only γ-Fe was present, which transformed into α-Fe upon cooling (C content <0.1 wt%). These results confirmed that iron could be regenerated at 1000 °C in the presence of either EFB or char produced through the liquefaction of EFB as reductant.

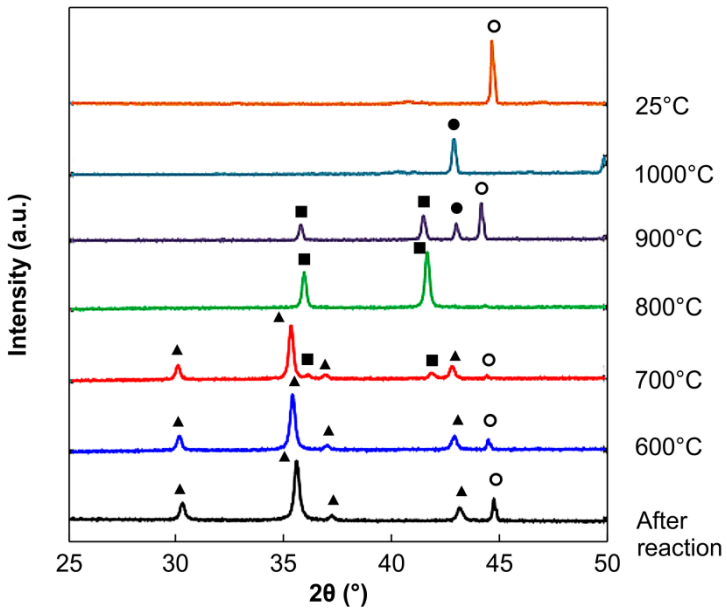

Figure 5. XRD patterns of the EFB/SR mixture containing oxidized Fe and heated at 600–1000 °C. (○) α-Fe, (●) γ-Fe, (▲) Fe_3O_4, and (■) FeO.

For evaluating the reusability of Fe, the SR containing oxidized Fe and char was mixed with EFB and treated under N_2 at 1000 °C for 2 h. The hydrothermal liquefaction of EFB using regenerated Fe was conducted at a H_2O/EFB ratio of 40:1, and Table 7 summarizes the results. Compared to fresh Fe, using the regenerated Fe reduced the yield of bio-oil slightly from 84% to 73%, indicating that Fe is partly deactivated during

regeneration. The increased peak intensities in the XRD patterns (Figure 6(a)) confirmed the presence of comparatively larger metal crystallites after regeneration. By field-emission transmission electron microscopy (FE-TEM), the average particle sizes of the fresh, used, and regenerated samples were 110 nm, 85 nm, and 548 nm, respectively, suggesting that Fe particles agglomerate during regeneration. In the first reuse cycle, the yields of hydroxyacetone and 3-hydroxy-2-butanone decreased (Table 7), but these yields were constant in the second cycle. This result indicated that the amount of generated hydrogen decreases with Fe regeneration. Therefore, it is possible that the decrease in bio-oil yields is attributed to increased char formation, which is due to the reduced amount of hydrogen generated from the reaction between aggregated Fe and H_2O.

Table 7. Reuse of Fe regenerated from the solid residue using EFB at 1000 °C

Fe sample	Carbon yield (%C)					
	WS			WI	Bio-oil	Gas
	WS	HA[a]	HB[b]			
Fresh	69	20	7	15	84	5
Reuse #1	66	14	4	17	83	7
Reuse #2	64	14	5	9	73	8

Reaction conditions: EFB = 1 g, H_2O = 40 g, P_{N2} = 1.0 MPa, temperature = 300 °C, time = 10 min. [a] Hydroxyacetone and [b] 3-hydroxy-2-butanone.

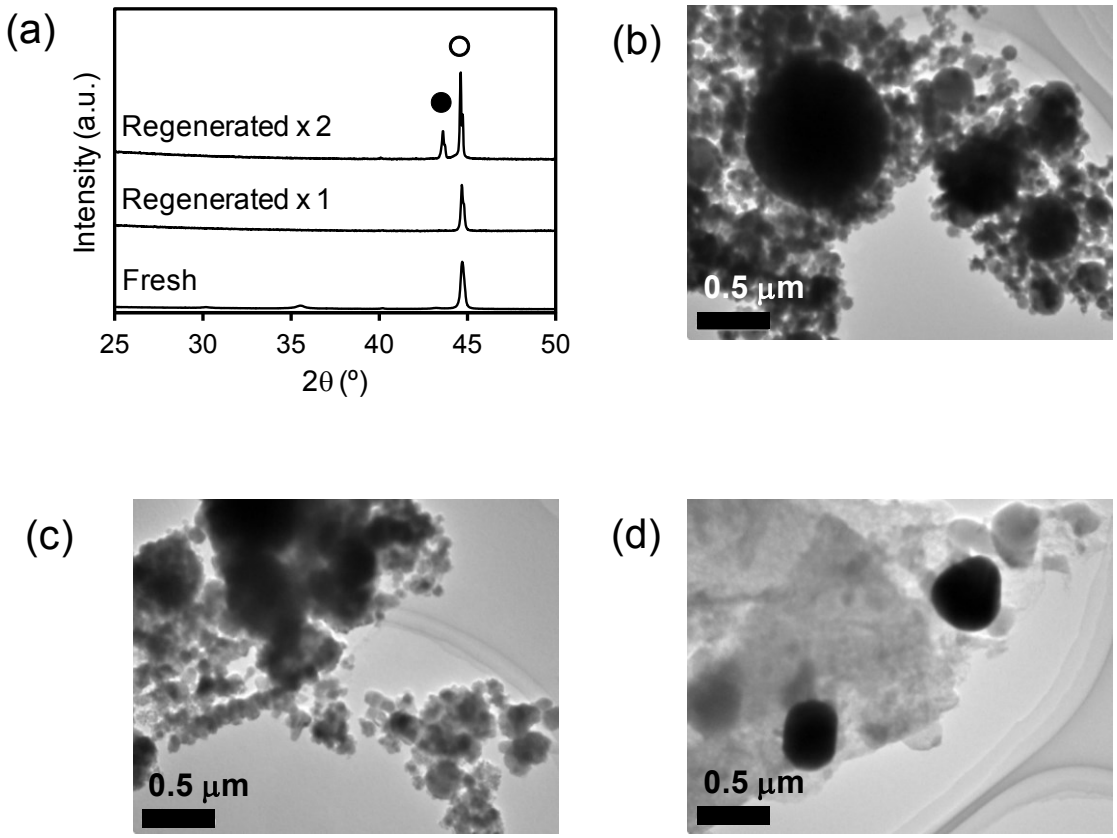

Figure 6. (a) XRD patterns ((○) α-Fe, (●) γ-Fe), and (b–d) FE-TEM images of the fresh, spent, and regenerated Fe samples, respectively.

1.3.4. Catalytic cracking of the WS fraction

The catalytic cracking of biomass pyrolysis vapors or bio-oil using solid acid catalysts could provide valuable hydrocarbons, which are currently obtained from fossil fuels (Table 8).[15, 32-35] Hence, the production of hydrocarbon from the WS fraction (40:1 H_2O/EFB) via catalytic cracking using HZSM-5 was evaluated (Table 9). The main gaseous products were observed in amounts with the following order: C_2–C_4 olefins > CO_2, CO > C_1–C_5 alkanes > BTX. Coke formation was not observed. Importantly, using WS obtained from the Fe-containing system, the yields of C_2–C_4 olefins and BTX were 1.9 times greater than those observed for the Fe-free system, although the formed

amounts of CO_2, CO, and alkanes were comparable. The increase in the C_2–C_4 olefin yield is expected to be attributed to higher quantities of hydroxyketones in the WS fraction. Indeed, Vispute and co-workers have reported that the yields of C_2–C_4 olefins and BTX from the catalytic cracking of water-soluble bio-oil increase after introducing an upgrading step of hydrogenation over Ru/C and Pt/C catalysts.[35]

Table 9 summarizes the results obtained from the catalytic cracking of the WS fraction using regenerated Fe. The total yields of C_2–C_4 olefins and BTX decreased over two reuse cycles. Therefore, the decrease in olefin yields is attributed to the decreased hydrogenated compound formation during the hydrothermal liquefaction of EFB.

Table 8. Yields of light olefins obtained via the catalytic cracking of biomass, biomass pyrolysis vapors, bio-oil, and bio-oil model compounds

Entry	Catalyst (Si/Al ratio)	Feed	Reactor	T (°C)	Feed/Cat. ratio (Feeding rate)	Olefin yield	Ref
1	HZSM-5 (24:1)	WS without Fe (C = 7299 ppm)	Fixed bed	600	1.1 g feed/g cat./h	14%-C	This study
2	HZSM-5 (24:1)	WS with Fe (C = 5584 ppm)	Fixed bed	600	1.1 g feed/g cat./h	27%-C	This study
3	HZSM-5 (24:1)	Tetrahydrofuran (12.5 wt%, C = 78690 ppm)	Fixed bed	600	9.7 g feed/g cat./h	46%-C	This study
4	HZSM-5 (24:1)	Tetrahydrofuran (2.9 wt%, C = 15441 ppm)	Fixed bed	600	1.3 g feed/g cat./h	44%-C	This study
5	HZSM-5 (24:1)	Tetrahydrofuran (12.5 wt%)	Fixed bed	600	11.7 g feed/g cat./h	51%-C	[35]
6	HZSM-5 (30:1)	WSBO[a] (12.5 wt%)	Fixed bed	600	11.7 g feed/g cat./h	19%-C	[35]
7	HZSM-5 (30:1)	WSBO[a] hydrogenation over Ru/C	Fixed bed	600	11.7 g feed/g cat./h	33%-C	[35]
8	HZSM-5 (30:1)	WSBO[a] hydrogenation over Ru/C and Pt/C	Fixed bed	600	11.7 g feed/g cat./h	51%-C	[35]
9	HZSM-5 (30:1)	40 wt% pine sawdust bio-oil, 60 wt% methanol	Fluidized bed	500	2.7 g feed/g cat./h	22 wt%	[36]
12	ZSM-5	Pine wood	Fluidized bed	600	0.35 g feed/g cat./h	9%	[37]
13	LOSA-1 and 10% Al_2O_3	Rice stalk	Fluidized bed	550	44 g/h	11%	[38]
14	ZSM-5	Rice stalk	Fluidized bed	550	44 g/h	11%	[39]

[a]WSBO = Water-soluble fraction of pinewood bio-oil.

Table 9. Yields of carbon products obtained from the catalytic cracking of the WS fraction

Production system of WS fraction	Carbon yield (%C)												Carbon balance (%)
	Olefins				Alkanes			BTX	CO_x			Water solubles	
	C_2	C_3	C_4	Sum	C_1	C_{2-5}	Sum		CO	CO_2	Sum		
H_2O/EFB	6	7	1	14	3	1	4	1	10	8	18	27	64
H_2O/EFB/Fe (fresh)	13	13	1	27	3	1	4	2	11	5	16	27	76
H_2O/EFB/Fe (reuse #1)	11	10	2	23	5	–	5	2	9	7	16	33	79
H_2O/EFB/Fe (reuse #2)	9	11	2	22	3	3	6	3	8	6	14	32	77

1.4. Conclusion

As demonstrated by the experimental results discussed above, zero-valent Fe was successfully used for the hydrothermal liquefaction of EFB to produce bio-oil. This method, in which the hydrogen produced in the reaction was consumed to stabilize the degradation products of EFB, was more successful than the conventional H_2O/EFB approach. In addition, the used Fe was regenerated by heating it with SR and EFB at 1000 °C, although slightly lower product yields were obtained using the regenerated Fe. The H_2O/EFB/Fe system was demonstrated to be suitable for the liquefaction of EFB to produce bio-oil, and it allows the control of the selectivity of the WS and WI components by varying the H_2O content. In addition, C_2–C_4 olefins were produced in good yields via the catalytic cracking of the WS fraction using the HZSM-5 zeolite catalyst. Nevertheless, additional studies must be conducted to further develop this system to transform biomass into valuable resources. Potential areas of study include: the identification of the most efficient iron species for hydrogen generation, improvement of the hydrogen utilization efficiency, regeneration method for the oxidized Fe, and possible extension of this system to other biomass resources (e.g. other lignocellulosic biomass, algae, food waste, and sewage sludge). The author believes that the Fe/H_2O system developed herein can pave the route toward better utilization of biomass resources.

1.5. References

1. Ragauskas, A. J.; Williams, C. K.; Davison, B. H.; Britovsek, G.; Cairney, J.; Eckert, C. A.; Frederick, W. J.; Hallett, J. P.; Leak, D. J.; Liotta, C. L.; Mielenz, J. R.; Murphy, R.; Templer, R.; Tschaplinski, T., The Path Forward for Biofuels

and Biomaterials. *Science* **2006,** *311* (5760), 484–489.

2. Huber, G. W.; Iborra, S.; Corma, A., Synthesis of Transportation Fuels from Biomass: Chemistry, Catalysts, and Engineering. *Chem. Rev.* **2006,** *106* (9), 4044–4098.

3. Corma, A.; Iborra, S.; Velty, A., Chemical Routes for the Transformation of Biomass into Chemicals. *Chem. Rev.* **2007,** *107* (6), 2411–2502.

4. Swain, P. K.; Das, L. M.; Naik, S. N., Biomass to Liquid: A Prospective Challenge to Research and Development in 21st Century. *Renew. Sust. Energy Rev.* **2011,** *15* (9), 4917–4933.

5. Kan, T.; Strezov, V.; Evans, T. J., Lignocellulosic Biomass Pyrolysis: A Review of Product Properties and Effects of Pyrolysis Parameters. *Renew. Sust. Energy Rev.* **2016,** *57*, 1126–1140.

6. Collard, F.-X.; Blin, J., A Review on Pyrolysis of Biomass Constituents: Mechanisms and Composition of the Products Obtained from the Conversion of Cellulose, Hemicelluloses and Lignin. *Renew. Sust. Energy Rev.* **2014,** *38*, 594–608.

7. Tekin, K.; Karagöz, S.; Bektaş, S., A Review of Hydrothermal Biomass Processing. *Renew. Sust. Energy Rev.* **2014,** *40*, 673–687.

8. Akhtar, J.; Amin, N. A. S., A Review on Process Conditions for Optimum Bio-Oil Yield in Hydrothermal Liquefaction of Biomass. *Renew. Sust. Energy Rev.* **2011,** *15* (3), 1615–1624.

9. Arturi, K. R.; Kucheryavskiy, S.; Søgaard, E. G., Performance of Hydrothermal Liquefaction (HTL) of Biomass by Multivariate Data Analysis. *Fuel Process. Technol.* **2016,** *150*, 94–103.

10. Bi, Z.; Zhang, J.; Peterson, E.; Zhu, Z.; Xia, C.; Liang, Y.; Wiltowski, T., Biocrude from Pretreated Sorghum Bagasse through Catalytic Hydrothermal Liquefaction. *Fuel* **2017,** *188*, 112–120.

11. Nazari, L.; Yuan, Z.; Souzanchi, S.; Ray, M. B.; Xu, C., Hydrothermal Liquefaction of Woody Biomass in Hot-Compressed Water: Catalyst Screening and Comprehensive Characterization of Bio-Crude Oils. *Fuel* **2015,** *162*, 74–83.

12. Li, H.; Yuan, X.; Zeng, G.; Tong, J.; Yan, Y.; Cao, H.; Wang, L.; Cheng, M.; Zhang, J.; Yang, D., Liquefaction of Rice Straw in Sub- and Supercritical 1,4-Dioxane–Water Mixture. *Fuel Process. Technol.* **2009,** *90* (5), 657–663.

13. Zacher, A. H.; Olarte, M. V.; Santosa, D. M.; Elliott, D. C.; Jones, S. B., A Review and Perspective of Recent Bio-Oil Hydrotreating Research. *Green Chem.* **2014,** *16* (2), 491–515.

14. Patil, P. T.; Armbruster, U.; Martin, A., Hydrothermal Liquefaction of Wheat Straw in Hot Compressed Water and Subcritical Water–Alcohol Mixtures. *J. Supercrit. Fluids* **2014,** *93*, 121–129.

15. Vispute, T. P.; Zhang, H. Y.; Sanna, A.; Xiao, R.; Huber, G. W., Renewable Chemical Commodity Feedstocks from Integrated Catalytic Processing of Pyrolysis Oils. *Science* **2010,** *330* (6008), 1222–1227.

16. Heo, E.; Kim, J.; Cho, S., Selecting Hydrogen Production Methods Using Fuzzy Analytic Hierarchy Process with Opportunities, Costs, and Risks. *Int. J. Hydrogen Energy* **2012,** *37* (23), 17655–17662.

17. Huisman, G. H.; Van Rens, G. L. M. A.; De Lathouder, H.; Cornelissen, R. L., Cost Estimation of Biomass-to-Fuel Plants Producing Methanol, Dimethylether or Hydrogen. *Biomass Bioenergy* **2011,** *35*, S155–S166.

18. Kamarudin, S. K.; Daud, W. R. W.; Yaakub, Z.; Misron, Z.; Anuar, W.; Yusuf, N. N. A. N., Synthesis and Optimization of Future Hydrogen Energy Infrastructure Planning in Peninsular Malaysia. *Int. J. Hydrogen Energy* **2009,** *34* (5), 2077–2088.

19. Mueller-Langer, F.; Tzimas, E.; Kaltschmitt, M.; Peteves, S., Techno-Economic Assessment of Hydrogen Production Processes for the Hydrogen Economy for the Short and Medium Term. *Int. J. Hydrogen Energy* **2007,** *32* (16), 3797–3810.

20. Olateju, B.; Kumar, A., Hydrogen Production from Wind Energy in Western Canada for Upgrading Bitumen from Oil Sands. *Energy* **2011,** *36* (11), 6326–6339.

21. Shibata, M.; Varman, M.; Tono, Y.; Miyafuji, H.; Saka, S., Characterization in Chemical Composition of the Oil Palm (*Elaeis Guineensis*). *J. Jpn. Inst. Energy* **2008,** *87* (5), 383–388.

22. Sun, P.; Heng, M.; Sun, S.-H.; Chen, J., Analysis of Liquid and Solid Products from Liquefaction of Paulownia in Hot-Compressed Water. *Energy Convers. Manage.* **2011,** *52* (2), 924–933.

23. Mullen, C. A.; Strahan, G. D.; Boateng, A. A., Characterization of Various Fast-Pyrolysis Bio-Oils by NMR Spectroscopy. *Energy Fuels* **2009,** *23* (5), 2707–2718.

24. Kawamoto, H.; Hatanaka, W.; Saka, S., Thermochemical Conversion of Cellulose in Polar Solvent (Sulfolane) into Levoglucosan and Other Low Molecular-Weight Substances. *J. Anal. Appl. Pyrolysis* **2003,** *70* (2), 303–313.

25. Singh, R.; Balagurumurthy, B.; Prakash, A.; Bhaskar, T., Catalytic Hydrothermal Liquefaction of Water Hyacinth. *Bioresour. Technol.* **2015,** *178*, 157–165.

26. Hirano, Y.; Kasai, Y.; Sagata, K.; Kita, Y., Unique Approach for Transforming Glucose to C3 Platform Chemicals Using Metallic Iron and a Pd/C Catalyst in Water. *Bull. Chem. Soc. Jpn.* **2016,** *89* (9), 1026–1033.

27. Kabyemela, B. M.; Adschiri, T.; Malaluan, R. M.; Arai, K., Glucose and Fructose Decomposition in Subcritical and Supercritical Water: Detailed Reaction Pathway, Mechanisms, and Kinetics. *Ind. Eng. Chem. Res.* **1999,** *38*, 2888–2895.

28. Tang, H.; Qi, T.; Qin, Y., Production of Low-Phosphorus Molten Iron from High-Phosphorus Oolitic Hematite Using Biomass Char. *JOM* **2015,** *67* (9), 1956–1965.

29. Strezov, V., Iron Ore Reduction Using Sawdust: Experimental Analysis and Kinetic Modelling. *Renew. Energy* **2006,** *31* (12), 1892–1905.

30. Purwanto, H.; Selamat, N. F. M.; Anto, P. b.; Akiyama, T., Pre-Reduced Iron Produced from Low Grade Ore Using Biomass. *SEAISI Q. J.* **2010,** *39* (2), 18–22.

31. Rashid, R. Z. A.; Salleh, H. M.; Ani, M. H.; Yunus, N. A.; Akiyama, T.; Purwanto, H., Reduction of Low Grade Iron Ore Pellet Using Palm Kernel Shell. *Renew. Energy* **2014,** *63*, 617–623.

32. Chen, N. Y.; Degnan, T. F.; Koenig, L. R., Liquid Fuel from Carbohydrates. *CHEMTECH* **1986,** *16* (8), 506–511.

33. Adjaye, J. D.; Bakhshi, N. N., Production of Hydrocarbons by Catalytic Upgrading of a Fast Pyrolysis Bio-Oil. Part I: Conversion over Various Catalysts. *Fuel Process. Technol.* **1995,** *45* (3), 161–183.

34. Rezaei, P. S.; Shafaghat, H.; Daud, W. M. A. W., Production of Green Aromatics

and Olefins by Catalytic Cracking of Oxygenate Compounds Derived from Biomass Pyrolysis: A Review. *Appl. Catal., A* **2014,** *469*, 490–511.

35. Zhang, H.; Cheng, Y.-T.; Vispute, T. P.; Xiao, R.; Huber, G. W., Catalytic Conversion of Biomass-Derived Feedstocks into Olefins and Aromatics with ZSM-5: The Hydrogen to Carbon Effective Ratio. *Energy Environ. Sci.* **2011,** *4* (6), 2297–2307.

36. Valle, B.; Gayubo, A. G.; Alonso, A.; Aguayo, A. T.; Bilbao, J., Hydrothermally Stable HZSM-5 Zeolite Catalysts for the Transformation of Crude Bio-Oil into Hydrocarbons. *Appl. Catal., B* **2010,** *100* (1), 318–327.

37. Zhang, H.; Carlson, T. R.; Xiao, R.; Huber, G. W., Catalytic Fast Pyrolysis of Wood and Alcohol Mixtures in a Fluidized Bed Reactor. *Green Chem.* **2012,** *14* (1), 98–110.

38. Zhang, H.; Xiao, R.; Jin, B.; Xiao, G.; Chen, R., Biomass Catalytic Pyrolysis to Produce Olefins and Aromatics with a Physically Mixed Catalyst. *Bioresour. Technol.* **2013,** *140*, 256–262.

39. Zhang, H.; Xiao, R.; Jin, B.; Shen, D.; Chen, R.; Xiao, G., Catalytic Fast Pyrolysis of Straw Biomass in an Internally Interconnected Fluidized Bed to Produce Aromatics and Olefins: Effect of Different Catalysts. *Bioresour. Technol.* **2013,** *137*, 82–87.

Chapter 2. Quantitative analysis of the aqueous fraction from the Fe-assisted hydrothermal liquefaction of oil palm empty fruit bunches

2.1. Introduction

The effective utilization of biomass resources, such as agricultural residues, algae, and sewage sludge, is an urgent and important issue that will help society prepare for the depletion of fossil-based resources in the future. Fast pyrolysis and hydrothermal liquefaction reactions have been extensively studied as methods for the liquefaction of biomass resources and their subsequent use as fuels and chemical feedstocks.[1-2] The hydrothermal liquefaction reaction is a promising method for the liquefaction of biomass, and operates at moderate temperatures (280–370 °C) and high pressures (10–25 MPa).[3-6] During this process, ubiquitous water is used as the solvent, which is advantageous since wet biomass can be used without any pre-drying. The product of the hydrothermal liquefaction reaction is separated into four fractions, namely water-soluble (WS) and water-insoluble (WI) fractions, as well as solid residues (SRs), and gases (Figure 1).[7] Increasing the levels of the WS and WI fractions, which can be used as fuels and chemical feedstocks, is important in order to improve biomass-utilization efficiency. Until now, the WI fractions (biocrudes) have largely been regarded as useful resources and the focus of analytical research has almost exclusively been directed toward these fractions; however, the use of the WS fraction also needs to be considered as a possible strategy in this regard.[8-13]

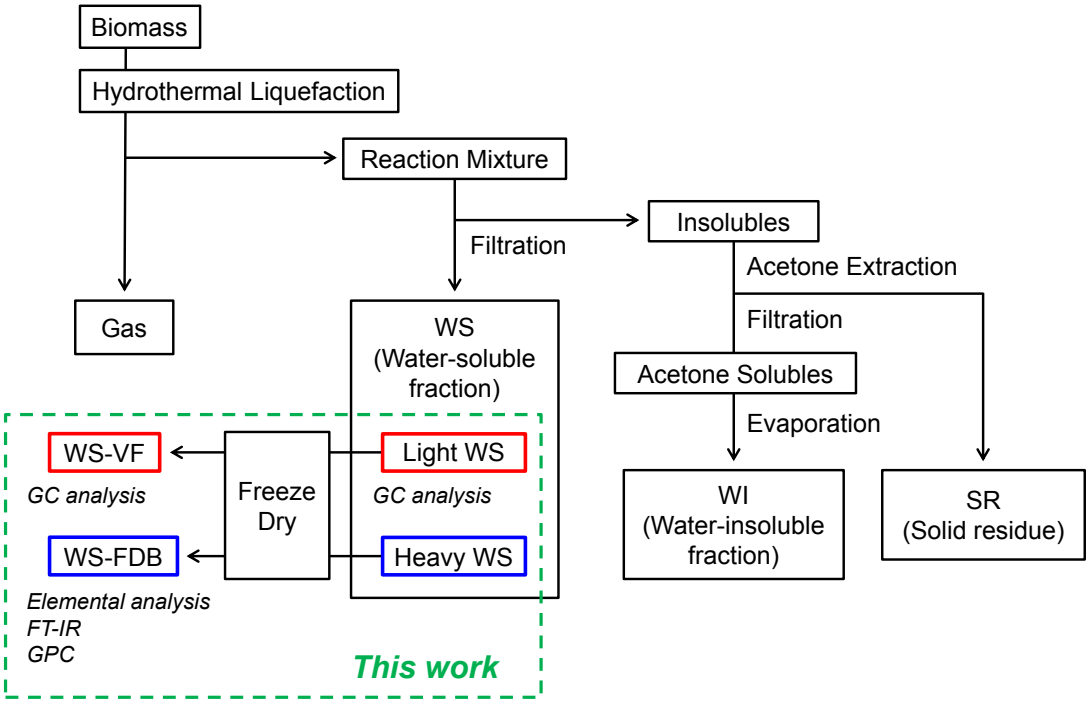

Figure 1. Products from the hydrothermal liquefaction of biomass and an overview of analysis strategy.

As described in chapter 1, the author demonstrated the hydrothermal liquefaction of palm empty fruit bunches (EFBs) and showed that the use of Fe-metal powder, as an additive, considerably increased the yield of the WS fraction. In addition, catalytic cracking of the WS fraction over a solid acid catalyst (HZSM-5 zeolite) afforded hydrocarbons, such as olefinic and aromatic compounds, that can be used as basic chemical raw materials. During the cracking reaction, the WS fraction obtained from the Fe-assisted hydrothermal system contained higher levels of hydrocarbon products than that obtained from a conventional hydrothermal system, revealing that Fe not only accelerates decomposition, but also affords more upgraded products. Preliminary analysis of the WS fraction revealed that the product composition had changed significantly following addition of Fe. However, further analysis of the WS fraction was

difficult due to its complex composition; consequently, only a qualitative discussion on the effect of Fe was provided. In order to clarify the role of Fe, optimize the hydrothermal decomposition process, and develop methods that use the WS fraction, a rapid and accurate method for the evaluation of the WS fraction is a key technological objective.

Reports on the analysis of the aqueous fractions from the hydrothermal liquefaction of biomass have been published; however, quantitative analyses are limited to only a few cases.[14-18] As analytical methods, gas chromatography–mass spectrometry (GC–MS) and gas chromatography–flame ionization detection (GC–FID) are often used; these methods are powerful because they can rapidly analyze multicomponent mixtures. For quantitative analysis by GC, the preparation of calibration curves using authentic samples is necessary. The analysis of complex mixtures, such as those from the thermochemical decomposition of biomass, is labor-intensive and costly. In particular, when no standard reagents are on hand, and when they cannot be easily purchased, it becomes necessary to synthesize authentic samples, which is not a realistic approach for trace amounts of product.

Even when standards are not available, relative response factors (RRFs) of analytes for FID analysis can be estimated from the chemical structures of the analytes; consequently, calibration curves can still be prepared. Sternberg and co-workers proposed a method for predicting the RRF of a compound bearing heteroatoms by introducing the concept of effective carbon number (ECN).[19] They showed that the effect of heteroatoms on the ECN of a molecule depended on the nature of the functional groups and empirically quantified the contribution of each functional group to the ECN. A number of studies on predicting RRF have been reported,[20-23] and the

predicted RRFs have been shown to be useful for the analysis of scent [24] and taste,[25] and in other areas.[26] Biomass-derived components produced by thermochemical conversion were also analyzed using predicted RRFs.[27-30] For example, Undri and co-workers successfully quantified the composition of the biocrude obtained by rapid pyrolysis using an independently developed RRF prediction method.[31]

In this study, the author developed a modified technique for predicting ECN based on the above-mentioned method, quantitatively analyzed the crude WS fraction from the hydrothermal liquefaction of biomass, and clarified the composition of the volatile components. In addition, the author introduces a freeze-drying method[32-33] and succeeded in isolating non-volatile WS components that cannot be detected by GC. The compositions and properties of the isolated heavy components were determined by elemental analysis, Fourier-transform infrared spectroscopy (FT-IR) and gel-permeation chromatography (GPC). Combining these methods has enabled the comprehensive analysis of the WS fraction and a detailed discussion of the effect of the Fe additive. In addition, by examining the cracking characteristics of the volatile and heavy components of the WS fraction, guidelines for the optimization of the hydrothermal liquefaction process are proposed.

2.2. Materials and Methods

2.2.1. Materials

Oil palm empty fruit bunches (EFBs) from Indonesia were supplied by the Nippon Shokubai Co., Ltd. (Japan), and were used as the lignocellulosic-biomass feedstock. The EFBs were dried at 25 °C and crushed into particles less than 300 μm in size. Fe powder (99.9%, NM-0029-UP) was purchased from Ionic Liquids Technologies

GmbH (Germany). HZSM-5 zeolite with a Si/Al ratio of 24:1 was supplied by the Nippon Shokubai Co., Ltd. (Japan). Internal standards and authentic samples for GC analyses were obtained commercially. 2-Methoxyethanol, cyclopentanone, 1-hydroxy-2-propanone, propanol, acetic acid, propanoic acid, cyclopentanol, cyclohexanol, propyleneglycol, 1,2-ethanediol, 1,2-butanediol, 1,4-butanediol, 1,2-pentanediol, 1,2-hexanediol, 1,2-cyclohexanediol, 4-oxopentanoic acid, furfural, phenol, methyl *p*-hydroxybenzoate, cinnamaldehyde, and 3-phenyl-2-propen-1-ol from purchased from Wako Pure Chemical Industries, Ltd., while cyclohexanone, 3-hydroxy-2-butanone, methyl DL-2-hydroxy-3-butenoate, 2-butanone, 2,3-butanediol, *tert*-butyl alcohol, *tert*-amyl alcohol, 5-hydroxymethyl-2-furaldehyde, guaiacol, syringol, syringaldehyde, and vanillin were purchased from Tokyo Chemical Industry Co., Ltd.

2.2.2. Preparation of the WS fraction

EFB liquefaction and separation experiments were conducted following the method described in chapter 1. Briefly, EFB (4.0 g), Fe powder (0 or 6.256 g), and H_2O (40 g) were introduced into a Hastelloy C high-pressure reactor, which was purged four times with nitrogen. The initial pressure was set to 1.0 MPa with nitrogen, and the stirring rate was adjusted to 700 rpm. The reactor was then heated to 300 °C and maintained at this temperature for 10 min. The reactor was then rapidly cooled to 25 °C using ice-water. The reaction mixture was filtered and the filtrate was collected as the WS fraction. The total organic carbon (TOC) content of the WS fraction was determined using a total organic carbon analyzer (Shimadzu, TOC-LCSH/CSN). The pH of the WS fraction was measured with a LAQUAtwin B-711 pH analyzer (HORIBA). Sample

information is summarized in Table 1. Each reaction was carried out in quadruplicate and product yields were calculated as averages.

Table 1. Results of Fe-assisted and conventional hydrothermal liquefaction of EFB.[a]

Reaction system	Carbon yield (%C)					pH of the
	Gas	WS	WI	SR	total	WS fraction
Fe-assisted	4%	56%	23%	10%	93%	4.5
Conventional	7%	33%	38%	17%	95%	3.4

[a] Reaction conditions: EFB = 4 g, H_2O = 40 g, Fe = 6.256 g or 0 g, initial pressure = 1.0 MPa (N_2), temperature = 300°C, time = 10 min. Yields were calculated based on the carbon content of raw EFB.

2.2.3. Gas Chromatographic analysis of the WS fraction

The WS fraction sample was diluted with acetone (1:1 v/v) and 2-methoxyethanol (0.05 wt%) was added as an internal standard. Samples were analyzed by gas chromatography–mass spectrometry (GC–MS) on a Shimadzu QP-2010 system equipped with a capillary column (GL Sciences, Inert-cap® WAX-HT, 30 m × 0.25 mm ID × 0.25 μm film thickness), and gas chromatography (Shimadzu, GC-2014) using the same capillary column described above, but equipped with a flame ionization detector (GC–FID). The split ratio was set to 1:50 and the injection volume was 1.0 μL. The oven was operated at 50 °C for 3 min, then heated at 10 °C/min to 260 °C, and maintained at this temperature for 16 min; the total run time was 30 min. All compounds were identified by comparing their mass spectra with those from the National Institute of Standards and Technology (NIST) library of mass spectral data. When authentic samples were available, product retention times were confirmed to

coincide with those of the authentic samples.

2.2.4. Quantitative GC–FID method

Quantitative calculations based on the GC–FID data were carried out using relative response factors (RRFs). The RRF is defined by eq. 1:[34]

$$\mathrm{RRF} = \frac{A_i \times C_{IS}}{C_i \times A_{IS}} \quad (1)$$

where "*C*" is the concentration, "*A*" is the peak area, and the subscripts "*i*" and "*IS*" refer to the analyte and internal standard, respectively.

The concentration of the analyte can be calculated from eq. 2:

$$C_i = C_{IS} \times \frac{A_i}{A_{IS}} \times \frac{1}{\mathrm{RRF}} \quad (2)$$

where the RRF was obtained by eq. 1 for compounds that are available as authentic sample; quantitative analysis is then carried out according to eq. 2.

On the other hand, the relationship between RRF and the effective carbon number (ECN) is given by eq. 3:[23]

$$\mathrm{RRF} = \frac{\mathrm{ECN_i} \times \mathrm{MW_{IS}}}{\mathrm{MW_i} \times \mathrm{ECN_{IS}}} \quad (3)$$

From eqs. 2 and 3, the concentration of an analyte (C_i) can be calculated if the ECN of each compound in the analytical sample can be determined. Based on Sternberg's concept, the ECN can be determined using the following equation:[35]

$$\mathrm{ECN} = \sum_k (\mathrm{N}_k \times \mathrm{Cnt}_k) \quad (4)$$

where "N" is the number of atoms or functional groups in the compound and "Cnt" is the ECN contribution coefficient, which is an empirical factor. Cnt values have been summarized by Sternberg and co-workers; however, there are differences between the calculated and measured RRF values since response depends subtly on equipment and

conditions. In order to correct for this difference, authentic samples were selected and mixtures of known concentrations of authentic samples and internal standards were analyzed. Cnt values were recursively optimized to give the best correlation between predicted and measured RRF values.

2.2.5. Freeze-dry separation of the WS fraction and subsequent analysis

The freeze-drying apparatus was assembled using a round-bottom flask, glass adapters, a vacuum trap, manometer, and vacuum pump (Figure 2). The crude WS fraction sample (10 mL) was placed in the round-bottom flask, after which it was rapidly frozen by immersing the flask in liquid nitrogen. The frozen samples were immediately connected to the apparatus and maintained under vacuum (< 0.2 kPa) for 5 h. Sublimated water and volatile compounds were collected in a cold trap cooled by liquid nitrogen.

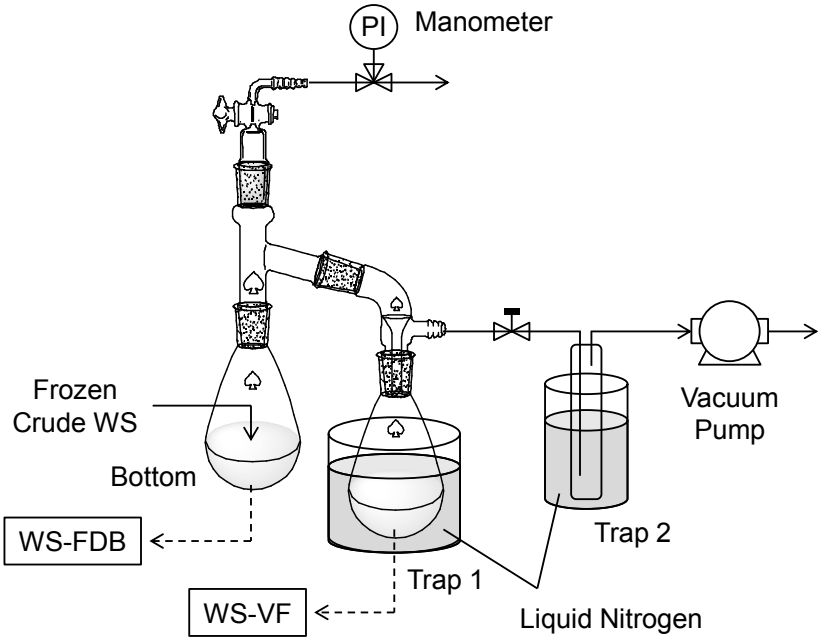

Figure 2. Schematic layout of the freeze-drying apparatus.

The moisture content of the residue in the flask was determined using a Karl Fischer moisture titrator (MKV-710, Kyoto Electronics Manufacturing Co., Ltd.); AQUAMICRON® Titrant SS 3mg and AQUAMICRON® Solvent CP (Mitsubishi Chemical Corporation) were used for titration. Elemental analysis (CHN) of the freeze-dried WS-fraction sample was performed using an elemental analyzer (Elementar Vario EL cube) and sulfanilamide as the calibration standard. The oxygen mass content was calculated by difference. The FT-IR spectrum (KBr smear) of the freeze-dried WS-fraction sample was acquired on a Thermo Nicolet NEXUS 670 Fourier-transform infrared spectrometer operating in transmission mode between 4000 and 400 cm^{-1}. The sample was dried under vacuum to remove water. Gel-permeation chromatography (GPC) of the dried WS-fraction samples was performed using a TOSOH HLC-8320GPC GPC system equipped with a refractive index detector and fitted with a series of four TOSOH TSKgel SuperH2000 columns (3 μm, 150 mm × 6 mm ID). Before analysis, the sample was dissolved in tetrahydrofuran (THF) and filtered through a 0.45 μm syringe filter. Chromatograms were recorded at 40 °C over 30 min using THF as the eluent at a rate of 0.6 mL/min. Polyethylene glycol was used as the molecular-weight calibration standard.

2.2.6. Catalytic cracking of the WS fraction and subsequent analysis

Catalytic cracking of the WS fraction was performed using a fixed-bed continuous flow reactor composed of a stainless-steel tube reactor, gas-feeding system, liquid-feeding pump, heating system, gas wash bottle filled with ice-cold water, and a gas sampling system (see chapter 1). HZSM-5 zeolite (3.3 g, spherical, with particle diameters of 0.85–1.7 mm) was added to the reactor, followed by the addition of

stainless-steel beads for liquid-feedstock vaporization. The catalyst was flushed with nitrogen (50 mL/min) for 1 h at 25 °C, followed by heating to 600 °C under nitrogen (50 mL/min). The WS fraction was fed into the reactor using a plunger pump at a weight hourly space velocity (WHSV) of 1.1 h^{-1}. During the reaction, the condensed products were collected using a gas wash bottle with either water or acetonitrile. All gaseous products were collected in a gas-sampling bottle. Gaseous products were analyzed using two gas chromatography systems: a Shimadzu GC-8A chromatograph equipped with silica-gel (Shinwa Chemical Industries, ZS-74) and 5A-molecular-sieve (Shinwa Chemical Industries, ZM-1) columns, and a thermal conductivity detector for CO_2 and CO, and a Shimadzu GC-2014 instrument equipped with a Sunpak-A column (Shinwa Chemical Industries, ZS-72) and a flame ionization detector for hydrocarbons.

2.2.7. Product yield

The yields from hydrothermal liquefaction and catalytic cracking were calculated as follows:

$$\text{Yield of each fraction from hydrothermal liquefaction (\%)} = \frac{\text{Moles of carbon in the product}}{\text{Moles of carbon in the raw material}} \times 100 \qquad (5)$$

and

$$\text{Yield of each product from catalytic cracking (\%)} = \frac{\text{Moles of carbon in the product}}{\text{Moles of carbon in the WS-feed fraction}} \times 100 \qquad (6)$$

2.3. Results and Discussion

2.3.1. GC analysis of the WS fraction

2.3.1.1. Predicting the RRF

As discussed in chapter 1, the WS fraction produced by hydrothermal liquefaction contained functionalized aliphatic compounds such as alcohols, ketones, and carboxylic acids, among others. In order to determine the influence of the functional groups borne by these compounds on the ECN, 14 parameters (three elements (C, H, O) and 11 functional groups) were used in eq. 4. To optimize the Cnt value, 32 authentic samples were selected; these samples were either present in the WS fraction or had similar compositions to those present. The RRFs of the authentic samples (RRF_{found}) were calculated using eq. 1 and experimental data. Cnt values were optimized recursively so that the RRF values calculated from eqs. 3 and 4 (RRF_{calc}) were close to the values of RRF_{found}. The data were optimized using the "solver" plug-in of Excel® (Microsoft Corp.).[31] Cnt, RRF_{found}, and RRF_{calc} values are summarized in Table 2. Figure 3 reveals a good linear relationship between RRF_{calc} and RRF_{found}, with a correlation coefficient (R^2) of 0.9859. Even when no authentic sample is available and a calibration curve cannot be created, it is now possible to calculate the RRF of a compound from its chemical structure in order to perform quantitative analyses.

Table 2. Optimized Cnt and RRF values of authentic samples.

Functional group	Cnt
C	1
H	-0.075
O	0.226
C(alkyl)	0.037
C(olefin)	-0.208
C(aromatic)	-0.01
C=O(ketone)	-1.389
C=O(aldehyde)	-0.753
C=O(acid)	-1.417
O(ether)	-0.906
OH(1°)	-0.651
OH(2°)	-0.754
OH(3°)	0.567
OH(Aryl)	-0.857

Authentic samples	RRF_{calc}	RRF_{found}
Cyclopentanone	2.18	2.26
3-Hydroxy-2-butanone	1.12	1.19
1-hydroxy-2-Propanone	0.76	0.63
Acetic acid	0.7	0.73
Propanoic acid	1.21	1.23
Propyleneglycol	1.11	1.18
1,2-Ethanediol	0.68	0.79
1,2-Butanediol	1.47	1.52
4-Oxopentanoic acid	1.11	1.12
5-hydroxymethyl-2-furaldehyde	1.34	1.34
Phenol	2.8	2.7
Guaiacol	2.21	2.23
Cyclohexanone	2.35	2.4
Propanol	1.88	1.89
Cyclopentanol	2.45	2.31
Cyclohexanol	2.59	2.49
Furfural	1.5	1.53
2-Butanone	1.76	1.9
1,2-Pentanediol	1.73	1.59
1,2-Hexanediol	1.93	1.93
1,2-Cyclohexanediol	1.99	2.09
2,3-Butanediol	1.41	1.43
1,4-Butanediol	1.53	1.63
Syringol	1.85	1.98
Methyl DL-2-Hydroxy-3-butenoate	1.2	1.12
Methyl p-Hydroxybenzoate	2.06	2.01
Cinnamaldehyde	3.03	2.96
Syringaldehyde	1.71	1.74
3-Phenyl-2-propen-1-ol	2.97	3.04
Vanillin	1.97	1.98
tert-Butyl alcohol	2.34	2.32
tert-Amyl alcohol	2.36	2.38

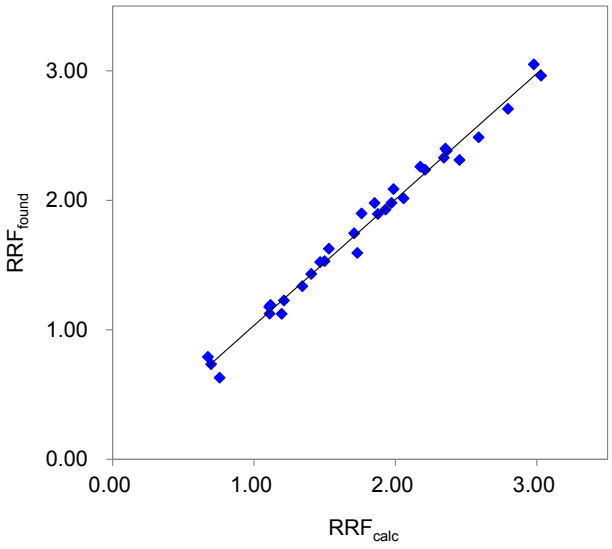

Figure 3. Comparison between RRF_{found} and optimized RRF_{calc} for authentic samples.

2.3.1.2. Quantitative GC analysis of the WS fraction

The crude WS fractions obtained by the hydrothermal liquefaction of the EFB in the presence and absence of Fe were analyzed by GC–MS. Compounds were identified from their MS fragmentation patterns by comparisons with spectra in the NIST database. The light WS components were quantified using the RRF_{found} and RRF_{calc} values, the results of which are summarized in Table 3. Furthermore, the carbon yields (eq. 5) were grouped according to compound classification, as showed in Figure 4.

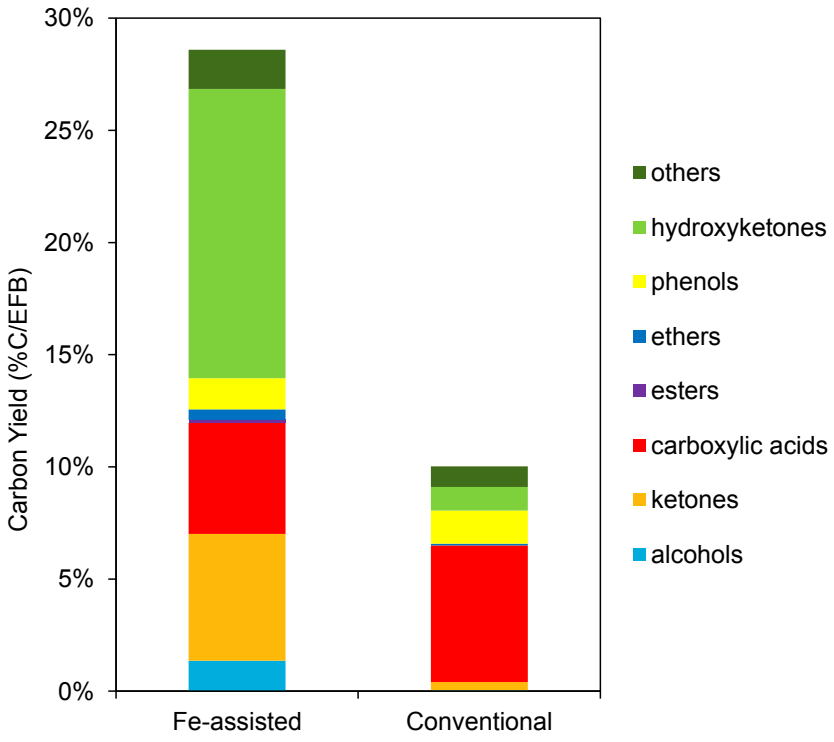

Figure 4. Distributions of compounds in the light WS components.

As shown in chapter 1, hydroxyketones, such as hydroxyacetone or 3-hydroxy-2-butanone were detected as characteristic compounds in Fe-assisted hydrothermal liquefaction reactions. The yield of hydroxyketones in the Fe-assisted WS

fraction was quantified to be 12.9%, which represents half of the total yield of identified compounds. The yields of simple alcohols and ketones were determined to be 1.4% and 5.7% respectively. With the exception of acetic acid, carboxylic acids were hardly detected; their acidities are frequently problematic properties of thermal decomposition products. This result is consistent with the observation that the Fe-assisted WS fraction exhibited relatively mild acidity (Table 1). The total yield of identified products was 28.6%, which is half of the crude WS fraction yield.

On the other hand, fewer product peaks were detected in the WS fraction produced by conventional hydrothermal decomposition compared to those from the Fe-assisted process; the total product yield was determined to be 10.0%, which represents one third of the total WS fraction yield. The low proportion of GC-quantifiable components in the crude WS fraction indicates that this fraction has overall low volatility. The major compounds were carboxylic acids, mainly acetic acid; the pH value of 3.4 is also consistent with an abundance of acids (Table 1).

The yields of phenols are low in both processes; it seems that lignin cannot be decomposed to its phenylpropanoid monomeric units in this reaction system.

As shown above, the effect of Fe on the yields of light WS products can be evaluated quantitatively.

Table 3. Quantitative results from the GC analysis of the WS fraction prepared by the hydrothermal liquefaction of EFB.[a]

			Molecular		RRF		Fe-assisted		Conventional	
R.T.	Compound name	Formula	Weight	Classification	Found/Calculated	Value	Area	Yield (%C)	Area	Yield (%C)
5.841	2-Methoxyethanol	$C_3H_8O_2$	76.09	Internal standard			30197		28442	
5.909	Cyclopentanone	C_5H_8O	84.12	ketone	Found	2.22	4876	0.50%	3454	0.09%
7.567	3-Hydroxy-2-butanone	$C_4H_8O_2$	88.11	hydroxyketone	Found	1.41	24176	2.98%	5207	0.17%
7.803	Hydroxyacetone	$C_3H_6O_2$	74.08	hydroxyketone	Found	0.67	31393	7.24%	11888	0.65%
8.437	2-Methyl-3-hexanone	$C_7H_{14}O$	114.19	ketone	Calculated	2.37	18513	1.83%	1482	0.04%
8.677	2-Methyl-2-cyclopenten-1-one	C_6H_8O	96.13	ketone	Calculated	2.21	30748	3.32%	11106	0.08%
8.846	1-Hydroxy-2-butanone	$C_4H_8O_2$	88.11	hydroxyketone	Calculated	1.18	10684	1.57%	6204	0.24%
8.86	Tetrahydro-2-(methoxymethyl)furan	$C_6H_{12}O_2$	116.16	ether	Calculated	1.85			2893	0.08%
9.439	Cyclohexanol	$C_6H_{12}O$	100.16	alcohol	Found	2.49	2865	0.26%		
9.68	2-pentyl methoxyacetate	$C_8H_{16}O_3$	160.21	ester/ether	Calculated	1.83	5612	0.59%		
9.776	4-Heptanol	$C_7H_{16}O$	116.2	alcohol	Calculated	2.57	7154	0.64%		
9.912	1-Hydroxy-2-pentanone	$C_5H_{10}O_2$	102.13	hydroxyketone	Calculated	1.49	8822	1.11%		
10.001	Acetic acid	$C_2H_4O_2$	60.05	carboxylic acid	Found	0.71	24852	4.49%	137968	5.77%
10.143	Furfural	$C_5H_4O_2$	96.08	ether/aldehyde	Found	1.53			9321	0.26%
10.629	Tetrahydro-2-furanmethanol	$C_5H_{10}O_2$	102.13	alcohol/ether	Calculated	1.76	2388	0.25%		
10.695	2,5-Hexanedione	$C_6H_{10}O_2$	114.14	ketone	Calculated	1.46			4304	0.16%
11.155	Propanoic acid	$C_3H_6O_2$	74.08	carboxylic acid	Found	1.16	3428	0.46%	9881	0.32%
12.03	1-Ethoxy-3-pentanol	$C_7H_{16}O_2$	132.2	alcohol/ether	Calculated	1.98	4415	0.45%		
12.227	1,2-Ethanediol	$C_2H_6O_2$	62.07	alcohol	Found	0.77	2824	0.45%		
12.295	Butyrolactone	$C_4H_6O_2$	86.09	ester	Calculated	1.7	1293	0.14%		
13.928	1,2-Pentanediol	$C_5H_{12}O_2$	104.15	alcohol	Found	1.59			1314	0.04%
14.952	Guaiacol	$C_7H_8O_2$	124.14	ether/phenol	Found	2.11	1787	0.18%	6243	0.15%
16.437	Phenol	C_6H_6O	94.11	phenol	Found	2.63	14854	1.38%	60946	1.48%
18.759	1,1'-[Ethylidenebis(oxy)]bis[2-methyl-propane]	$C_{10}H_{22}O_2$	174.28	ether	Calculated	2.28	4929	0.47%		
18.952	Syringol	$C_8H_{10}O_3$	154.16	ether/phenol	Found	1.97	2655	0.27%	10953	0.27%
19.423	4-Oxopentanoic acid,	$C_5H_8O_3$	116.12	ketone/carboxylic acid	Found	0.98			5657	0.24%
	total							29%		10%

[a] Yields were calculated based on the carbon content of the raw EFB.

2.3.2. Insight into the heavy WS components

2.3.2.1. Separation of the heavy WS components

It was only possible to detect and quantify the light WS components by GC; however, in order to clarify the composition of the entire WS fraction, information on the remaining heavy WS components must be obtained. Since water and the light WS components are analysis obstacles, determination of only the heavy WS components is difficult. Therefore, the author attempted to remove water and the low molecular-weight compounds from the crude WS fraction. Since distillation or evaporation would add thermal history to the sample, there is a decomposition risk to the WS fraction; consequently, the author chose to use the freeze-drying method. The liquid-nitrogen-frozen crude WS fraction was evacuated to a pressure below 0.2 kPa at room temperature. After the water had sublimed, a viscous residue remained in the bottom of the flask, as shown in Figure 5 (freeze-dried bottom, FDB). The sublimed water and other volatile compounds were collected in a liquid-nitrogen trap and recovered as a clear aqueous solution (volatile fraction, VF). The mass balances before and after separation were consistent, and the carbon yield was confirmed by TOC measurements (Table 4); the carbon yield of the VF was determined to be 52% and 32% for the Fe-assisted and conventional hydrothermal WS fractions, respectively, which is in agreement with the carbon-yield proportion of the light WS components in the crude WS fraction determined by GC. In addition, the gas chromatogram of each VF was almost identical to that of the crude WS fraction, whereas the corresponding chromatograms of the FDB exhibited peaks that were significantly lower in intensity than those observed for the crude WS fractions (Figure 6). Furthermore, the Karl Fischer method also confirmed that the moisture contents of the residues were less than

5%. The author concludes from these results that the light WS components and water were separated by freeze-drying in the VF, while heavy WS components were condensed in the FDB.

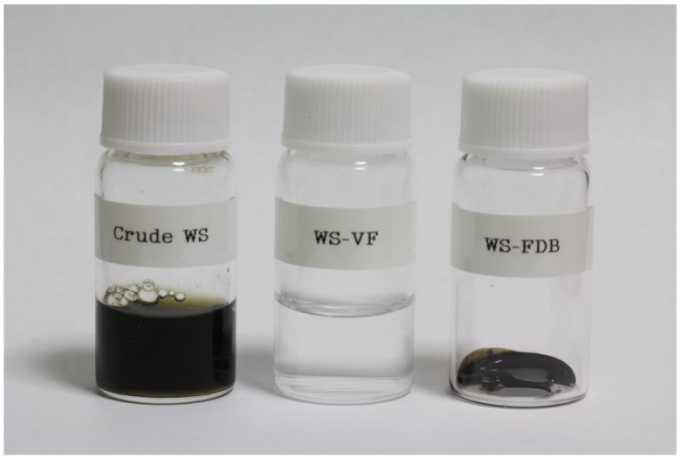

Figure 5. Photographic images before and after the freeze-dry separation of the WS fraction. From left to right: Crude WS fraction, volatile fraction, freeze-dried bottom.

Table 4. Mass balances and carbon balances following freeze-dry separations of the crude WS fractions.

	Mass balance (wt%)[a]			Carbon balance (%C)[b]		
	WS-FDB	WS-VF	total	WS-FDB	WS-VF	total
Fe-assisted	2%	97%	99%	46%	52%	98%
Conventional	2%	98%	100%	68%	32%	100%

[a] Calculated based on the weight of the freeze-dried crude WS fraction.

[b] Calculated based on the carbon content of the freeze-dried crude WS fraction.

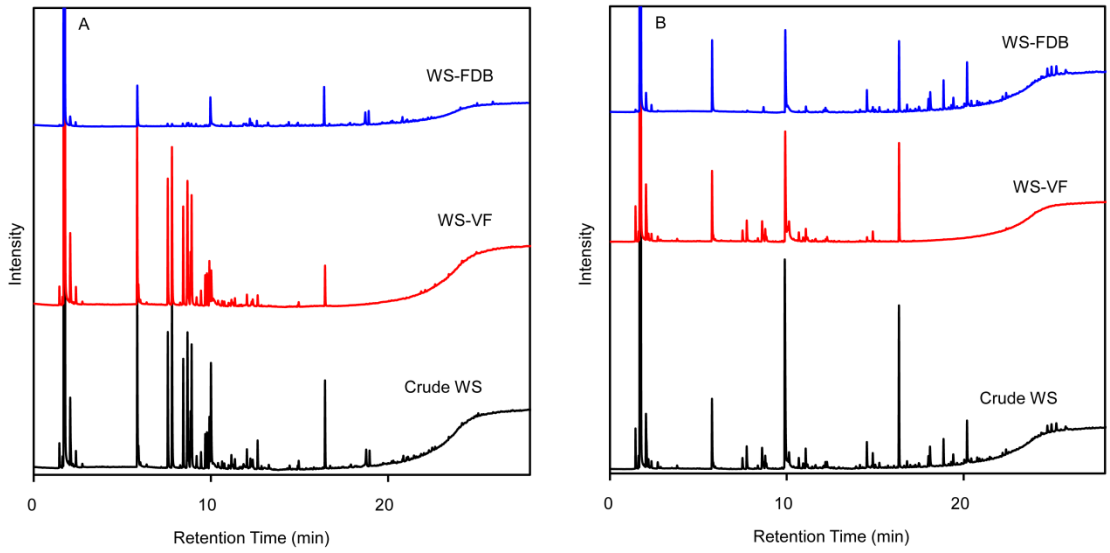

Figure 6. Comparisons of the GC–FID chromatogram of the crude WS fraction with those of WS-VF and WS-FDB; (a) Fe-assisted, (b) conventional.

2.3.2.2. Elemental composition of the WS fraction

Elemental compositions of the light WS components were calculated by counting the elements in each GC-quantified compound. Elemental compositions of the heavy WS components were quantified by elemental analyses of the FDBs (the influences of residual moisture and the light WS components were subtracted). Elemental compositions of the crude WS fractions were calculated by combining the light and heavy WS elemental compositions by considering the proportion of each components. The results are displayed in the forms of H/C and O/C ratios mapped on a van Krevelen diagram and compared with those of biomass feedstocks such as raw EFBs, cellulose, hemicellulose, lignin, as well as biomass-derived chemicals and petrochemicals (Figure 7).[36]

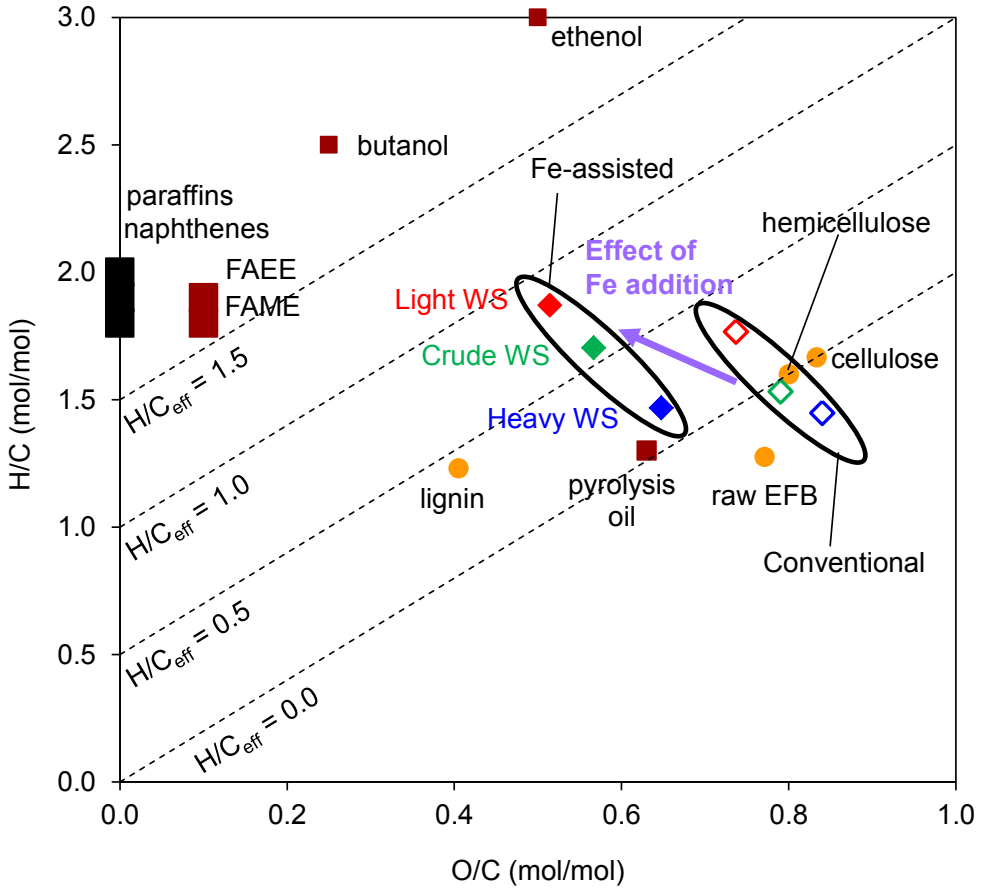

Figure 7. van Krevelen diagram of the WS fractions, biomass feedstocks, biomass-derived chemicals, and petrochemicals.

The diagonal lines in the diagram are hydrogen-to-carbon effective-ratio (H/C_{eff}) contour lines (eq. 7), which are often used to estimate and describe biomass upgrading.[37] To bring the elemental composition of biomass-derived compounds close to those of petrochemicals, oxygen should be removed in the form of H_2O; consequently, one mole of oxygen reduces two moles of effective hydrogen, as shown in eq. 7. A higher H/C_{eff} value indicates more efficient reforming during this process.

$$H/C_{eff} = \frac{[H]-2[O]}{[C]} \quad (7)$$

The author found that the H/C ratio was higher and the O/C ratio was lower when the sample was prepared in the presence of Fe. The crude WS fraction prepared by conventional hydrothermal liquefaction had a similar composition to cellulose or hemicellulose, the H/C_{eff} of which was almost zero. The H/C and O/C ratios apparently improved by employing Fe as an additive, with the H/C_{eff} increasing to 0.57. These results suggest that Fe is capable of hydrodeoxygenating the sample, which effectively improves the hydrothermal liquefaction reaction. Vispute and co-workers demonstrated the two-step hydrodeoxygenation of the aqueous fraction extracted from a pyrolysis oil.[38] The extracted aqueous fraction of the pyrolysis oil (water-soluble fraction of pinewood bio-oil, WSBO) has a composition close to that of the WS fraction obtained by hydrothermal liquefaction since their H/C_{eff} ratios are similar; the H/C_{eff} of the WSBO increased from 0.14 to 0.71 by ruthenium-catalyzed hydrodeoxygenation. Hence, one-step Fe-assisted hydrothermal liquefaction process is nearly equivalent to this two-step system. However, when compared to other biomass-derived chemicals and petrochemicals, the H/C_{eff} ratio is still low. Improvement in the reaction conditions during Fe-assisted hydrothermal liquefaction, or the development of an additional upgrading catalyst, is required to increase the efficiency of this process.

2.3.2.3. FT-IR spectrum of the freeze-dried WS fraction

The FDB samples were examined by FT-IR spectroscopy in order to obtain information on the functional groups present in the heavy WS components; the IR spectra are shown in Figure 8.

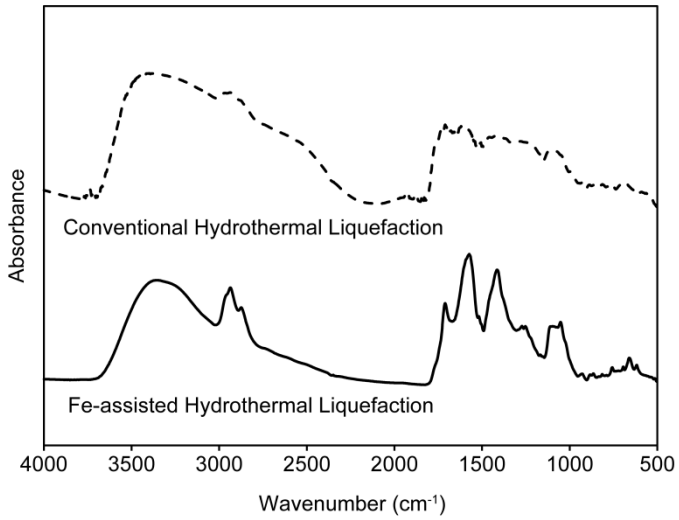

Figure 8. FT-IR spectra of WS-FDB.

The heavy WS components were presumed to contain complicated mixtures since few sharp peaks attributable to specific functional groups are observed in the spectra. Broad strong absorptions were observed at around 3400 cm^{-1} in both samples, consistent with the presence of OH groups (and residual water).[39] These OH groups originate from cellulose and hemicellulose, and the water-solubilities and non-volatilities of the heavy WS components are due to these groups. A shoulder observed at around 2500 cm^{-1} in the conventional hydrothermally liquefacted sample indicates the intermolecular hydrogen bonding of carboxylic acid,[40] suggesting that COOH groups are more abundant in this sample than in that produced by Fe assistance. The peaks observed between 3000 and 2800 cm^{-1} in both samples are attributed to the C-H stretching vibrations of alkyl groups. The peak around 1450 cm^{-1} is due to C-H deformation vibrations of alkyl groups. In the case of the Fe-assisted sample, these alkyl peak were slightly more intense than those corresponding to the conventionally liquefacted sample, suggesting that dehydration and hydrodeoxygenation reactions are promoted by Fe. Both samples exhibited absorptions in the 1700 cm^{-1} region, consistent

with C=O stretching vibrations and suggestive of the presence of carbonyl compounds. The peak at 1600 cm^{-1} is attributed to aromatic C=C stretching or quinone C=O stretching. The peak at 1250 cm^{-1} and 1050 cm^{-1} arising from C-O stretching indicates the presence of alcohols, ethers, esters, or phenols. Overall, peaks between 1700 and 1000 cm^{-1} were unclear in the spectrum of the conventionally liquefacted sample, indicating that this sample is a more complicated mixture than the Fe-assisted sample. The IR spectrum profiles of FDBs are analogous with those of humins or biochars,[41-43] suggesting these substances are structurally similar.

2.3.2.4. Molecular-weight distributions of the freeze-dried WS samples

In order to investigate the molecular-weight distributions of the heavy WS components, the FDB samples were analyzed by GPC, and the differential molecular-weight distribution profiles are displayed in Figure 9, with the average molecular weights listed in Table 5. Molecular weight distributions were measured in poly(ethylene glycol) equivalents.

Table 5. Average molecular weights of WS-FDB.[a]

	M_n	M_w	M_z
Fe-assisted	219	277	321
Conventional	194	252	299

[a] Poly(ethylene glycol) equivalent.

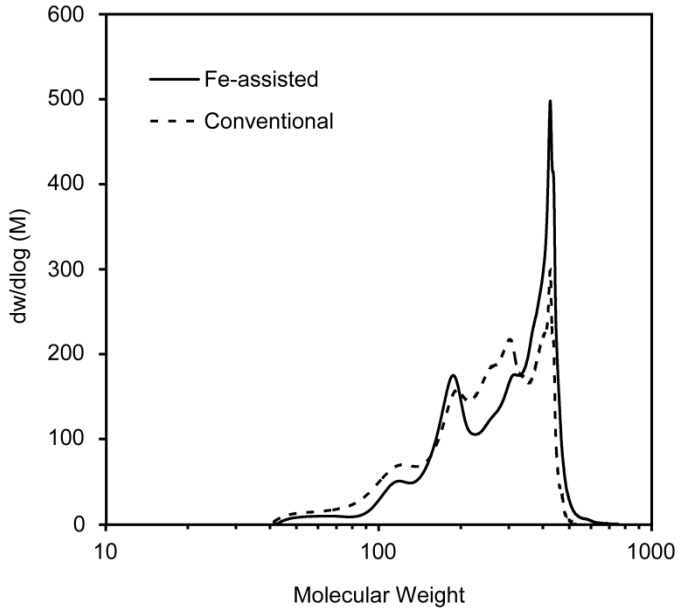

Figure 9. Molecular weight distributions of WS-FDB (poly(ethylene glycol) equivalents).

Figure 9 reveals that a group of compounds with molecular weights distributed in the 100 to 500 range can be separated by the freeze-drying method. A molecular weight of 500 corresponds to a trimer of sugars or monomeric lignin units.[44] The mass-average molecular weight (Mw) was around 250 for both Fe-assisted and conventional samples. The author concludes, therefore, that the heavy WS components are composed of oligomers containing polar functional groups (OH, COOH), rather than polymers; these components are formed by the denaturation of oligomeric sugars or lignin that were incompletely decomposed during the hydrothermal process, or by the condensation of low molecular-weight products. Considering that humins are produced through similar pathways[43] but have large molecular weight distributions[45] and low solubilities in water, the heavy WS components are considered to be a precursor of humins.[46] As shown in Table 4, the proportion of the heavy WS components contained

in the crude WS fraction prepared by Fe-assisted hydrothermal decomposition was lower than that of the sample prepared by conventional hydrothermal decomposition. In addition, the molecular-weight profiles of the two FDB samples are slightly different (Figure 9). These results indicate that the reaction route changes following the addition of Fe. A likely explanation is that Fe accelerates biomass decomposition and/or suppresses the re-condensation of the decomposition products. As discussed above, detailed analyses of the light and heavy WS components verify that Fe has a remarkable effect on the hydrothermal liquefaction of biomass.

2.3.3. Catalytic cracking of the WS-VF and WS-FDB

Catalytic cracking of the WS fractions obtained from EFBs produced hydrocarbons such as olefins, as well as benzene, toluene, and xylenes (BTX). As mentioned in chapter 1, the WS fraction obtained by the Fe-assisted hydrothermal decomposition of the EFB exhibited a higher yield of hydrocarbons than that obtained by conventional hydrothermal decomposition, which the author considers to be due to the higher concentrations of light compounds in the Fe-assisted WS fraction. In order to verify this hypothesis, cracking experiments were carried out on the VF and FDB of the Fe-assisted WS fraction, the results which were compared with those of the crude WS fraction and displayed in Table 6.

Table 6. Catalytic cracking of WS-VF and WS-FDB and comparisons with the crude WS fraction.[a]

	Carbon yields (%C)													Carbon balance (%C)
	olefins				BTX	Olefin + BTX	Alkanes			COx			Water solubles[b]	
	C_2	C_3	C_4	Sum	Sum	Sum	C_1	C_{2-5}	Sum	CO	CO_2	Sum		
Crude WS	12	14	2	28	7	35	3	2	5	9	4	13	13	66
WS-VF	17	20	4	41	8	49	3	3	6	13	9	22	11	88
WS-FDB	4	6	1	11	3	14	2	1	3	5	4	9	24	50

[a] Preparation conditions of WS: EFB = 4 g, H_2O = 40 g, Fe = 6.256 g or 0 g, initial pressure = 1.0 MPa (N_2), temperature = 300°C, time = 10 min.

Cracking conditions: HZSM-5 = 3.3 g (6 mL, d = 0.55), WS feed = weight hourly space velocity of 1.1 h^{-1}, N_2 = 50 mL/min, temperature = 300 °C. Yields were calculated based on the fed-in WS fraction.

[b] Collected carbon in the gas wash bottle.

As expected, the VF produced cracking products in higher yields. When the unseparated WS sample was used, the carbon balance between the fed carbon and the product was poor, whereas when the VF was used the carbon balance was almost 90%. On the other hand, when the FDB was used, the hydrocarbon yield was lower and the carbon balance decreased to less than 50%.

The low carbon balances observed for the crude WS fraction and the FDB are ascribed to non-volatile (heavy) compounds that become carbonized and fixed as coke in the vaporizer of the reactor. Therefore, in order to improve the hydrocarbon yield, it is important that the proportion of the light WS components in the crude WS fraction is increased. The development of a catalyst that promotes decomposition and suppresses re-condensation of the WS components is therefore required.

2.3.4. Summary of the product distributions obtained by hydrothermal liquefaction

Figure 10 provides an overview of the products obtained by hydrothermal liquefaction including those that are not in WS fractions. By quantitatively analyzing the WS fractions, the changes in product distribution due to the addition of Fe become clear. The author showed that the addition of Fe significantly increases the proportion of the WS fraction, which is discussed in chapter 1. Herein, it was confirmed that the proportion of highly volatile compounds (light WS components) had increased remarkably. On the other hand, the acetone-soluble and water-insoluble (WI) fractions, and the solid residues (SRs), which are considered to be complex polymeric compounds, both decreased. As a result, the addition of Fe to the system resulted in a shift of the molecular-weight distribution of the products to a lower average value.

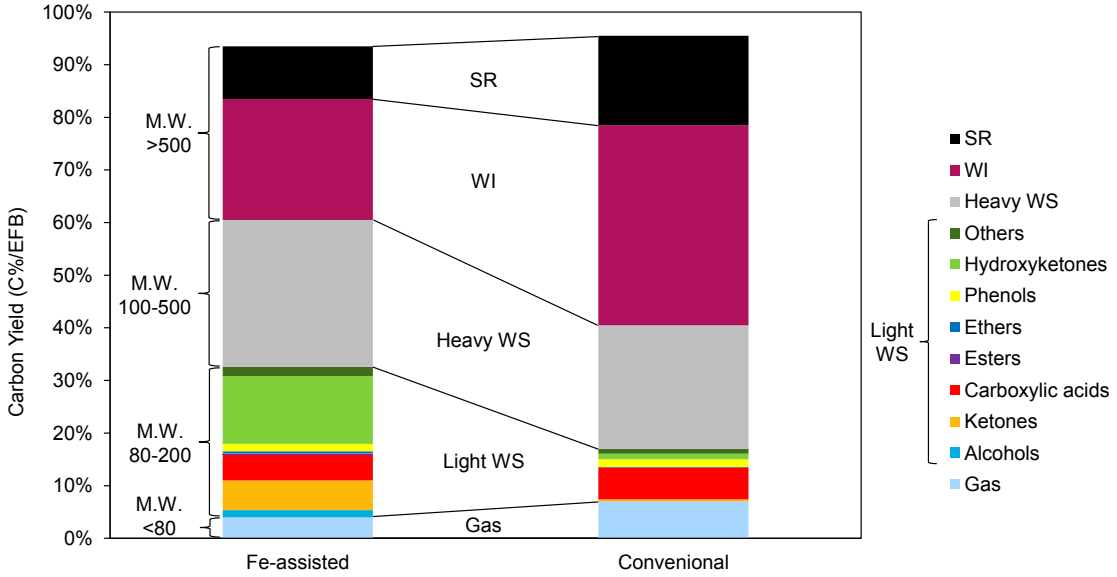

Figure 10. Summary of product yields from the hydrothermal liquefaction of EFB.

2.4. Conclusions

In this study, The author developed a method for the quantification of the WS fraction from the hydrothermal liquefaction of biomass. The composition of the light WS components was revealed through a combination of GC–MS (for identification) and GC–FID (for quantification). An empirical RRF estimation method, based on the ECN concept, was developed to quantify compounds with unknown FID sensitivities. A good correlation was obtained between the experimental and the calculated RRF values through the optimization of the ECN contribution coefficient (Cnt) of each analyte functional group against the analysis data of 32 standard samples. GC analyses of the WS fractions revealed that the addition of Fe during hydrothermal liquefaction altered the product distribution and increased the yield of the light WS components.

Heavy WS components were isolated by removing water and the light WS

components by freeze-drying, which enabled various analyses to be performed. Quantitative information on the heavy WS components was obtained by elemental analysis and GPC, while qualitative information was provided by FT-IR spectroscopy. These results suggest that the addition of Fe affects the composition and structure of the heavy WS components.

Catalytic cracking of each WS fraction using the HZSM-5 zeolite was investigated under the same conditions, which revealed that the light WS components gave high yields of olefins. These results confirm the importance of improving the yield of the light WS components, and provide guidance for improving the economics of the hydrothermal liquefaction and cracking system. The development of improved catalysts and the optimization of the reaction condition are currently in progress.

2.5. References

1. Xiu, S.; Shahbazi, A., Bio-Oil Production and Upgrading Research: A Review. *Renew. Sust. Energy Rev.* **2012,** *16* (7), 4406–4414.
2. Kumar, G.; Shobana, S.; Chen, W.-H.; Bach, Q.-V.; Kim, S.-H.; Atabani, A. E.; Chang, J.-S., A Review of Thermochemical Conversion of Microalgal Biomass for Biofuels: Chemistry and Processes. *Green Chem.* **2017,** *19* (1), 44–67.
3. Peterson, A. A.; Vogel, F.; Lachance, R. P.; Fröling, M.; Antal, J. M. J.; Tester, J. W., Thermochemical Biofuel Production in Hydrothermal Media: A Review of Sub- and Supercritical Water Technologies. *Energy Environ. Sci.* **2008,** *1* (1), 32–65.
4. Akhtar, J.; Amin, N. A. S., A Review on Process Conditions for Optimum Bio-Oil Yield in Hydrothermal Liquefaction of Biomass. *Renew. Sust. Energy*

Rev. **2011,** *15* (3), 1615–1624.

5. Xue, Y.; Chen, H.; Zhao, W.; Yang, C.; Ma, P.; Han, S., A Review on the Operating Conditions of Producing Bio-Oil from Hydrothermal Liquefaction of Biomass. *Int. J. Energy Res.* **2016,** *40* (7), 865–877.
6. Toor, S. S.; Rosendahl, L.; Rudolf, A., Hydrothermal Liquefaction of Biomass: A Review of Subcritical Water Technologies. *Energy* **2011,** *36* (5), 2328–2342.
7. Sun, P.; Heng, M.; Sun, S.-H.; Chen, J., Analysis of Liquid and Solid Products from Liquefaction of Paulownia in Hot-Compressed Water. *Energy Convers. Manage.* **2011,** *52* (2), 924–933.
8. Kurimoto, Y.; Takeda, M.; Koizumi, A.; Yamauchi, S.; Doi, S.; Tamura, Y., Mechanical Properties of Polyurethane Films Prepared from Liquefied Wood with Polymeric Mdi. *Bioresour. Technol.* **2000,** *74* (2), 151–157.
9. Ramos-Tercero, E. A.; Bertucco, A.; Brilman, D. W. F., Process Water Recycle in Hydrothermal Liquefaction of Microalgae to Enhance Bio-Oil Yield. *Energy Fuels* **2015,** *29* (4), 2422–2430.
10. Cherad, R.; Onwudili, J. A.; Biller, P.; Williams, P. T.; Ross, A. B., Hydrogen Production from the Catalytic Supercritical Water Gasification of Process Water Generated from Hydrothermal Liquefaction of Microalgae. *Fuel* **2016,** *166*, 24–28.
11. Tommaso, G.; Chen, W. T.; Li, P.; Schideman, L.; Zhang, Y., Chemical Characterization and Anaerobic Biodegradability of Hydrothermal Liquefaction Aqueous Products from Mixed-Culture Wastewater Algae. *Bioresour. Technol.* **2015,** *178*, 139–46.
12. Wu, K.; Yang, M.; Chen, Y.; Pu, W.; Hu, H.; Wu, Y., Aqueous-Phase

Ketonization of Acetic Acid over Zr/Mn Mixed Oxides. *AlChE J.* **2017,** *63* (7), 2958–2967.

13. Zou, S.; Wu, Y.; Yang, M.; Kaleem, I.; Zhou, J.; Li, C.; Tong, J., Response to "Comments on 'Thermochemical Catalytic Liquefaction of the Marine Microalgae *Duanaliella Tertiolecta* and Characterization of Bio-Oils' by Zou Et Al.". *Energy Fuels* **2010,** *24* (6), 3710–3712.
14. Villadsen, S. R.; Dithmer, L.; Forsberg, R.; Becker, J.; Rudolf, A.; Iversen, S. B.; Iversen, B. B.; Glasius, M., Development and Application of Chemical Analysis Methods for Investigation of Bio-Oils and Aqueous Phase from Hydrothermal Liquefaction of Biomass. *Energy Fuels* **2012,** *26*, 6988–6998.
15. Panisko, E.; Wietsma, T.; Lemmon, T.; Albrecht, K.; Howe, D., Characterization of the Aqueous Fractions from Hydrotreatment and Hydrothermal Liquefaction of Lignocellulosic Feedstocks. *Biomass Bioenergy* **2015,** *74*, 162–171.
16. Maddi, B.; Panisko, E.; Albrecht, K.; Howe, D., Qualitative Characterization of the Aqueous Fraction from Hydrothermal Liquefaction of Algae Using 2D Gas Chromatography with Time-of-Flight Mass Spectrometry. *J. Vis. Exp.* **2016,** (109), 1–11.
17. Madsen, R. B.; Biller, P.; Jensen, M. M.; Becker, J.; Iversen, B. B.; Glasius, M., Predicting the Chemical Composition of Aqueous Phase from Hydrothermal Liquefaction of Model Compounds and Biomasses. *Energy Fuels* **2016,** *30* (12), 10470–10483.
18. Maddi, B.; Panisko, E.; Wietsma, T.; Lemmon, T.; Swita, M.; Albrecht, K.; Howe, D., Quantitative Characterization of Aqueous Byproducts from Hydrothermal Liquefaction of Municipal Wastes, Food Industry Wastes, and

Biomass Grown on Waste. *ACS Sustain. Chem. Eng.* **2017,** *5* (3), 2205–2214.

19. Sternberg, J. C.; Gallaway, W. S.; Jones, D. T. L., Mechanism of Response of Flame Ionization Detectors. In *Gas Chromatography*, Brenner, N.; Callen, J. E.; Weiss, M. D., Eds. Academic Press: New York, 1962; pp 231–267.
20. Cicchetti, E.; Merle, P.; Chaintreau, A., Quantitation in Gas Chromatography: Usual Practices and Performances of a Response Factor Database. *Flavour Fragr. J.* **2008,** *23* (6), 450–459.
21. de Saint Laumer, J.-Y.; Leocata, S.; Tissot, E.; Baroux, L.; Kampf, D. M.; Merle, P.; Boschung, A.; Seyfried, M.; Chaintreau, A., Prediction of Gas Chromatography with Flame Ionization Detection Response Factors: Algorithm Improvement, Extension to Silylated Compounds, and Application to the Quantification of Metabolites. *J. Sep. Sci.* **2015,** *38*, 3209–3217.
22. Tissot, E.; Rochat, S.; Debonneville, C.; Chaintreau, A., Rapid GC–FID Quantification Technique without Authentic Samples Using Predicted Response Factors. *Flavour Fragr. J.* **2012,** *27* (4), 290–296.
23. de Saint Laumer, J.-Y.; Cicchetti, E.; Merle, P.; Egger, J.; Chaintreau, A., Quantification in Gas Chromatography: Prediction of Flame Ionization Detector Response Factors from Combustion Enthalpies and Molecular Structures. *Anal. Chem.* **2010,** *82* (15), 6457–6462.
24. Filippi, J. J.; Belhassen, E.; Baldovini, N.; Brevard, H.; Meierhenrich, U. J., Qualitative and Quantitative Analysis of Vetiver Essential Oils by Comprehensive Two-Dimensional Gas Chromatography and Comprehensive Two-Dimensional Gas Chromatography/Mass Spectrometry. *J. Chromatogr. A* **2013,** *1288*, 127–148.

25. Cachet, T.; Brevard, H.; Chaintreau, A.; Demyttenaere, J.; French, L.; Gassenmeier, K.; Joulain, D.; Koenig, T.; Leijs, H.; Liddle, P.; Loesing, G.; Marchant, M.; Merle, P.; Saito, K.; Schippa, C.; Sekiya, F.; Smith, T., Iofi Recommended Practice for the Use of Predicted Relative-Response Factors for the Rapid Quantification of Volatile Flavouring Compounds by GC–FID. *Flavour Fragr. J.* **2016,** *31* (3), 191–194.

26. Neuenschwander, U.; Negron, A.; Jensen, K. F., A Clock Reaction Based on Molybdenum Blue. *J. Phys. Chem. A* **2013,** *117* (21), 4343–51.

27. Dalluge, D. L.; Daugaard, T.; Johnston, P.; Kuzhiyil, N.; Wright, M. M.; Brown, R. C., Continuous Production of Sugars from Pyrolysis of Acid-Infused Lignocellulosic Biomass. *Green Chem.* **2014,** *16* (9), 4144–4155.

28. Olcese, R.; Carré, V.; Aubriet, F.; Dufour, A., Selectivity of Bio-Oils Catalytic Hydrotreatment Assessed by Petroleomic and GC*GC/MS–FID Analysis. *Energy Fuels* **2013,** *27* (4), 2135–2145.

29. Djokic, M. R.; Dijkmans, T.; Yildiz, G.; Prins, W.; Van Geem, K. M., Quantitative Analysis of Crude and Stabilized Bio-Oils by Comprehensive Two-Dimensional Gas-Chromatography. *J. Chromatogr. A* **2012,** *1257*, 131–140.

30. Michailof, C.; Sfetsas, T.; Stefanidis, S.; Kalogiannis, K.; Theodoridis, G.; Lappas, A., Quantitative and Qualitative Analysis of Hemicellulose, Cellulose and Lignin Bio-Oils by Comprehensive Two-Dimensional Gas Chromatography with Time-of-Flight Mass Spectrometry. *J. Chromatogr. A* **2014,** *1369*, 147–160.

31. Undri, A.; Abou-Zaid, M.; Briens, C.; Berruti, F.; Rosi, L.; Bartoli, M.; Frediani, M.; Frediani, P., A Simple Procedure for Chromatographic Analysis of Bio-Oils from Pyrolysis. *J. Anal. Appl. Pyrolysis* **2015,** *114*, 208–221.

32. Addis, G.; Baskaran, R.; Raju, M.; Ushadevi, A.; Asfaw, Z.; Woldu, Z.; Baskaran, V., Effect of Blanching and Drying Process on Carotenoids Composition of Underutilized Ethiopian (*Coccinia Grandis* L. Voigt) and Indian (*Trigonella Foenum-Graecum* L.) Green Leafy Vegetables. *J. Food Process. Preserv.* **2009,** *33* (6), 744–762.

33. Tejada, L.; Vioque, M.; Gómez, R.; Fernández-Salguero, J., Effect of Lyophilisation, Refrigerated Storage and Frozen Storage on the Coagulant Activity and Microbiological Quality of *Cynara Cardunculus* L. Extracts. *J. Sci. Food Agric.* **2008,** *88* (8), 1301–1306.

34. Michailof, C. M.; Kalogiannis, K. G.; Sfetsas, T.; Patiaka, D. T.; Lappas, A. A., Advanced Analytical Techniques for Bio-Oil Characterization. *WIREs Energy Environ.* **2016,** *5* (6), 614–639.

35. Szulejko, J. E.; Kim, Y. H.; Kim, K. H., Method to Predict Gas Chromatographic Response Factors for the Trace-Level Analysis of Volatile Organic Compounds Based on the Effective Carbon Number Concept. *J. Sep. Sci.* **2013,** *36* (20), 3356–3365.

36. O'Connor, P., Chapter 1 - a General Introduction to Biomass Utilization Possibilities. In *The Role of Catalysis for the Sustainable Production of Bio-Fuels and Bio-Chemicals*, Triantafyllidis, K. S.; Lappas, A. A.; Stöcker, M., Eds. Elsevier: Amsterdam, 2013; pp 1–25.

37. Chen, N. Y.; Degnan, T. F.; Koenig, L. R., Liquid Fuel from Carbohydrates. *CHEMTECH* **1986,** *16* (8), 506–511.

38. Vispute, T. P.; Zhang, H. Y.; Sanna, A.; Xiao, R.; Huber, G. W., Renewable Chemical Commodity Feedstocks from Integrated Catalytic Processing of

Pyrolysis Oils. *Science* **2010,** *330* (6008), 1222–1227.

39. Mei, Y.; Liu, R., Effect of Temperature of Ceramic Hot Vapor Filter in a Fluidized Bed Reactor on Chemical Composition and Structure of Bio-Oil and Reaction Mechanism of Pine Sawdust Fast Pyrolysis. *Fuel Process. Technol.* **2017,** *161*, 204–219.

40. Sahoo, S.; Chakraborti, C.; Behera, P.; Mishra, S., Ftir and Raman Spectroscopic Investigations of a Norfloxacin/Carbopol934 Polymeric Suspension. *J. Young Pharm.* **2012,** *4* (3), 138–145.

41. Zhang, S.; Yuan, L.; Li, W.; Lin, Z.; Li, Y.; Hu, S.; Zhao, B., Characterization of pH-Fractionated Humic Acids Derived from Chinese Weathered Coal. *Chemosphere* **2017,** *166*, 334–342.

42. Rasrendra, C. B.; Windt, M.; Wang, Y.; Adisasmito, S.; Makertihartha, I. G. B. N.; van Eck, E. R. H.; Meier, D.; Heeres, H. J., Experimental Studies on the Pyrolysis of Humins from the Acid-Catalysed Dehydration of C6-Sugars. *J. Anal. Appl. Pyrolysis* **2013,** *104*, 299–307.

43. Sevilla, M.; Fuertes, A. B., The Production of Carbon Materials by Hydrothermal Carbonization of Cellulose. *Carbon* **2009,** *47* (9), 2281–2289.

44. Zakzeski, J.; Bruijnincx, P. C. A.; Jongerius, A. L.; Weckhuysen, B. M., The Catalytic Valorization of Lignin for the Production of Renewable Chemicals. *Chem. Rev.* **2010,** *110* (6), 3552–3599.

45. Almendros, G.; Sanz, J.; Sobrados, L., Characterization of Synthetic Carbohydrate-Derived Humic-Like Polymers. *Sci. Total Environ.* **1989,** *81-82*, 91–98.

46. van Zandvoort, I.; Wang, Y.; Rasrendra, C. B.; van Eck, E. R.; Bruijnincx, P. C.;

Heeres, H. J.; Weckhuysen, B. M., Formation, Molecular Structure, and Morphology of Humins in Biomass Conversion: Influence of Feedstock and Processing Conditions. *ChemSusChem* **2013,** *6* (9), 1745–1758.

Chapter 3. Mechanism of the Fe-Assisted hydrothermal liquefaction of lignocellulosic biomass

3.1. Introduction

Reduction of greenhouse gas emissions to mitigate climate change is an urgent global issue given the ever-increasing worldwide energy consumption. An effective means to achieve a sustainable society is switching the source of chemical feedstocks from fossil fuels to carbon-neutral resources. Since biomass is one of the most abundant renewable resources, various biological and thermochemical methods have been developed to convert it into the easily manageable liquid form. Hydrothermal liquefaction (HTL) is a promising technology because it simply uses water as the solvent and directly converts biomass without any energy-consuming pre-drying step.[1-3] In HTL, biomass is treated with hot compressed water to afford water-soluble (WS) and water-insoluble (WI) fractions as main products and the gaseous fraction and solid residue (SR) as byproducts.[4]

While the WI fraction (so-called biocrude) has been investigated because of its utilization as a feedstock for liquid fuel, the WS fraction has attracted attention because its effective use is the key to making the whole process commercially feasible.[5] One of several methods of utilizing the WS fraction is recirculation into HTL itself, which enables the greater recovery of the oil yield and reduction of the loss of organics.[6-8] Anaerobic digestion to produce methane, which will maximize energy production, has also been proposed.[9] Gasification is a viable option to obtaining hydrogen for the biocrude upgrading process.[10] Organic acids in the WS fraction can be converted to ketones,[11] and subsequently, to liquid fuels or olefins through catalytic processes.[5] In

addition, high-value specialty chemicals, such as ethanol, acetic acid, and acetone, can be produced by extraction and subsequent catalytic processes.[12]

As shown in chapter 1 and 2, the author developed an HTL process for lignocellulosic biomass conversion using metallic Fe as an additive. Oil palm empty fruit bunch (EFB) was efficiently liquefied to afford an especially large amount of WS fraction. The author focused on the WS fraction because it is a promising source of renewable chemical feedstocks; its aggressive utilization by catalytic cracking using a solid acid catalyst (HZSM-5 zeolite) produces hydrocarbons, such as olefinic and aromatic compounds.[13] The WS fraction produced through Fe-assisted HTL exhibited higher hydrocarbon yields than conventional HTL. The hydrocarbon yield of catalytic cracking is known to depend on the elemental composition of the feedstock.[14] Qualitative and quantitative analyses revealed that the Fe additive improved the elemental composition (i.e., increased H/C and decreased O/C ratios) in the WS fraction. In addition, Fe significantly increased the yield of light compounds. The WS fraction was successfully separated into a volatile fraction (light WS), containing mainly small compounds, and a non-volatile fraction (heavy WS), containing mainly oligomeric compounds. Catalytic cracking of light WS afforded more hydrocarbons than that of heavy WS, indicating that the degree of degradation in HTL is an important factor in the economics of the integrated process (HTL + cracking).

The main components of biomass — cellulose, hemicellulose, and lignin — are decomposed under hydrothermal condition to form various products. Because of the complexity of the biomass composition, the reaction chemistry and mechanism of HTL are also complicated. The main pathway of HTL is believed to involve three steps: (i) depolymerization of biomass, (ii) decomposition of biomass monomers, and (iii)

recondensation of reactive intermediates.[3] On the basis of the reactivity of saccharides and a few possible intermediates in Fe-assisted HTL, the author hypothesized that step (ii) is accelerated, while step (iii) is suppressed in the Fe/H_2O system. However, as discussed in chapter 1, the effect of Fe on the reactivity was investigated about carbohydrate substrates and their decomposition products. The effect on lignin reactivity was not evaluated and the detailed role of Fe in the hydrothermal system remains unclear. These unresolved issues are obstacles to the optimization of the HTL process conditions.

In the present study, the author further investigated the Fe-assisted HTL of biomass by evaluating the reactivity of each biomass component in the presence of Fe. Commercially available carbohydrates (including polysaccharides and monomeric sugars) and enzymatically isolated lignin were used as model substrates. Experiments were conducted in the presence and absence of Fe to elucidate the role of Fe and reaction mechanism in the Fe/H_2O system. The contribution of each component of EFB to the products of Fe-assisted HTL was discussed on the basis of the results of the HTL of these model substrates.

3.2. Experimental Section

3.2.1. Materials

EFB from Indonesia was used as the lignocellulosic biomass feedstock and supplied by Nippon Shokubai Co., Ltd. It was dried at 25 °C and crushed into particles less than 300 μm in size. Fe powder (99.9%, NM-0029-UP) and Fe_3O_4 (98%, NO-0049-HP) were purchased from Ionic Liquids Technologies GmbH. Cellulose (Avicel® PH-101), alkali lignin, Celluclast® 1.5 L, and Novozyme 188 were purchased

from Sigma-Aldrich Co., LLC. D-(+)-glucose and xylan from corn core were purchased from Wako Pure Chemical Industries, Ltd. and Tokyo Chemical Industry Co., Ltd., respectively.

3.2.2. HTL Process

HTL and separation experiments were performed according to the method described in chapter 1. Briefly, the substrate, Fe powder, and deionized water were introduced into the Hastelloy C high-pressure reactor (MMJ-100, OM Labotech), which was purged four times with nitrogen after introduction of the materials. The initial pressure was set to 1.0 MPa with nitrogen, and the stirring rate was adjusted to 700 rpm. The reactor was then heated to 300 °C. After 10 min, the reactor was rapidly cooled to 25 °C using ice-water.

Gaseous products were collected in a gas sampling bag, and water-soluble products were isolated by filtration and denoted as the "WS" fraction. The water-insoluble solids in the filter cake were extracted with acetone and concentrated under reduced pressure as the "WI" fraction. The residue from the filter paper was dried and designated as "SR."

The crude WS fraction (10 mL) was placed in a round-bottom flask and frozen by immersing the flask in liquid nitrogen. Immediately after connecting the flask to a freeze dryer (FDS-1000, Tokyo Rikakikai Co., Ltd.), the sample was maintained under reduced pressure (< 0.2 kPa) for 6 h. The volatile fraction was removed as "light WS" fraction, whereas the residue in the flask was collected by redissolution in water and denoted as "heavy WS" fraction.

3.2.3. Analysis of HTL Products

Gaseous products were analyzed using the Shimadzu GC-8A chromatograph equipped with silica-gel and 5A-molecular-sieve columns (ZS-74 and ZM-1, respectively, Shinwa Chemical Industries), and a thermal conductivity detector (TCD). The total organic carbon (TOC) contents of the crude and heavy WS fractions were measured using a TOC analyzer (TOC-LCSH/CSN, Shimadzu). The TOC of the light WS fraction was the difference between those of the crude and heavy WS fractions. Identification of each product in the WS fraction was performed by gas chromatography-mass spectrometry (GC-MS) on the Shimadzu QP-2010 system equipped with a capillary column (Inert-cap® WAX-HT, 30 m × 0.25 mm ID × 0.25 μm film thickness, GL Sciences), while quantification was performed by gas chromatography-flame ionization detection (GC-FID) on the Shimadzu GC-2014 system equipped with the same capillary column. The WS fraction samples were diluted with acetone (1:1 v/v), and 2-methoxyethanol (0.05 wt%) was added as an internal standard. Compounds were identified by comparing their mass spectra to those from the National Institute of Standards and Technology library of mass spectral data. Elemental analysis (CHN) of WI and SR was performed using an elemental analyzer (vario EL cube, Elementar) and sulfanilamide as the calibration standard. The oxygen mass content was calculated from the difference.

The product yields from HTL were calculated as follows:

$$\text{Yield of each product from HTL (\%)} = \frac{\text{Moles of carbon in the product}}{\text{Moles of carbon in the raw material}} \times 100 \quad (1)$$

3.2.4. Gas chromatography quantification of light water-soluble fraction from hydrothermal liquefaction of glucose

The volatile compounds in the water-soluble (WS) fraction, detected by gas chromatography (GC), were quantified using the relative response factor (RRF). RRF is defined by

$$\mathrm{RRF} = \frac{A_i \times C_{IS}}{C_i \times A_{IS}} \quad (2)$$

where C is the concentration, A is the peak area, and the subscripts i and IS refer to the analyte and internal standard, respectively.

The RRF of commercially available compounds were determined from experimental data. If the authentic sample was not available, the RRF was predicted following the method described in chapter 2.

3.2.5. Hydrothermal reaction of benzaldehyde

The reaction of benzaldehyde (1 g, Wako Pure Chemical Industries, Ltd.), Fe powder (1.564 g, NM-0029-UP, Ionic Liquids Technologies GmbH), and deionized water (40 g) were carried out under the same condition as other substrates. The filtered reaction mixture was analyzed by GC-MS and GC-FID.

3.2.6. Enzymatic Lignin Preparation

Lignin was isolated by removal of cellulose and hemicellulose through ball-milling pretreatment and subsequent enzymatic saccharification.[15] EFB was introduced into a ball-mill (Simoloyer CM01, Zoz GmbH) and crushed at 1000 rpm for 120 min using 5-mm stainless steel beads. The vessel was kept at 5 °C during milling. Enzymatic saccharification was performed using an enzyme cocktail consisting of

Celluclast® 1.5 L (280 Units/g EFB) and Novozyme 188 (10 Units/g EFB). The crushed EFB (30 g), enzyme cocktail, and 0.1 M sodium acetate buffer (pH 5.0, 260 g) were placed in a plastic container with a lid and then, the reaction mixture was incubated at 50 °C for 21 h with agitation using a shaker. The solid content was collected from the resulting slurry by centrifugation and washed with deionized water. Saccharification was repeatedly performed on the solid residue, and wet enzymatic lignin was obtained in 27 wt% yield as a solid.

3.2.7. Analysis of Carbohydrates and Total Lignin

The compositions of raw EFB and enzymatic lignin were determined using the analytical procedure reported by the National Renewable Energy Laboratory (NREL).[16] Quantification of carbohydrates (cellulose and hemicellulose) and acetic acid was performed by high-performance liquid chromatography (Prominence, Shimadzu) equipped with Aminex® HPX-87H columns (300 mm × 7.8 mm ID, Bio-Rad) and a refractive index detector. The acid-soluble lignin was determined using a UV-visible spectrophotometer (UVmini-1240, Shimadzu), and the acid-insoluble lignin was defined as the ash-free solid residue (Klason lignin).

3.3. Results and Discussion

3.3.1. Hydrothermal Liquefaction of Carbohydrates

3.3.1.1. Effect of Metallic Fe

To investigate the effect of Fe on the HTL of carbohydrates, various carbohydrates including mono- and polysaccharides were reacted under hydrothermal condition (10 wt% substrates, 300 °C, 10 min) both in the presence and absence of Fe.

The results are compared to that for EFB, as shown in Figure 1. Products were collected as four fractions: WS, WI, gaseous products, and SR. In all cases, the addition of Fe significantly increases the yield of WS, and lowers those of WI and SR. As discussed in chapter 1, Fe-assisted HTL of carbohydrates afforded significant amounts of alcohols (hydroxyketones such as hydroxyacetone), which contributed to a higher WS fraction. Retro-aldol condensation of sugars was considered to be promoted by the oxidized Fe generated in situ, and subsequent hydrogenation of the resulting aldehydes afforded alcohols. There is only minor difference between the HTL of cellulose and glucose both in the presence and absence of Fe. This implies that Fe has an insignificant effect on the depolymerization of cellulose to glucose by hydrolysis since this process is known to occur rapidly under hydrothermal condition.[17] The C5 sugar (xylan) exhibits lower WS yield and higher WI yield in the presence of Fe than the C6 sugar. Nevertheless, both C5 and C6 sugars show increased WS yield and suppressed char production after the addition of Fe. These results confirm that Fe is effective for the conversion of the carbohydrate components of biomass feedstocks into the WS fraction. In contrast, Fe has less effect on lignin; compared with carbohydrates, HTL of EFB results in lower WS yield and higher WI yield both in the presence and absence of Fe. Therefore, the lignin in EFB is more likely to be converted to WI rather than WS under hydrothermal condition. This is supported by the fact that the WS fraction produced from HTL of EFB contained only small amounts of phenolic products produced by depolymerization of lignin (see chapter 2).[3] At least Fe is not considered to have the ability to decompose lignin into monomeric units.

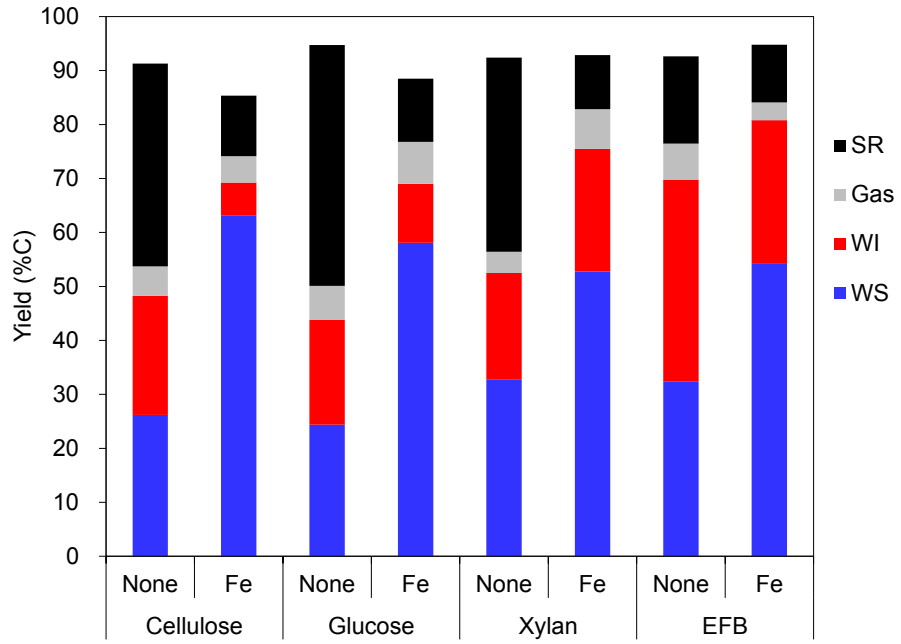

Figure 1. Product yields of HTL of carbohydrates and EFB in the presence and absence of Fe.

3.3.1.2. Effect of Oxidized Fe

A number of studies on the effect of various catalysts in HTL have been reported.[18-21] Bases (e.g., K_2CO_3, KOH) are representative catalysts that promote the hydrolysis of glycosidic linkages and facilitate the endwise depolymerization of carbohydrates.[18] Fe compounds (e.g., $FeCl_3$, Fe_2O_3, $FeSO_4$) also act as catalysts in HTL, which increase the yield of biocrude (WI fraction) while suppressing the formation of char (SR).[21] Hirano and co-workers have demonstrated the transformation of glucose to C3 chemicals in water using oxidized metals or metallic Fe.[22-23] In these works, they considered the oxidized Fe species as a retro-aldol catalyst.[24-26] To investigate the role of oxidized Fe, HTL of glucose using Fe and/or Fe_3O_4 was performed (Figure 2). When Fe_3O_4 is the only additive, the WS yield is higher than that of normal HTL; however, its effect is smaller than that of Fe even though the same amount of additive (based on Fe)

is used. The WI yield increases, while SR production is suppressed, compared with product yields obtained without catalyst loading, which is consistent with the results of other HTL using an oxidized Fe catalyst.[21] However, higher WS yield and lower WI yield are obtained using both additives compared with using Fe alone, indicating the synergistic effect of Fe and Fe_3O_4. The author determined the ratio of the volatile and non-volatile fractions in WS (indicated as light and heavy WS in Figure 2, respectively) using the freeze-dry method. In addition, GC analysis of the WS fraction and quantification of the products were conducted (Figure 3, Table 1). Although a smaller quantity of volatile compounds is detected using Fe_3O_4 compared with using Fe, the WS profile using Fe_3O_4 was different from that using conventional HTL. For example, 4-oxo-pentanoic acid, which is produced by dehydration of glucose, was not detected in the Fe_3O_4 system. On the other hand, small amounts of C2-C4 products were detected. The combination of Fe and Fe_3O_4 was also found to maximize the yield of small molecules. These results indicate that the catalytic activity of oxidized Fe alone is relatively low and only efficiently increases the amount of volatile WS products by coexisting with metallic Fe in the system. Since only Fe is used as an additive in the present system, the concentration of oxidized Fe and consequently, the retro-aldol activity, were initially low. The WS yield can be improved by using oxidized Fe (i.e., incompletely reduced Fe) or other retro-aldol catalysts as co-additive.

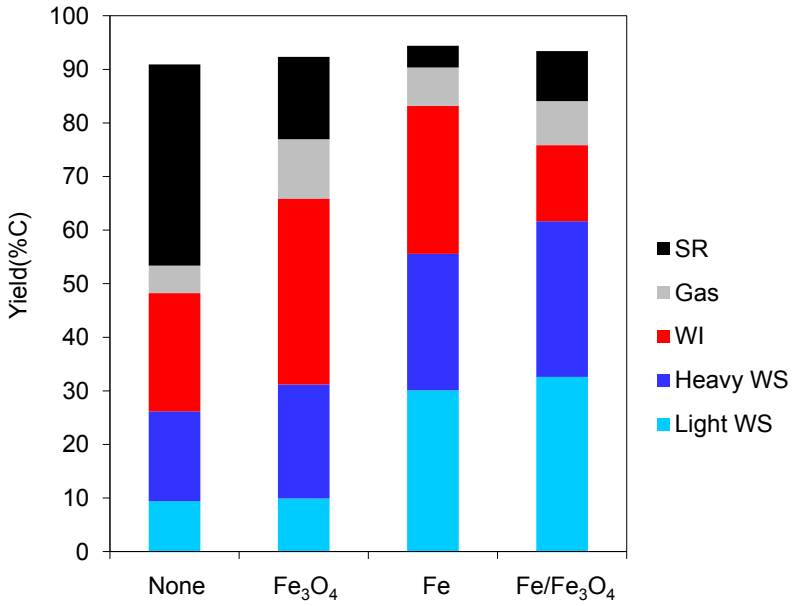

Figure 2. Product profile of HTL of glucose in the absence and presence of various additives (Reaction conditions: Glucose = 4 g, Fe_3O_4 = 0g or 8.646 g, Fe = 0 g or 6.256 g, H_2O = 40 g, initial pressure = 1.0 MPa (N_2), temperature = 300 °C, time = 10 min).

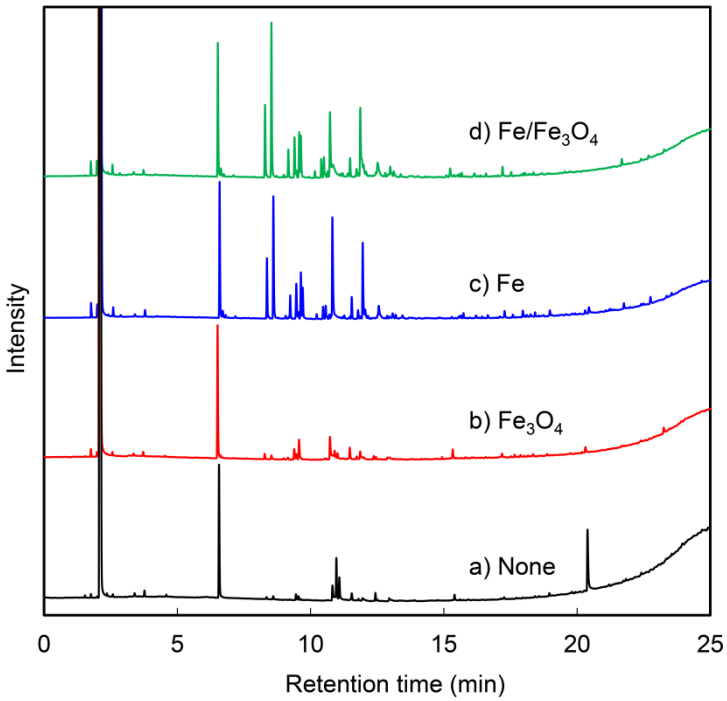

Figure 3. GC-FID chromatograms of the WS fraction from HTL of glucose (a) without additive and in the presence of (b) Fe_3O_4, (c) Fe, and (d) Fe/Fe_3O_4.

Table 1. Quantitative analysis of WS fraction from HTL of glucose[a]

Retention time (min)	compound	none		Fe_3O_4[b]		Fe[c]		Fe + Fe_3O_4[d]	
		Area	Yield (%C)	Area	Yield (%C)	Area	Yield (%C)	Area	Yield (%C)
2.6	2-Butanone	319	0.06	572	0.08	1668	0.23	1884	0.25
2.9	Ethanol					497	0.07	515	0.08
3.4	2-Pentanone	474	0.08	547	0.08	581	0.08	637	0.08
6.7	Cyclopentanone			1094	0.15	1884	0.23	2290	0.28
6.7	2-Methylcyclopentanone			221	0.03	738	0.09	648	0.08
8.3	2-Hydroxy-3-butanone	297	0.05	1272	0.19	12250	1.69	16267	2.21
8.6	Hydroxyacetone	609	0.17	1023	0.23	26579	5.64	34857	7.30
9.6	2-Methyl-2-cyclopenten-1-one			5283	0.73	9626	1.23	9983	1.26
9.7	1-Hydroxy-2-butanone					6999	1.07	10211	1.53
10.2	4-Hydroxy-3-hexanone					973	0.13	1405	0.19
10.5	2-Pentyl-methoxyacetate					2577	0.35	4141	0.56
10.6	4-Heptanol					2822	0.33	4570	0.53
10.6	1-Hydroxy-2-pentanone					1001	0.14	1533	0.21
10.8	Acetic acid	3120	0.86	6504	1.44	30588	6.32	19416	3.95
11	Furfural	7262	1.55	2977	0.51				
11.5	2,5-Hexanedione	1459	0.28	2898	0.44	4441	0.64	4209	0.59
11.9	Propanoic acid	1107	0.23	2927	0.49	17459	2.71	17713	2.72
12.5	Propylene glycol	226	0.05	610	0.10	4624	0.73	1002	0.16
13	1,2-Ethanediol	598	0.14	1033	0.20	445	0.08	797	0.14
13	Butanoic acid			878	0.14				
13.1	γ-Butyrolactone			340	0.05	774	0.10	2265	0.30
15.4	3-Methyl-1,2-cyclopentanedione	995	0.18	2363	0.34			867	0.12
17.3	Phenol	411	0.06	1607	0.19	1673	0.18	2182	0.23
20.4	4-Oxopentanoic acid	12670	2.79	1727	0.30	2029	0.33		
21.8	5-Hydroxymethyl-2-furaldehyde	298	0.06						
	Unknowns		2.85		4.22		7.75		9.84
	Light WS total		9.41		9.91		30.12		32.61

[a]General reaction conditions: Glucose = 4 g, H_2O = 40 g, atmosphere = 1.0 MPa (N_2), temperature = 300 °C, time = 10 min. Yields were calculated as carbon yield based on glucose. [b]Fe_3O_4 = 8.646 g. [c]Fe = 6.256 g. [d]Fe = 6.256 g, Fe_3O_4 = 8.646 g.

3.3.1.3. Hydrogenation by Metallic Fe

As shown in Section 3.1.2, efficient decomposition of sugars is achieved by the combined effects of oxidized and metallic Fe. Unstable carbonyl compounds, especially aldehydes, produced via retro-aldol condensation of sugars can easily undergo recondensation to form insoluble polymers (WI) and char (SR). Fe is considered to reduce these labile intermediates to stable alcohols, which suppresses the formation of byproducts. In chapter 1, the author confirmed that pyruvaldehyde could be

hydrogenated under hydrothermal condition in the presence of Fe to produce hydroxyacetone. According to the literature,[27-29] there are a few possible hydrogenation pathways using zero-valent metal in water (Scheme 1). Pathway (i) is initiated by the attack of a highly active hydrogen radical, generated from metallic Fe and a proton, on the carbonyl group. Pathway (ii) is initiated by hydride transfer from an iron hydride species generated from metallic Fe and a proton. Pathway (iii) involves single-electron transfer from metallic Fe to the substrate as the key step. The hydrogen radical in pathway (i) was originally assigned as the so-called "nascent hydrogen"; however, its existence was rejected by several succeeding studies.[27-28] Fábos and co-wokers proposed pathway (ii) as an alternate explanation for the "nascent hydrogen" in their work on the mechanism of hydrogenation using metallic Fe and acids.[29] The most general explanation for hydrogenation reactions using zero-valent metals is pathway (iii), which is analogous to the Bouveault-Blanc reduction in which esters are converted into alcohols by metallic Na.[30-31] Reduction of aldehydes had also been achieved using Fe, Zn, Mg, Al and Mn as a reductant.[32-36] Mechanism has been proposed in which aldehydes adsorbed on the surface of Fe are reduced by single electron transfer from Fe to form radical intermediates.[34] In addition, The author found that the reaction of benzaldehyde in this hydrothermal reduction system affords benzyl alcohol and diphenyl acetaldehyde as byproduct (Scheme 2. The latter is considered to form through pinacol-type homocoupling of radical intermediates[33, 36-37] and subsequent pinacol rearrangement,[38] which is circumstantial evidence for the generation of radical intermediates. According to these considerations, the author concludes that pathway (iii) is the most plausible route for the present reaction system.

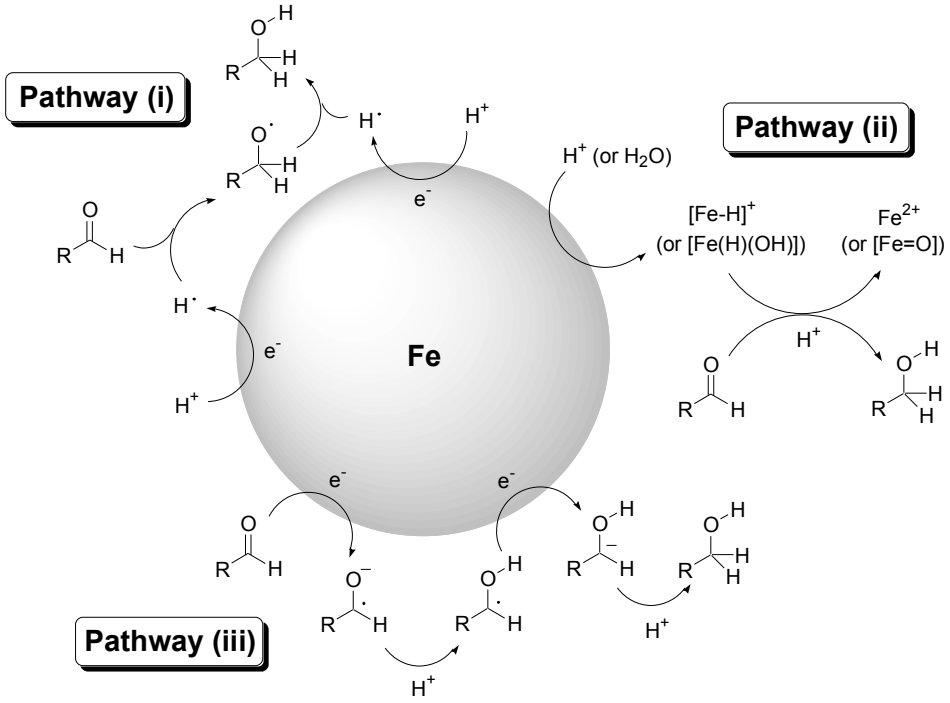

Scheme 1. Possible pathways of hydrogenation by metallic Fe under hydrothermal condition

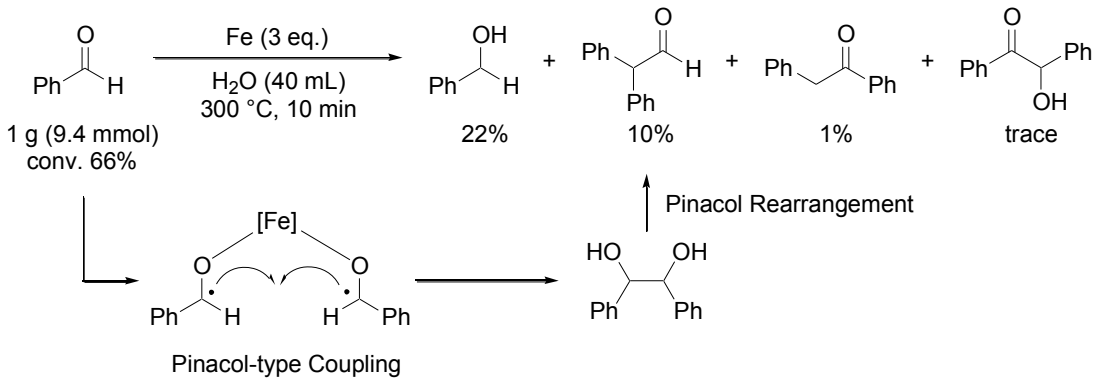

Scheme 2. Product yields and plausible mechanism of hydrothermal reaction of benzaldehyde.

It should be noted that H_2 does not participate in hydrogenation in any of the three pathways despite being present in the gas phase of Fe-assisted HTL of biomass due to the direct reaction of Fe and water ($3Fe + 4H_2O \rightarrow Fe_3O_4 + 4H_2$). The author

estimated how much the reducing capacity of Fe was used for the reduction of the products. The balance of elements in the starting material, products [WS, water-insoluble (WI), gas, and solid residue (SR)], and byproducts of hydrothermal liquefaction of oil palm empty fruit bunch (EFB) is summarized in Table 2. Elemental compositions were calculated using carbon yields and elemental ratios analyzed in chapter 2 (Table 3). The hydrogen generated from Fe was calculated assuming the reaction $3Fe + 4H_2O \rightarrow Fe_3O_4 + 4H_2$. Oxidation degrees of Fe were estimated using Rietveld X-ray diffraction (XRD) quantification of raw and spent iron powder (Table 4). The hydrogen and oxygen contents in SR could not be determined because of the interference of oxygen contained in oxidized Fe mixed in SR. H_2O produced through dehydration of alcoholic products could not be quantified since the solvent was also H_2O. Therefore, it was impossible to completely balance the elements before and after the reaction. However, the total elemental compositions of the products, excluding those that cannot be calculated, do not largely diverge from those of the starting materials, indicating that the calculated values can be considered reasonable. On the basis of the calculations, the hydrogen expected to be generated from Fe is 182 mmol as H atom. The author assumes this amount is the reducing capacity of Fe. On the other hand, the H_2 in gas phase, quantified by GC-TCD after the reaction, is 93 mmol as H atom. Considering the difference between expected and generated H_2 in the gas phase, the author estimates that, in the HTL of EFB, about half of the reducing capacity of Fe was used for the reduction of the products, while the remaining half was used for the reaction with water to generate H_2. To efficiently utilize the reducing capacity of Fe, other hydrogenation catalysts are required.

Table 2. Elemental compositions of substrates and products of Fe-assisted HTL of EFB[a]

			Elemental composition (mmol)		
			C	H	O
Before Reaction	EFB		148	188	114
	Expected H_2 from Fe[b]		-	182	-
	Before Reaction total		148	370	114
After Reaction	Products	WS	83	141	47
		WI	34	42	8
		Gas	6	1	10
		SR	15	N/A	N/A
		total	138	184	65
	H_2 in gas phase[c]		-	93	-
	H_2O		-	N/A	N/A
	After Reaction total		138	277	65

[a]Reaction conditions: EFB = 4 g, Fe =6.256 g, H_2O = 40 g, initial pressure = 1.0 MPa (N_2), temperature = 300 °C, time = 10 min. [b]$3Fe + 4H_2O \rightarrow Fe_3O_4 + 4H_2$. [c]Quantified by GC-TCD.

Table 3. Carbon yield and elemental ratio of each product from HTL of EFB[a]

	Yield (%C)	H/C	O/C
WS	56	1.7	0.57
WI	23	1.24	0.23
Gas[b]	4	0.21	1.68
SR	10	N/A	N/A
total	93		

[a]Reaction conditions: EFB = 4 g, Fe = 6.256 g, H_2O = 40 g, initial pressure = 1.0 MPa (N_2), temperature = 300 °C, time = 10 min. Yields were calculated as carbon yield based on EFB. Data are from reference 1. [b]H/C and O/C ratios were calculated on the basis of GC analysis.

Table 4. Rietveld XRD quantification of raw and spent Fe powder[a]

	Fe	Fe_3O_4
Raw Fe	70.6	29.4
Spent Fe (SR of HTL)	9.8	90.2

[a]XRD patterns were collected by the Rigaku SmartLab X-ray diffractometer using CuKα radiation at a voltage of 45 kV and current of 200 mA. Divergence slit = 1º, vertical divergence limitation = 20 mm, 2θ = 5–90º, step width = 0.02º, scanning speed = 5º min^{-1}. Reitveld analysis was conducted using the Rigaku-manufactured integrated X-ray powder diffraction software PDXL ver. 2.1.

3.3.2. Effect of Fe on HTL of Lignin

3.3.2.1. Preparation of Enzymatic Lignin

To evaluate the reactivity of lignin in HTL of lignocellulosic biomass and the effect of Fe, it is crucial to examine the reaction of pure lignin. However, there are no known methods to isolate lignin in its natural form. Commercially available lignins (e.g., alkali lignin, lignosulfonic acid) have undergone strong alkali and high-temperature treatments. Under these harsh conditions, deconstruction of ether bonds (β-O-4 bond cleavage) and condensation (C–C bond formation) simultaneously occur,[39] making these substrates unsuitable for accurate evaluation of HTL of lignin. Therefore, the author chose enzymatic lignin as the model substrate for HTL. It is prepared by ball-milling of raw biomass and subsequent enzymatic hydrolysis of carbohydrates. The lignin produced by this process is known to have a structure relatively close to that of natural lignin and is sometimes used as model substrate for lignin depolymerization.[40-41] The composition of the prepared enzymatic lignin was determined using the NREL method[16] and is summarized in Figure 4. The amount of lignin is the sum of

acid-soluble and acid-insoluble fractions. Compared with the raw material before enzymatic hydrolysis, enzymatic lignin has a significantly reduced proportion of C6 and C5 carbohydrates, although its lignin content increases from 27% to 61% by weight.

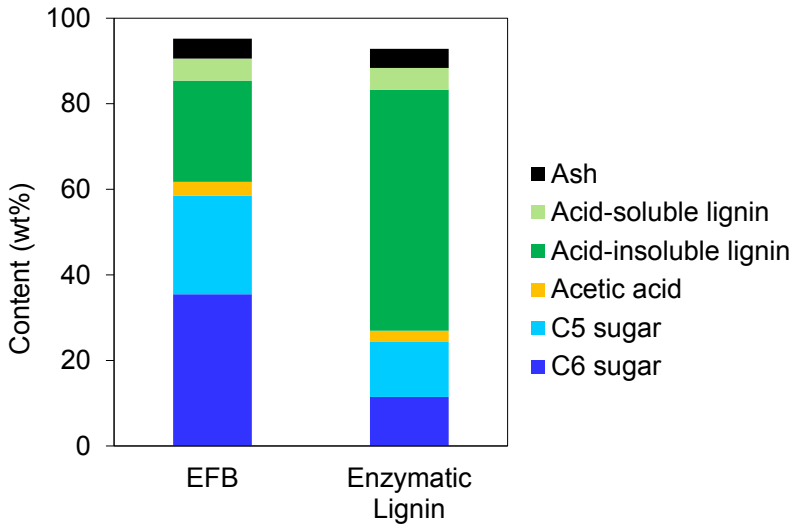

Figure 4. Compositions of EFB and enzymatic lignin determined using the NREL method.

3.3.2.2. Effect of Lignin Concentration on HTL

The reactivity of lignin in HTL in the presence and absence of Fe was estimated by testing various substrates with different lignin contents: (A) a mixture of cellulose and xylan (6:4 by weight, the same proportion in EFB, 0% lignin), (B) EFB (27% lignin), and (C) enzymatic lignin (61% lignin). In addition, (D) alkali lignin (100% lignin) was used as the reference sample. The product yields are summarized in Table 5, and plots of each product yield versus lignin content are shown in Figure 5.

Table 5. Hydrothermal liquefaction of model substrates bearing various lignin contents[a]

Substrate	Lignin content (%)	Fe (g)	Yields (%C)				Carbon Balance (%C)
			WS	WI	Gas	SR	
(A) Cellulose/Xylan (6:4)	0	1.564	94	1	2	4	101
(A) Cellulose/Xylan (6:4)	0	0	60	22	5	6	94
(B) EFB	27	1.564	69	15	5	8	97
(B) EFB	27	0	51	31	6	6	94
(C) Enzymatic lignin	61	1.564	43	35	4	11	93
(C) Enzymatic lignin	61	0	34	40	5	13	93
(D) Alkali lignin	100	1.564	18	65	1	17	103
(D) Alkali lignin	100	0	14	56	1	31	102

[a]Reaction conditions: Substrates = 1 g (as solid), H_2O = 40 g, atmosphere = 1.0 MPa (N_2), temperature = 300 °C, time = 10 min. Yields were calculated as carbon yield based on the starting materials.

The yields using the mixture of cellulose and xylan (A) are similar to those using cellulose or xylan alone. There are significant differences between the WS and WI yields of Fe-assisted and conventional HTL. On the other hand, for lignin-containing substrates (B and C), the WS yield decreases linearly, while the WI yield increases linearly, with lignin content, and the difference between the product yields of Fe-assisted and conventional HTL is smaller. In the presence of Fe, enzymatic lignin affords only 9% higher WS fraction and 5% lower WI fraction compared with the product yields obtained in conventional HTL. When each yield is extrapolated to 100% lignin content, there is only minor difference between Fe-assisted and conventional HTL. The reaction of alkali lignin (D) results in low WS yield as well as high WI yield, which are close to the extrapolated values (Table 5). In all cases, small amounts of phenolic compounds, which are the products of lignin depolymerization, were observed

in WI by GC analysis. These results indicate that lignin is easily converted to the WI fraction through the HTL process owing to their high molecular weight and hydrophobicity, and Fe is not effective for depolymerizing lignin to small compounds. In addition, the elemental compositions of WI from Fe-assisted and conventional HTL, determined by CHN analysis, were almost the same, showing that hydrodeoxygenation of lignin did not proceed after the addition of Fe. Based on the aforementioned results, Fe as an additive is considered to exhibit insignificant effect on the HTL of lignin in biomass feedstocks.

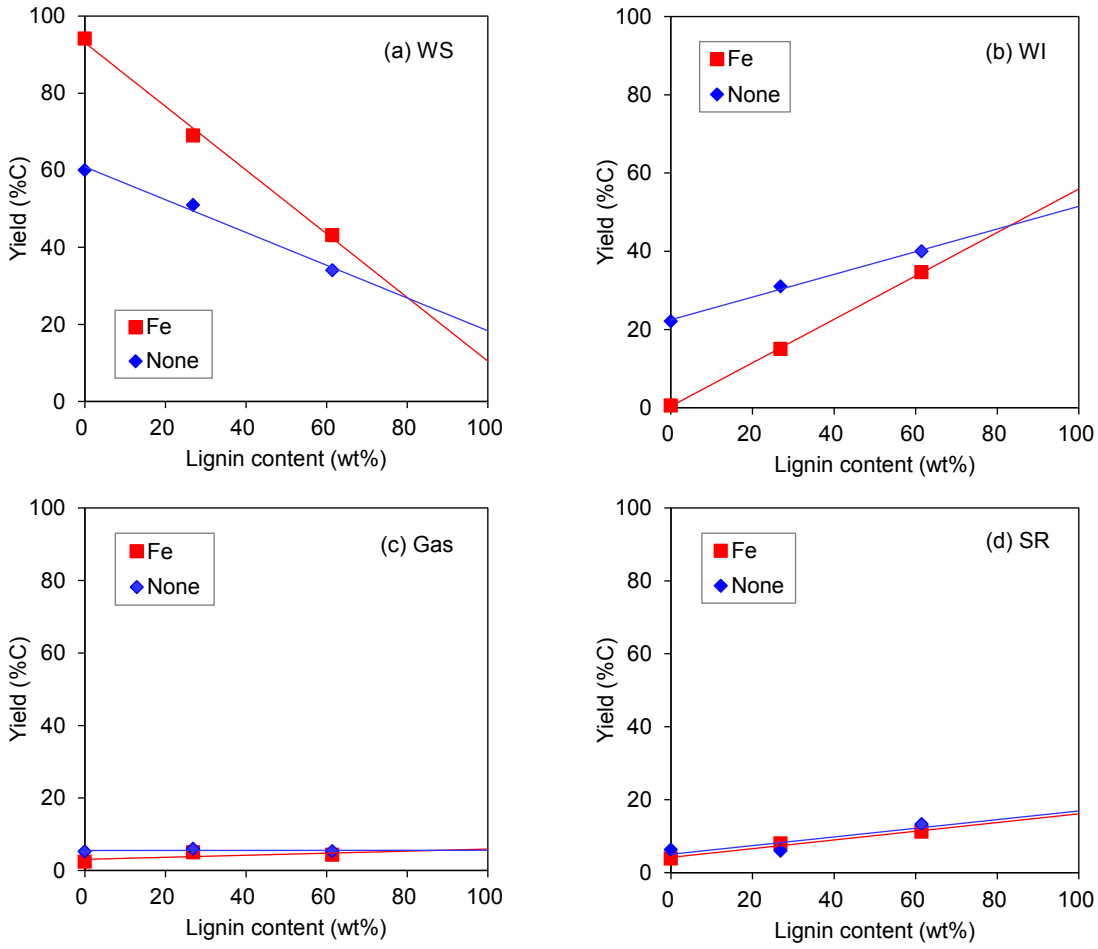

Figure 5. Product yields from HTL at various lignin contents of model substrates: 0% (6:4 mixture of cellulose/xylan), 27% (EFB), and 61% (enzymatic lignin). (a) WS, (b) WI, (c) Gas, and (d) SR fractions.

3.3.3. Contribution of Each Component of EFB to Fe-Assisted HTL Yields

After evaluating the reactivity of all components of the biomass, the author estimated the material balance of Fe-assisted HTL. The composition of 4 g of EFB determined using the NREL method is shown in Table 6. The yields of Fe-assisted HTL of individual components at quantities close to their concentrations in EFB are summarized in Table 7. Using the data in Tables 6 and 7, the contributions of each component to each fraction were calculated and summed to obtain the estimated yield of Fe-assisted HTL of EFB (Table 8). These estimated values are close to the actual performance of Fe-assisted HTL of EFB (Figure 6). Therefore, the Fe-assisted reaction of EFB can be approximated by summing the reaction of individual components. Table 8 reveals the breakdown of the products from each component, showing that cellulose and xylan mainly contribute to the WS yield, whereas the amount of WS products derived from lignin is small.

Table 6. Composition of EFB (4 g)[a]

	Content (wt%)	Weight (g)
Cellulose	39	1.4
Xylan	23	0.9
Lignin[b]	29	1.2
Total	87	3.4

[a]Determined using NREL method. [b]Sum of acid-soluble and acid-insoluble lignin.

Table 7. HTL of model substrates in the presence of Fe [a]

	Substrate	Product Yields (%C/Substrate)				Carbon Balance
	(g)	WS	WI	Gas	SR	(%C)
Cellulose	1.5	77	2	6	4	89
Xylan	1	80	4	7	3	94
Lignin[b]	1	11	56	6	16	89

[a]Reaction conditions: H_2O = 40 g, Fe = 1.564 g/substrate, atmosphere = 1.0 MPa (N_2), temperature = 300 °C, time = 10 min. Yields were calculated as carbon yield based on the starting materials. [b]Yields were estimated from Figure 5 by extrapolating to 100% lignin content.

Table 8. Estimated contributions to the yield of EFB liquefaction (%C) [a]

	Contribution (%C/EFB)				Carbon balance
	WS	WI	Gas	SR	(%C)
Cellulose	26	1	2	1	30
Xylan	18	1	1	1	21
Lignin	4	22	2	6	34
Total	48	24	5	8	85

[a]Contribution of each component was calculated by multiplying the carbon content of the component in EFB by its HTL yield.

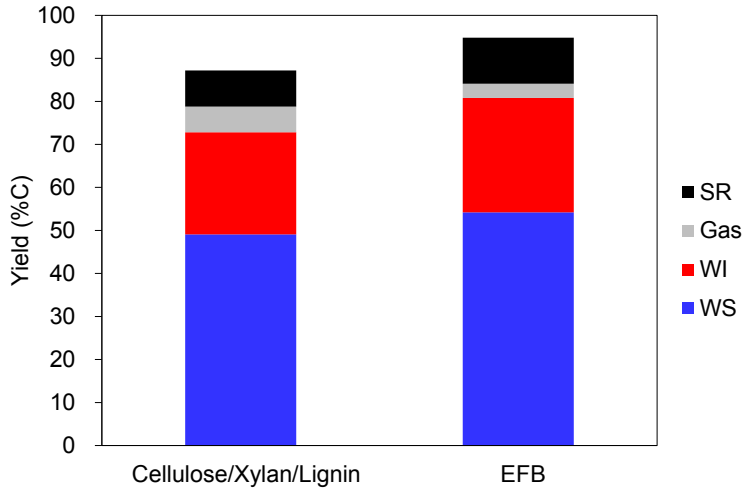

Figure 6. Yields estimated from HTL of each model substrate (cellulose, xylan, and lignin) (left) and obtained from HTL of EFB (right).

3.3.4. Proposed Overall Reaction Pathway

On the basis of reaction routes investigated herein and chapter 1 and 2, the author proposes the overall reaction pathway shown in Scheme 3. Polysaccharides (cellulose and hemicellulose) are rapidly hydrolyzed under hydrothermal condition to C6 and C5 sugars. These sugars isomerize between their aldose and ketose forms and are cleaved through retro-aldol condensation catalyzed by oxidized Fe. The resulting C2-C4 intermediates easily undergo isomerization (keto-enol tautomerization), dehydration/hydration, or recondensation owing to the presence of the carbonyl group, which makes the reaction system more complex. Recondensation increases the fractions of insoluble polymers (WI) and char (SR). However, hydrogenation in the presence of zero-valent Fe converts unstable aldehydes to alcohols, which are stable under hydrothermal condition and consequently increases the WS fraction. In contrast, lignin is hardly depolymerized in the present Fe-assisted system and therefore recovered largely as the WI fraction.

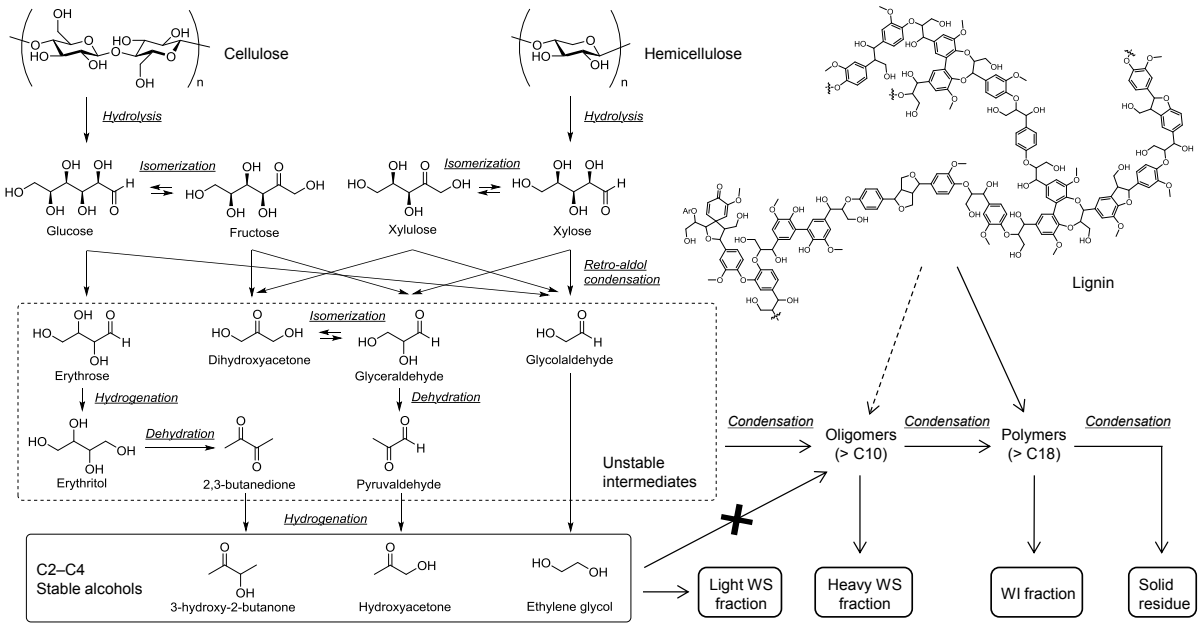

Scheme 3. Plausible overall reaction pathway of Fe-assisted HTL of lignocellulosic biomass

3.4. Conclusions

Metallic Fe and oxidized Fe generated in situ worked synergistically in HTL of biomass to increase the quantity of light compounds in the WS fraction. Oxidized Fe accelerated retro-aldol condensation of sugars, while Fe suppressed the recondensation of unstable intermediates. The Fe additive had minor effect on the degradation of enzymatic lignin. The material balance of Fe-assisted HTL of biomass was estimated from the reactions of individual model substrates. This HTL system can efficiently convert polysaccharides (e.g., cellulose and hemicellulose) to small compounds that can be used as feedstocks for production of specialty chemicals. Identification of reaction mechanisms will aid in the optimization of reaction conditions and development of a total reaction system.

3.5. References

1. Gollakota, A. R. K.; Kishore, N.; Gu, S., A Review on Hydrothermal Liquefaction of Biomass. *Renew. Sust. Energy Rev.* **2018,** *81*, 1378–1392.
2. Kumar, M.; Olajire Oyedun, A.; Kumar, A., A Review on the Current Status of Various Hydrothermal Technologies on Biomass Feedstock. *Renew. Sust. Energy Rev.* **2018,** *81*, 1742–1770.
3. Toor, S. S.; Rosendahl, L.; Rudolf, A., Hydrothermal Liquefaction of Biomass: A Review of Subcritical Water Technologies. *Energy* **2011,** *36* (5), 2328–2342.
4. Sun, P.; Heng, M.; Sun, S.-H.; Chen, J., Analysis of Liquid and Solid Products from Liquefaction of Paulownia in Hot-Compressed Water. *Energy Convers. Manage.* **2011,** *52* (2), 924–933.
5. Madsen, R. B.; Biller, P.; Jensen, M. M.; Becker, J.; Iversen, B. B.; Glasius, M., Predicting the Chemical Composition of Aqueous Phase from Hydrothermal Liquefaction of Model Compounds and Biomasses. *Energy Fuels* **2016,** *30* (12), 10470–10483.
6. Biller, P.; Madsen, R. B.; Klemmer, M.; Becker, J.; Iversen, B. B.; Glasius, M., Effect of Hydrothermal Liquefaction Aqueous Phase Recycling on Bio-Crude Yields and Composition. *Bioresour. Technol.* **2016,** *220*, 190–199.
7. Klemmer, M.; Madsen, R. B.; Houlberg, K.; Mørup, A. J.; Christensen, P. S.; Becker, J.; Glasius, M.; Iversen, B. B., Effect of Aqueous Phase Recycling in Continuous Hydrothermal Liquefaction. *Ind. Eng. Chem. Res.* **2016,** *55* (48), 12317–12325.
8. Ramos-Tercero, E. A.; Bertucco, A.; Brilman, D. W. F., Process Water Recycle in Hydrothermal Liquefaction of Microalgae to Enhance Bio-Oil Yield. *Energy*

Fuels **2015,** *29* (4), 2422–2430.

9. Tommaso, G.; Chen, W. T.; Li, P.; Schideman, L.; Zhang, Y., Chemical Characterization and Anaerobic Biodegradability of Hydrothermal Liquefaction Aqueous Products from Mixed-Culture Wastewater Algae. *Bioresour. Technol.* **2015,** *178*, 139–46.

10. Cherad, R.; Onwudili, J. A.; Biller, P.; Williams, P. T.; Ross, A. B., Hydrogen Production from the Catalytic Supercritical Water Gasification of Process Water Generated from Hydrothermal Liquefaction of Microalgae. *Fuel* **2016,** *166*, 24–28.

11. Wu, K.; Yang, M.; Chen, Y.; Pu, W.; Hu, H.; Wu, Y., Aqueous-Phase Ketonization of Acetic Acid over Zr/Mn Mixed Oxides. *AlChE J.* **2017,** *63* (7), 2958–2967.

12. Maddi, B.; Panisko, E.; Wietsma, T.; Lemmon, T.; Swita, M.; Albrecht, K.; Howe, D., Quantitative Characterization of Aqueous Byproducts from Hydrothermal Liquefaction of Municipal Wastes, Food Industry Wastes, and Biomass Grown on Waste. *ACS Sustain. Chem. Eng.* **2017,** *5* (3), 2205–2214.

13. Vispute, T. P.; Zhang, H. Y.; Sanna, A.; Xiao, R.; Huber, G. W., Renewable Chemical Commodity Feedstocks from Integrated Catalytic Processing of Pyrolysis Oils. *Science* **2010,** *330* (6008), 1222–1227.

14. Zhang, H.; Cheng, Y.-T.; Vispute, T. P.; Xiao, R.; Huber, G. W., Catalytic Conversion of Biomass-Derived Feedstocks into Olefins and Aromatics with ZSM-5: The Hydrogen to Carbon Effective Ratio. *Energy Environ. Sci.* **2011,** *4* (6), 2297–2307.

15. Zhang, Y.; Yang, L.; Wang, D.; Li, D., Structure Elucidation and Properties of

Different Lignins Isolated from Acorn Shell of Quercus Variabilis Bl. *Int. J. Biol. Macromol.* **2018,** *107* (Pt A), 1193–1202.

16. Sluiter, A.; Hames, B.; Ruiz, R.; Scarlata, C.; Sluiter, J.; Templeton, D.; Crocker, D. *Determination of Structural Carbohydrates and Lignin in Biomass*; Laboratory Analytical Procedure (LAP), NREL/TP-510-42618; National Renewable Energy Laboratory: Revised 2012.
17. Ehara, K.; Saka, S., Decomposition Behavior of Cellulose in Supercritical Water, Subcritical Water, and Their Combined Treatments. *J. Wood Sci.* **2005,** *51* (2), 148–153.
18. Singh, R.; Balagurumurthy, B.; Prakash, A.; Bhaskar, T., Catalytic Hydrothermal Liquefaction of Water Hyacinth. *Bioresour. Technol.* **2015,** *178*, 157–165.
19. Nazari, L.; Yuan, Z.; Souzanchi, S.; Ray, M. B.; Xu, C., Hydrothermal Liquefaction of Woody Biomass in Hot-Compressed Water: Catalyst Screening and Comprehensive Characterization of Bio-Crude Oils. *Fuel* **2015,** *162*, 74–83.
20. Xu, C.; Etcheverry, T., Hydro-Liquefaction of Woody Biomass in Sub- and Super-Critical Ethanol with Iron-Based Catalysts. *Fuel* **2008,** *87* (3), 335–345.
21. Li, H.; Hurley, S.; Xu, C., Liquefactions of Peat in Supercritical Water with a Novel Iron Catalyst. *Fuel* **2011,** *90* (1), 412–420.
22. Hirano, Y.; Sagata, K.; Kita, Y., Selective Transformation of Glucose into Propylene Glycol on Ru/C Catalysts Combined with Zno under Low Hydrogen Pressures. *Appl. Catal., A* **2015,** *502*, 1–7.
23. Hirano, Y.; Kasai, Y.; Sagata, K.; Kita, Y., Unique Approach for Transforming Glucose to C3 Platform Chemicals Using Metallic Iron and a Pd/C Catalyst in Water. *Bull. Chem. Soc. Jpn.* **2016,** *89* (9), 1026–1033.

24. Baeza, A.; Guillena, G.; Ramón, D. J., Magnetite and Metal-Impregnated Magnetite Catalysts in Organic Synthesis: A Very Old Concept with New Promising Perspectives. *ChemCatChem* **2016,** *8* (1), 49–67.

25. Ramón, D.; Cano, R.; Yus, M., Unmodified Nano-Powder Magnetite or Iron(Iii) Oxide Catalyze the Easy and Fast Synthesis of 4-Substituted-4*H*-Pyrans. *Synlett* **2011,** *2011* (14), 2017–2020.

26. Watanabe, H.; Seto, J., The Catalysis of Maghemite and Hematite on the Aldol and the Retro-Aldol Condensation of Acetone. *Bull. Chem. Soc. Jpn.* **1991,** *64* (8), 2411–2415.

27. Laborda, F.; Bolea, E.; Baranguan, M. T.; Castillo, J. R., Hydride Generation in Analytical Chemistry and Nascent Hydrogen: When Is It Going to Be Over? *Spectrochim. Acta, Part B* **2002,** *57* (4), 797–802.

28. Meija, J.; D'Ulivo, A., Solution to Nascent Hydrogen Challenge. *Anal. Bioanal. Chem.* **2008,** *392* (5), 771–772.

29. Fábos, V.; Yuen, A. K. L.; Masters, A. F.; Maschmeyer, T., Exploring the Myth of Nascent Hydrogen and Its Implications for Biomass Conversions. *Chem. Asian J.* **2012,** *7* (11), 2629–2637.

30. Bouveault, L.; Blanc, G., Préparation Des Alcools Primaires Au Moyen Des Acides Correspondants. *Compt. Rend.* **1903,** *136*, 1676–1678.

31. Bouveault, L.; Blanc, G., Transformation Des Acides Monobasiques Saturés Dans Les Alcools Primaires Correspondants. *Bull. Soc. Chim. Fr.* **1904,** *31*, 666–672.

32. Clarke, H. T.; Dreger, E. E., N-Heptyl Alcohol. *Org. Synth.* **1926,** *6*, 52–53.

33. Mandal, T.; Jana, S.; Dash, J., Zinc-Mediated Efficient and Selective Reduction

of Carbonyl Compounds. *Eur. J. Org. Chem.* **2017,** *2017* (33), 4972–4983.

34. Zhang, W.-C.; Li, C.-J., Magnesium-Mediated Carbon−Carbon Bond Formation in Aqueous Media: Barbier−Grignard Allylation and Pinacol Coupling of Aldehydes. *J. Org. Chem.* **1999,** *64* (9), 3230–3236.

35. Wei-Bo, W.; Li-Lan, S.; Yao-Zeng, H., A Novel Reduction System — $SbCl_3$-Al/ or $SbCl_3$-Zn/DMF-H_2O for Conversion of Aldehydes to Alcohols. *Tetrahedron Lett.* **1990,** *31* (8), 1185–1186.

36. Jiménez, T.; Barea, E.; Oltra, J. E.; Cuerva, J. M.; Justicia, J., Mn(0)-Mediated Chemoselective Reduction of Aldehydes. Application to the Synthesis of A-Deuterioalcohols. *J. Org. Chem.* **2010,** *75* (20), 7022–7025.

37. Li, C.-J., Organic Reactions in Aqueous Media with a Focus on Carbon−Carbon Bond Formations: A Decade Update. *Chem. Rev.* **2005,** *105* (8), 3095–3166.

38. Amedio, J. C.; Bernard, P. J.; Fountain, M.; VanWagenen, G. A., Practical Preparation of 4,4-Diphenylcyclohexanol: A Key Intermediate in the Synthesis of Ms-325. *Synth. Commun.* **1998,** *28* (20), 3895–3906.

39. Chakar, F. S.; Ragauskas, A. J., Review of Current and Future Softwood Kraft Lignin Process Chemistry. *Ind. Crops Prod.* **2004,** *20* (2), 131–141.

40. Jääskeläinen, A. S.; Sun, Y.; Argyropoulos, D. S.; Tamminen, T.; Hortling, B., The Effect of Isolation Method on the Chemical Structure of Residual Lignin. *Wood Sci. Technol.* **2003,** *37* (2), 91–102.

41. Shen, X.-J.; Wen, J.-L.; Huang, P.-L.; Zheng, K.; Wang, S.-F.; Liu, Q.-Y.; Charlton, A.; Sun, R.-C., Efficient and Product-Controlled Depolymerization of Lignin Oriented by Raney Ni Cooperated with $Cs_xH_{3-x}PW_{12}O_{40}$. *BioEnergy Res.* **2017,** *10* (4), 1155–1162.

Chapter 4. Fe-assisted hydrothermal liquefaction of cellulose: Effects of hydrogenation catalyst addition on properties of water-soluble fraction

4.1. Introduction

Biomass features the advantages of renewability, carbon neutrality, and high energy potential, and is therefore a promising substitute of fossil resources.[1-5] Consequently, numerous biochemical (fermentation) and thermochemical (gasification, pyrolysis, and hydrothermal liquefaction (HTL)) processes have been developed for the conversion of biomass into fuels and chemical feedstocks. In particular, HTL, which is a promising method of converting energy-rich biomass into bio-oil and is carried out in aqueous media at moderate temperatures (280–370 °C) and high pressures (10–25 MPa), does not require energy-intensive dewatering/pre-drying steps and is thus suitable for substrates with relatively high moisture contents.[6-15] Typically, the HTL of biomass affords four fractions, namely the water-soluble (WS) fraction, the water-insoluble (WI) fraction (bio-oil or biocrude), solid residue (char), and gases. Bio-oil obtained by HTL is rich in oxygenated compounds and therefore cannot be directly used in oil refineries, requiring an upgrade before use as a fuel or chemical feedstock.

Both homogenous and heterogeneous catalysts have been employed to improve the yield and quality of HTL-produced bio-oil.[16-30] For instance, homogeneous catalysts such as inorganic acids (H_3PO_4, HCOOH, CH_3COOH, $HClO_4$, HCl, and H_2SO_4) and alkalis (Na_2CO_3, NaOH, K_2CO_3, KOH, and $Ca(OH)_2$) suppress char formation and enhance the yield of bio-oil, although they do not have any effect on bio-oil quality. In contrast, metals (Pt, Pd, Ru, Ni, and Co) as heterogeneous hydrogenation catalysts and metal oxides (MgO, Al_2O_3, CaO, MnO, NiO, CuO, ZnO, ZrO_2, SnO, La_2O_3, CeO_2,

zeolites, and mixed oxides) as heterogeneous solid acid-base catalysts can improve both the yield and quality of bio-oil. The improvement of bio-oil quality in the presence of heterogeneous catalysts has been ascribed to their promotional effects on dehydration, decarbonylation, decarboxylation, hydrogenation, and hydrogenolysis reactions. However, as the choice of catalyst depends on the biomass feedstock and reaction conditions, further studies are needed to identify catalysts suitable for achieving the desired yield and quality of bio-oil produced by biomass HTL and to elucidate the mechanism of this quality improvement.[13]

From the viewpoint of making the whole HTL process commercially feasible, the utilization of the biomass HTL–produced WS fraction has attracted little attention.[31] Although the WS fraction produced by biomass HTL has not been extensively investigated, several studies on its anaerobic digestion,[32] gasification,[33] ketonization,[34] and hydroprocessing[35] have been reported. As described in chapter 1, the author has demonstrated that when the HTL of lignocellulosic biomass is performed in the presence of metallic Fe powder, char formation is dramatically suppressed and the yield of the WS fraction is significantly increased. Moreover, the catalytic cracking of the thus produced WS fraction over a zeolite catalyst affords high amounts of light olefins and BTX (benzene, toluene, and xylene) as basic chemicals. The author has also investigated the HTL of cellulose, hemicellulose, and lignin as model lignocellulose substrates and proposed an overall reaction pathway for the Fe-assisted HTL of lignocellulosic biomass, suggesting that metallic Fe and in situ generated Fe oxides synergistically promote the formation and hydrogenation of light compounds in the WS fraction. However, in order for biomass HTL to be economically viable, the efficiency of the system needs to be improved so that the yield and quality of the WS fraction get

further enhanced. A key challenge for Fe-assisted HTL is considered to be increasing the utilization efficiency of Fe.

Herein, the author investigated the effects of heterogeneous metal catalysts (Pd, Pt, Ru, Co, Ni, and Cu) on the yield and quality (e.g., hydrogen-to-effective-carbon ratio (H/C_{eff}) and the proportion of volatiles) of the WS fraction produced by Fe-assisted HTL of cellulose. Moreover, the author examined the conversion of the thus obtained WS into light olefins (ethylene, propylene, butene) and BTX by catalytic cracking and proposed a plausible explanation of the beneficial effect of hydrogenation catalysts on the yield and quality of the WS fraction.

4.2. Experimental

4.2.1. Materials

Cellulose (Avicel® PH-101) was purchased from Sigma-Aldrich Co., LLC. Fe powder (99.9%, NM-0029-UP) was purchased from Ionic Liquids Technologies GmbH (Germany). Noble metal–based hydrogenation catalysts (5 wt%-Pd/ Al_2O_3, 5 wt%-Pt/ Al_2O_3, 5 wt%-Ru/Al_2O_3) were purchased from N.E. CHEMCAT Corporation (Japan) and used as received. Transition metal–based hydrogenation catalysts, namely stabilized Ni (SN-250, 56 wt%-Ni/kieselguhr) and Cr-free Cu (KC-1, 48 wt%-CuO/CaO/SiO_2) were supplied by Sakai Chemical Industry Co., Ltd. (Japan). The catalytic cracking catalyst (HZSM-5 zeolite with a Si/Al molar ratio of 24:1) was supplied by Nippon Shokubai Co., Ltd. (Japan). Oxidized Fe was prepared by thermal treatment of Fe powder in water at 250 °C for 1 h, as is described in the next section.

4.2.2. HTL process and HTL product analysis

Cellulose liquefaction and fraction separation procedures were conducted as described in the previous chapter. Typically, cellulose (4.0 g), Fe powder (0 or 6.256 g), metal catalyst (0.400 g), and water (40 g) were loaded into a 100-mL autoclave equipped with an electric heater and an electromagnetic inductive agitator. The autoclave was purged with N_2 for four times to remove air, and the initial pressure (N_2) was set to 1.0 MPa. The reactor was rapidly heated to 250 °C, maintained at this temperature for 1 h at a stirring speed of 700 rpm, and then rapidly cooled to 25 °C by immersion into an ice-water bath. Gaseous products were collected in a gas sampling bag, and WS products were isolated by filtration of the reaction mixture slurry. The filter cake was extracted with acetone, and the extract was concentrated via rotary evaporation at reduced pressure (60 °C, 1 h) to afford the WI fraction. The solid residue (SR) of filtration was dried at 70 °C at reduced pressure overnight and weighed. Product yields and properties were determined as described in previous chapter. A total organic carbon analyzer (Shimadzu, TOC-$L_{CSH/CSN}$) was employed to determine the yield of the WS fraction. Elemental analysis (CHN; Elementar, vario EL cube) was performed to determine the carbon contents of the WI fraction and the SR. Gaseous products were analyzed using a gas chromatograph (Shimadzu, GC-8A) equipped with silica-gel and 5-Å-molecular-sieve columns and a thermal conductivity detector (TCD).

The yields of HTL-produced fractions were calculated as

$$\text{Yield (\%)} = \frac{\text{Moles of carbon in the fraction}}{\text{Moles of carbon in loaded cellulose}} \times 100 \quad (1)$$

4.2.3. Evaluation of WS fraction quality

The quality of the WS fraction (H/C_{eff} ratio and proportion of volatiles) was

evaluated by the methods described in chapter 2. A gas chromatograph (Shimadzu, GC-2014) equipped with a flame ionization detector (FID) and a capillary column (GL Sciences, Inert-cap® WAX-HT, 30 m × 0.25 mm ID × 0.25 μm film thickness) was used to calculate the concentration of each constituent in the WS fraction, and the H/C_{eff} ratio was estimated from the H, O, and C contents summed over all compounds quantified by GC analysis. The relative contents of light and heavy components in crude WS fractions were determined by a freeze-drying method.

4.2.4. Catalytic cracking and cracking product analysis

Catalytic cracking of the WS fraction was performed in a fixed-bed continuous-flow reactor (see chapter 1). Before cracking experiments, the reactor was loaded with HZSM-5 (6.0 mL) and heated at 600 °C for 1 h in a flow of N_2 (50 mL/min). The WS fraction was fed into the reactor at a weight hourly space velocity of 1.1 h^{-1} and a temperature of 600 °C. During the reaction, condensable and non-condensable gaseous products were collected for 120 min using gas wash bottles and gas sampling bottles, respectively. Two gas chromatography systems equipped with a TCD or an FID were employed to quantify CO_2, CO, alkanes (C_1–C_5), light olefins (ethylene, propylene, and butene), and BTX (benzene, toluene, and xylene).

The yields of catalytic cracking products were calculated as

$$\text{Yield}\ (\%) = \frac{\text{Moles of carbon in the product}}{\text{Moles of carbon in the WS-feed fraction}} \times 100 \qquad (2)$$

The yields of water-solubles were determined by the content of water-soluble species condensed in the gas wash bottle via total organic carbon analysis, eliminating the content of BTX carbon. Catalyst coking was rarely observed, and the carbon balances were slightly deficient because of the carbonization of non-volatile compounds

on the vaporizer in the reactor.

4.3. Results and discussion

4.3.1. Effect of hydrogenation catalysts on the HTL of cellulose

Fe-assisted HTL was performed in the presence of various noble and transition metal–based catalysts, and the product yields were compared to those obtained without catalysts in the presence/absence of Fe (Figure 1). The addition of metal catalysts increased the yield of the WS fraction (except for the case of Fe + Ru/Al_2O_3) and almost completely suppressed the formation of the WI fraction compared to those by Fe-assisted HTL, while Fe-assisted HTL remarkably suppressed the SR formation and increased the WS fraction. As a side reaction, Fe reacted with water to generate hydrogen ($3Fe + 4H_2O \rightarrow Fe_3O_4 + 4H_2$) during Fe-assisted HTL. The author has found that hydrogen in the gas phase did not affect the yields of HTL products (see chapter 1). Therefore, the reducing capacity of Fe was not fully utilized in the case of Fe-assisted HTL in the absence of hydrogenation catalyst. The author supposed that added metal catalysts activated gas-phase hydrogen so as to hydrogenate intermediate compounds formed in the WS fraction. As has been discussed in the previous chapter, the increased yield of the WS fraction during Fe-assisted HTL was ascribed to the increased production of hydroxyketones via the retro-aldol condensation of sugars and the subsequent hydrogenation of the resulting aldehydes. Thus, metal catalysts were considered to accelerate the hydrogenation of in situ formed unstable aldehydes, increase the yield of stable hydroxyketones, and suppress the formation of condensation products (WI fraction) to facilitate boosting the WS fraction.

The GC profiles/compositions of WS fractions recorded/determined according to

the method described in chapter 2 are shown in Figure 2/Table 1, respectively. In the presence of Fe + Pd/Al_2O_3, a larger quantity of high-boiling volatile compounds was produced than in the Fe-only case, while only few peaks were observed in the no-catalyst no-Fe profile. Fe-assisted HTL produced hydroxyketones such as 2-hydroxy-3-butanone, 1-hydroxy-2-propanone, and 1-hydroxy-2-butanone, while diol (ethylene glycol, propylene glycol, 2,3-butanediol, and 1,2-butanediol) formation was favored in the case of the Fe + Pd/Al_2O_3 system. Therefore, it was recognized that hydroxyketones were hydrogenated to diols in the presence of Pd/Al_2O_3. The above results indicated that metal catalysts promoted the hydrogenation of unstable intermediates of HTL by using gas-phase hydrogen formed in situ to achieve inhibiting the WI formation and increasing the WS formation.

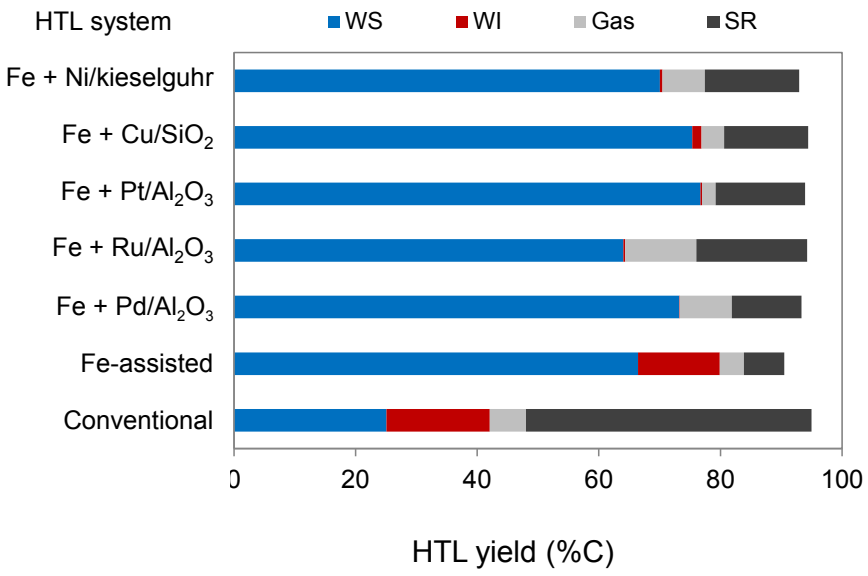

Figure 1. Effects of hydrogenation catalysts on the Fe-assisted HTL of cellulose.

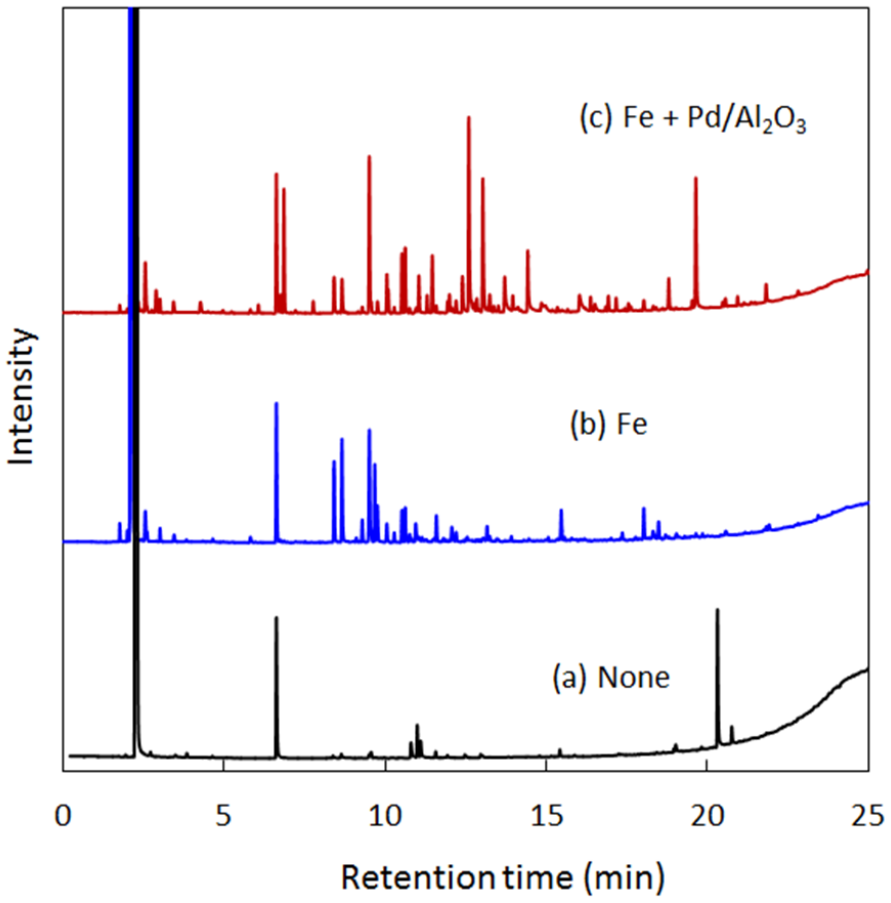

Figure 2. GC profiles of WS fractions produced by cellulose HTL (a) in the absence of additives and in the presence of (b) Fe, and (c) Fe + Pd/Al_2O_3.

Table 1. Quantitative analysis of the WS fraction obtained by cellulose HTL.

Retention time (min)	Compound	Yield[a] (%C)					
		none	Fe	FeO_x	Fe+Pd/Al_2O_3	Pd/Al2O_3+H_2	FeO_x+Pd/Al_2O_3+H_2
2.5	Methanol					0.30%	0.40%
2.6	2-Butanone	0.10%	0.20%	0.20%		0.00%	0.10%
2.9	Ethanol				0.70%		
3.4	2-Pentanone	0.10%	0.20%	0.10%	0.30%	0.10%	0.20%
4.2	Propanol				0.40%		0.10%
6.7	Cyclopentanone		0.10%		0.40%	0.80%	0.50%
6.7	2-Methyl-cyclopentanone		0.00%		2.60%	0.70%	2.00%
8.3	2-Hydroxy-3-butanone (acetoin)	0.10%	2.00%	0.20%	0.90%	0.60%	1.90%
8.6	1-Hydroxy-2-propanone (hydroxyacetone)	0.30%	6.00%	0.70%	2.00%	20.50%	11.20%
9.6	2-Methyl-2-cyclopenten-1-one			0.50%		0.50%	0.20%
9.7	1-Hydroxy-2-butanone		1.10%	0.10%	0.30%	4.90%	2.50%
9.9	Cyclohexanol		0.00%		0.50%		
10.2	4-Hydroxy-3-hexanone		0.20%		0.10%	0.20%	0.20%
10.5	2-Pentyl-methoxyacetate		0.80%	0.10%	1.40%	0.20%	2.80%
10.6	1-Hydroxy-2-pentanone					0.40%	0.90%
10.8	Acetic acid	0.80%	1.10%	1.70%		0.40%	
11.0	Furfural	1.00%		0.30%		0.20%	
11.2	Tetrahydro-2-furanmethanol		0.10%		1.40%	1.20%	1.00%
11.5	2,5-Hexanedione	0.20%	0.70%	0.50%	0.20%	0.80%	0.20%
11.6	2,3-Butanediol	0.10%		0.50%	0.30%		
11.9	Propanoic acid				0.50%	0.20%	0.40%
12.1	2,3-Butanediol				1.30%		
12.5	Propylene glycol (PG)		0.00%		5.90%		0.30%
12.8	1-Ethoxy-3-pentanol		0.00%		0.40%	0.30%	0.10%
13.0	Ethylene glycol (EG)		0.20%	0.10%	5.10%	0.70%	1.60%
13.0	Butanoic acid						
13.1	Butyrolactone		0.10%	0.10%	0.50%	0.30%	0.20%
13.4	1,2-Butanediol				1.70%		
14.5	1,2-Pentanediol			0.10%	0.60%		
15.4	3-Methyl-1,2-cyclopentanedione	0.20%		1.10%		0.80%	0.10%
15.7	1,2-Hexanediol				1.20%		
16.1	1,4-Butanediol				0.40%		0.10%
16.6	1,2-Cyclohexanediol				0.30%		
16.9	Cyclopentane-1,2-diol				0.30%		
17.3	Phenol		0.20%	0.10%			
17.4	Cinnamaldehyde			0.10%			
19.3	1,1'-[Ethylidenebis(oxy)]bis[2-methylpropane]		0.20%		3.70%	1.20%	1.90%
20.4	4-Oxopentanoic acid	5.10%		0.50%			
21.8	5-Hydroxymethyl-2-furaldehyde (5HMF)			0.20%		1.60%	

[a]Yields were calculated based on the carbon content of the loaded cellulose for HTL.

4.3.2. Evaluation of WS fraction quality

The elemental compositions of light WS components were estimated by summing the contents of elements in all compounds quantified by GC and were expressed as H/C, O/C, and H/C_{eff} ratios (Table 2). The H/C_{eff} ratio (eq. 3) is often used to describe the degree of biomass upgrading, with high H/C_{eff} values indicating efficient

reforming.[36] Generally, bio-based feedstocks such as lignocellulose and carbohydrates have H/C_{eff} ratios of 0–0.5, while petroleum-based feedstocks exhibit values of 1.0–2.0. Thus, H/C_{eff} ratios above 1.0 are benchmark for biomass upgrading.

$$H/C_{eff} = \frac{[H]-2[O]}{[C]} \quad (3)$$

Here, [H], [O], and [C] represent the total contents of hydrogen, oxygen, and carbon, respectively, in bio-oil.

Table 2 Evaluation of WS fraction quality.

System	Elemental ratios of light WS fraction components[a]			Relative contents of light and heavy WS	
	H/C	O/C	H/C_{eff}	Heavy	Light
no additive	1.60	0.65	0.30	71	29
Fe	2.00	0.72	0.56	64	36
Fe + Pd/Al_2O_3	2.33	0.50	1.33	37	63
Fe + Ru/Al_2O_3	2.24	0.49	1.25	28	72
Fe + Pt/Al_2O_3	2.21	0.51	1.19	26	74
Fe + Cu/SiO_2	2.04	0.52	0.99	47	53
Fe + Ni/kieselguhr	2.28	0.52	1.23	39	61

[a]Estimated by counting the sum of elements in each compound quantified by GC analysis. [b]Calculated based on the carbon content of the freeze-dried crude WS fraction.

The H/C ratios of light WS components obtained in the presence of hydrogenation catalysts were equal to or higher than those obtained in the Fe-only case, while the corresponding O/C ratios were lower than those obtained in the Fe-only case. Consequently, H/C_{eff} ratios above 1.0 were obtained in the presence of hydrogenation catalysts, with the maximal value (1.33) observed for Pd/Al_2O_3. These results suggest that hydrogenation catalysts can promote the hydrodeoxygenation of intermediates during the Fe-assisted HTL of cellulose and are effective for improving the quality of

the WS fraction. Vispute and co-workers studied the two-step hydrodeoxygenation of the water-soluble fraction of pinewood bio-oil,[35] showing that the upgrading of this fraction via hydrodeoxygenation over a Ru catalyst increased the H/C_{eff} ratio from 0.14 to 0.71. In contrast, present one-step Fe-assisted HTL with a hydrogenation catalyst improved the H/C_{eff} ratio from 0.30 (no additive), 0.56 (Fe only) to 1.33 (Fe + Pd) proving to be more valuable for upgrading WS fraction than the above two-step process.

The relative content of light components in WS fractions (calculated based on the carbon content of freeze-dried crude WS fractions) notably increased when HTL was performed in the presence of hydrogenation catalysts (Table 2), in agreement with the enhanced production of volatiles observed in this case by GC (Figure 2 and Table 1). As the author demonstrated that WS fractions rich in light components afforded light olefins in high yields upon catalytic cracking (see chapter 2), it was expected that the WS fractions obtained by Fe-assisted HTL with hydrogenation catalysts were suitable for producing light olefins via catalytic cracking.

4.3.3. Catalytic cracking of WS fractions

The author conducted catalytic cracking of WS fractions obtained by Fe-assisted HTL of cellulose with various hydrogenation catalysts (Figure 3). Major products were light olefins (ethylene, propylene, and butene), along with minor products such as BTX, alkanes, and CO_x (CO and CO_2).

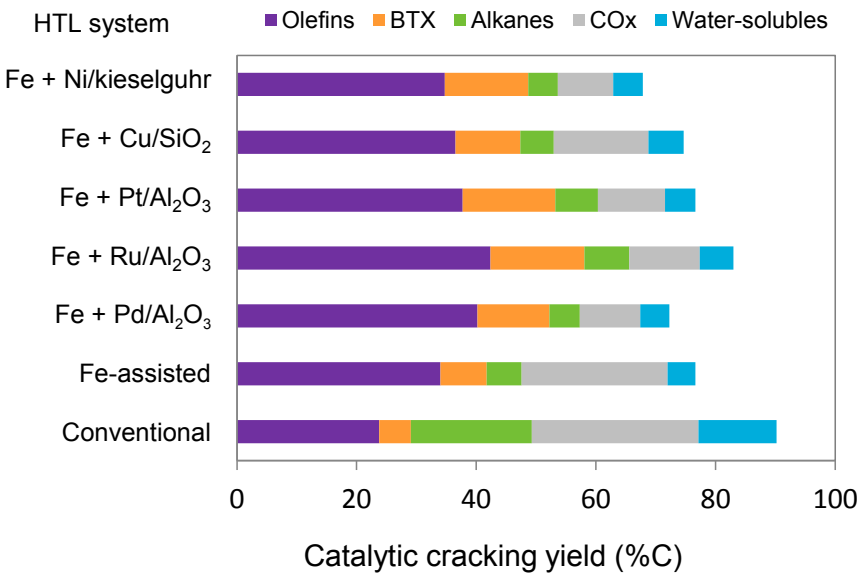

Figure 3. Effect of added catalyst on the catalytic cracking of WS fractions obtained by Fe-assisted HTL of cellulose.

WS fractions obtained by Fe-assisted HTL in the presence of hydrogenation catalysts featured catalytic cracking yields higher than those observed for conventional or Fe-assisted HTL, e.g., the yields of olefins obtained in the case of Pd or Ru catalysts (>40%) exceeded that (34%) obtained for the Fe-only case. Furthermore, the addition of hydrogenation catalysts increased BTX yields. As a consequence, the total yield of hydrocarbons produced by HTL/catalytic cracking equaled 42% for Fe + Pd/Al_2O_3 and Fe + Ru/Al_2O_3 systems, while a value of only 32% was observed for the Fe-only system.

To be suitable for biomass upgrading processes such as catalytic cracking, it is preferable that bio-based feedstocks have high H/C_{eff} ratios.[37] As described in the section 3.2, the H/C_{eff} ratios of light WS components obtained by Fe-assisted HTL in the presence of hydrogenation catalysts were higher than those of light WS components

obtained by Fe-assisted HTL in the absence of catalysts (Table 2). As expected, components with higher H/C_{eff} ratios were more efficiently converted into hydrocarbons during catalytic cracking (Figure 3), with the highest H/C_{eff} ratio and total hydrocarbon yield observed for the Pd/Al_2O_3 catalyst. There was a proportionate relationship between the H/C_{eff} ratios and catalytic cracking yields, in particular, olefins and BTX yields of the WS fractions (Figure 4).

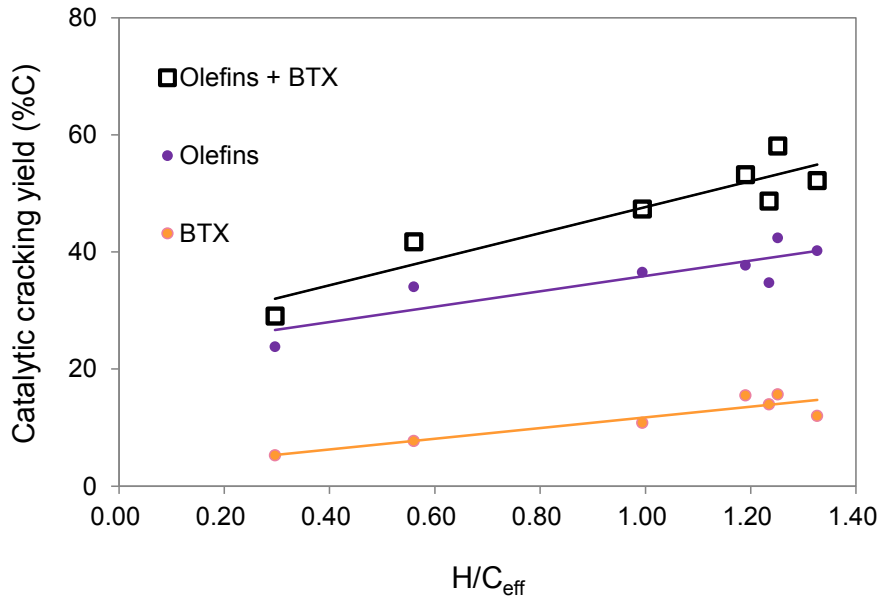

Figure 4. Relationship between the H/Ceff ratios and catalytic cracking yields of the WS fraction on the Fe-assisted HTL of cellulose with hydrogenation catalysts.

According to the results for Fe-assisted HTL of lignocellulose, the WS fraction obtained by Fe-assisted HTL exhibited a higher yield of olefins than that obtained by conventional HTL, due to the increased content of light components in the former fraction (Table 2). Actually, the content of light components was further increased upon the introduction of hydrogenation catalysts, e.g., WS fractions obtained in the presence

of Pt and Ru catalysts featured light component contents almost twice as high as that of the WS fraction obtained in the Fe-only case. There was a proportionate relationship between the content ratios of light WS fractions and catalytic cracking yields of the WS fractions (Figure 5), reconfirming that the hydrocarbon yield of the catalytic WS fraction cracking can be effectively increased by increasing the content of light components in this fraction.

These results indicate that the catalytic cracking of the WS fraction is influenced by the hydrodeoxygenation degree of WS component and the relative content of light components in the WS fraction.

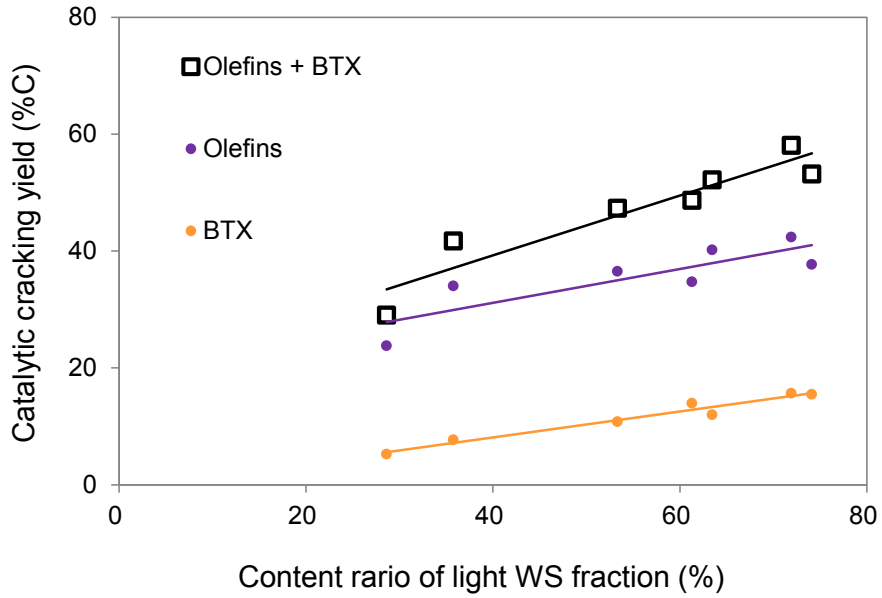

Figure 5. Relationship between the content ratios of light WS fractions and catalytic cracking yields of the WS fractions on the Fe-assisted HTL of cellulose with hydrogenation catalysts.

4.3.4. Plausible mechanism for hydrogenation catalyst effects

To determine the role of hydrogenation catalysts in the Fe-assisted HTL of cellulose, the author probed various (Fe species + Pd/Al_2O_3) HTL systems (Figure 6), investigated the catalytic cracking of the thus obtained WS fractions (Figure 7), and evaluated their quality (Table 3). The GC profiles/compositions of the thus obtained WS fractions are presented in Figure 8/Table 1, respectively.

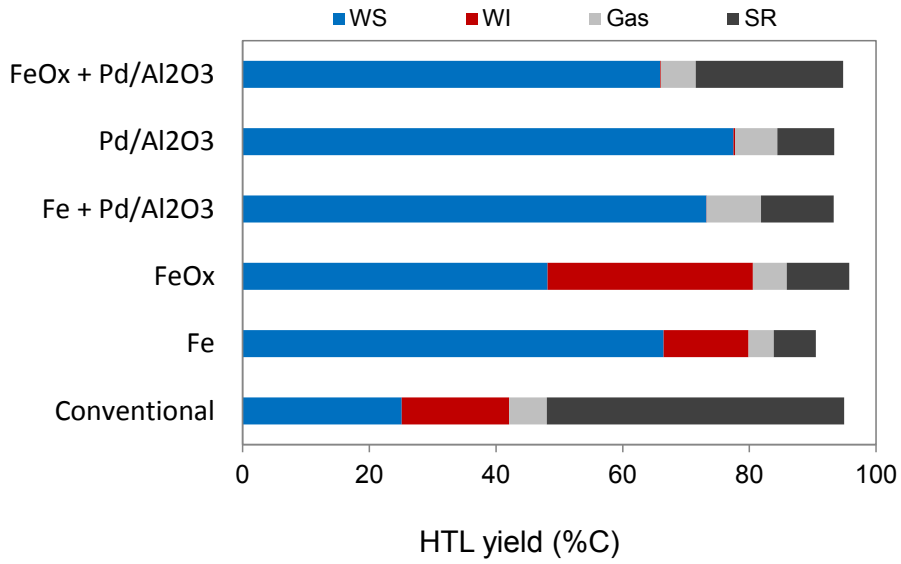

Figure 6. Effects of Fe additive and Pd catalyst on cellulose HTL.

[a]Initial pressure = 1.0 MPa N_2 + 1.5 MPa H_2, i.e., the atmosphere was identical to that used for Fe-assisted HTL.

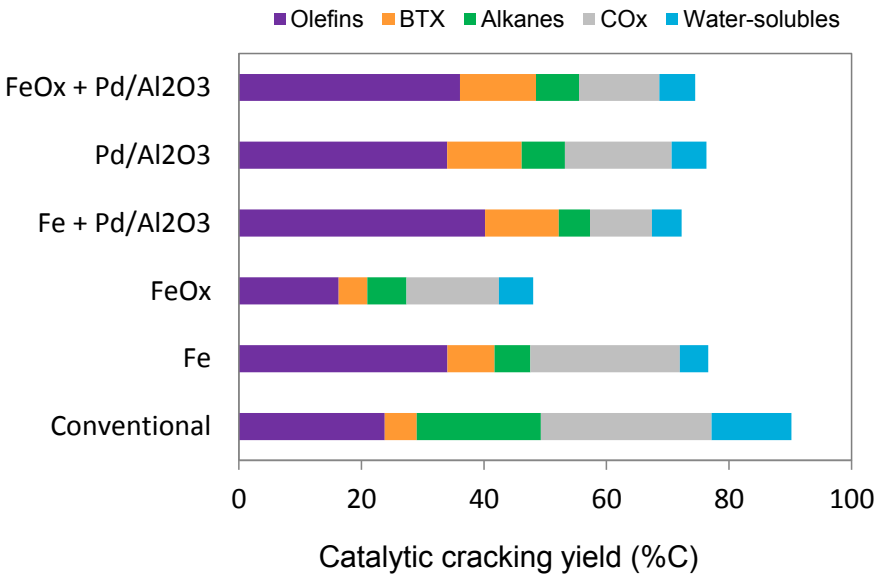

Figure 7. Effects of HTL system on the catalytic cracking of WS fractions.

Table 3. Quality evaluation of WS fractions obtained using systems listed in Figure 6.

System	Elemental ratios of light WS fraction components[a]			Relative contents of light and heavy WS	
	H/C	O/C	H/C_{eff}	Heavy	Light
Conventional	1.60	0.65	0.30	71	29
Fe	2.00	0.72	0.56	64	36
FeO_x	1.90	0.87	0.15	78	22
$Fe + Pd/Al_2O_3$	2.33	0.50	1.33	37	63
$Pd/Al_2O_3 + H_2$[c]	1.94	0.56	0.82	48	52
$FeO_x + Pd/Al_2O_3 + H_2$[c]	2.07	0.49	1.09	33	67

[a]Estimated by counting the sum of elements in each compound quantified by GC analysis. [b]Calculated based on the carbon content of the freeze-dried crude WS fraction. [c]Initial pressure = 1.0 MPa N_2 + 1.5 MPa H_2, i.e., the atmosphere was identical to that used for Fe-assisted HTL.

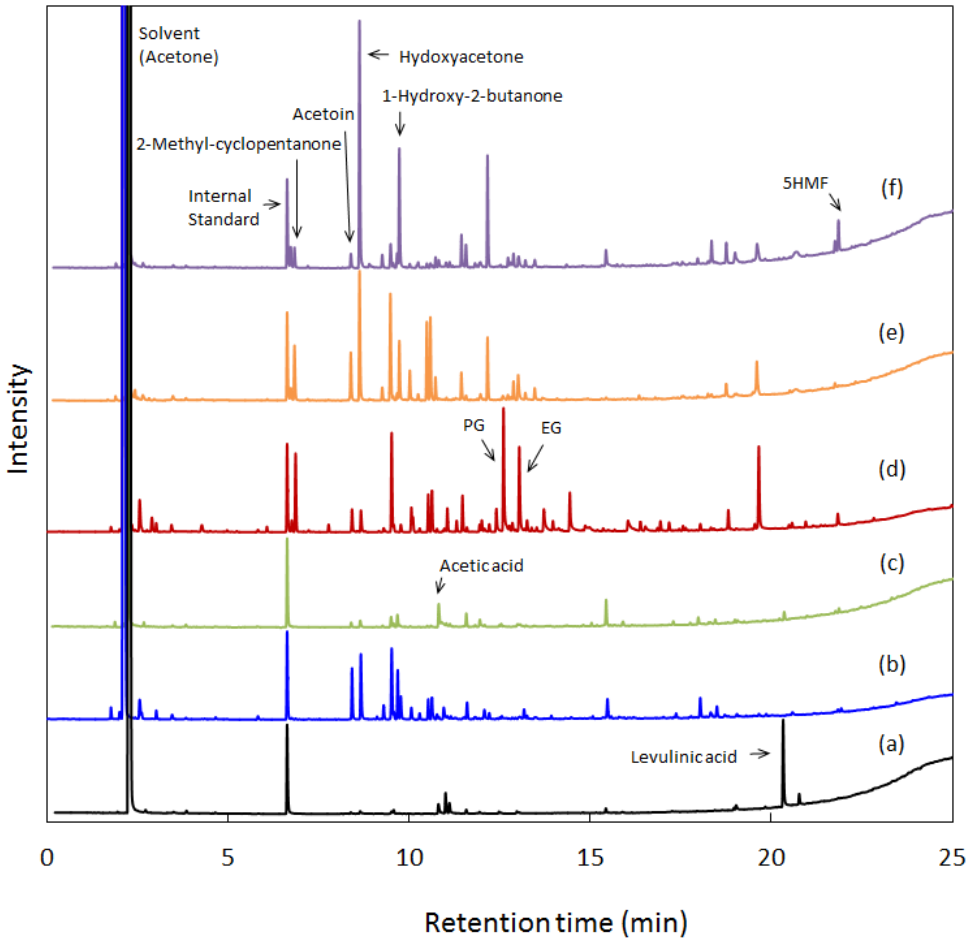

Figure 8. GC profiles of WS fractions produced by cellulose HTL (a) with no additive and in the presence of (b) Fe, and (c) FeO_x, (d) Fe + Pd/Al_2O_3, (e) FeO_x + Pd/Al_2O_3, and (f) Pd/Al_2O_3.

As described above, the addition of Pd/Al_2O_3 to the Fe-containing system increased the WS fraction and cracking yields relative to those observed for conventional HTL (no additive) and Fe-assisted (Fe alone) HTL systems due to the hydrogenation of unstable intermediates and the improvement of the WS fraction quality. When HTL was performed in the presence of Pd/Al_2O_3 alone (no Fe) under hydrogen atmosphere equal to that in the Fe-assisted HTL, the WS yield was slightly

higher than those of the Fe + Pd/Al_2O_3 system. In this instance, hydroxyacetone was detected at a yield of 20.5% as a primary product (Table 1). Therefore, it was inferred that the Pd catalyst hydrogenated unstable intermediates formed during the hydrothermal reaction into stable compounds such as hydroxyketones to suppress the condensation and re-polymerization to enhance the WS fraction yield. On the other hand, the quality of the thus obtained WS fraction was lower than that obtained in the case of the Fe + Pd/Al_2O_3 system (Table 3) so that the catalytic cracking yield was lower than that of the Fe + Pd system. The H/C_{eff} ratio and light component content of the WS fraction (0.99 and 53%, respectively) by Pd/Al_2O_3 alone were between those obtained for Fe-assisted (0.56 and 36%, respectively) and Fe + Pd/Al_2O_3 (1.33 and 63%, respectively) systems. The FeO_x (oxidized Fe) alone resulted in exceptionally low yield of WS fraction. The FeOx + Pd/Al_2O_3 system led to a high yield of WS fraction in HTL and hydrocarbons in catalytic cracking although the yields were less than those of the Fe + Pd/Al_2O_3 system. Thus, it was implied that Fe and Pd/Al_2O_3 acted synergistically to improve WS fraction quality by promoting the hydrogenation of intermediates and thus increasing the efficiency of catalytic cracking. This was supported by the fact that the HTL with Fe or Pd/Al_2O_3 alone remained as hydroxyacetone, while the Fe + Pd/Al_2O_3 system could sequentially hydrogenate to propylene glycol (Table 1). The author speculates that the Fe species can activate the carbonyl group of hydroxyacetone molecule to enable the Pd catalyst to hydrogenate into propylene glycol.[38]

Based on the above results (chapter 1, 3, 4) and previous studies,[38-39] the author proposes a plausible mechanism in this study explaining the effect of hydrogenation catalysts on the overall HTL reaction pathway (Scheme 1). In this mechanism, cellulose is rapidly hydrolyzed to glucose, which reversibly isomerizes into fructose. The

retro-aldol condensation of the (glucose + fructose) mixture catalyzed by oxidized Fe affords C_2–C_4 intermediates such as erythrose, glycolaldehyde, dihydroxyacetone, and glyceraldehyde. At this point, it is worth noting that oxidized Fe species were assumed to promote the retro-aldol and isomerization reactions.[38-39] In the absence of Fe, the unstable C_2–C_4 intermediates easily undergo isomerization (keto-enol tautomerization), dehydration, condensation, and carbonization to afford oligomers, polymers, and char as WI fraction or SR components.[40] Contrastingly, metallic Fe and Pd catalyze the hydrogenation of these aldehydes into stable alcohols under hydrothermal conditions to increase the WS fraction yield. As described above, a Pd catalyst activated gas-phase hydrogen derived from the reaction of Fe with water so as to effectively boost the hydrogenation of the intermediate compounds, while metallic Fe facilitated unstable intermediates to be stabilized by an electron-transfer-type reduction (see chapter 3). Finally, a key finding in this study is that the reduction of intermediates was dramatically accelerated by the both contributions of metallic Fe and a Pd catalyst. Moreover, Pd catalysts can additionally hydrogenate ketones into alcohols in cooperation with Fe, which helps via activation of carbonyl group, to improve the quality of the WS fraction. In agreement with the suggested mechanism, numerous diols (ethylene glycol, propylene glycol, 2,3-butanediol, 1,2-butanediol, 1,2-pentanediol, and 1,2-hexanediol) were formed in the Fe + Pd/Al_2O_3 system (Table 1).

The results of studies on the non-catalytic and catalytic HTL of various biomasses[1-30] demonstrated that the HTL process can be divided into three steps, namely depolymerization, decomposition, and re-polymerization (condensation). However, as biomass is a complex mixture of carbohydrates, lignin, proteins, and lipids, the exact mechanism of HTL has not yet been elucidated, with only few works dealing with the

effect of Fe powder on biomass HTL[41-42]. Chen and co-workers showed that a conversion of 89.45 wt% (sum of heavy bio-oil and aqueous product yields; 270 °C, 30 min) was achieved when wheat stalk liquefaction was performed in the presence of Na_2CO_3 and Fe, and probed the compositions of heavy bio-oil and the WS fraction by GC-MS. de Caprariis and co-workers demonstrated the effect of Fe powder addition on the HTL of oak wood, revealing that the use of Fe not only increased the yields of bio-oil, but also improved its quality by facilitating the in situ formation of H_2. However, neither of the two abovementioned studies proposed a detailed mechanism. The present work suggests a plausible mechanism of cellulose liquefaction to afford the WS fraction and therefore helps to unfold the mechanism of HTL and to speculate how the WS fraction is sequentially converted into the WI fraction (biocrude) and SR (char) when hydrogenation catalysts are used.

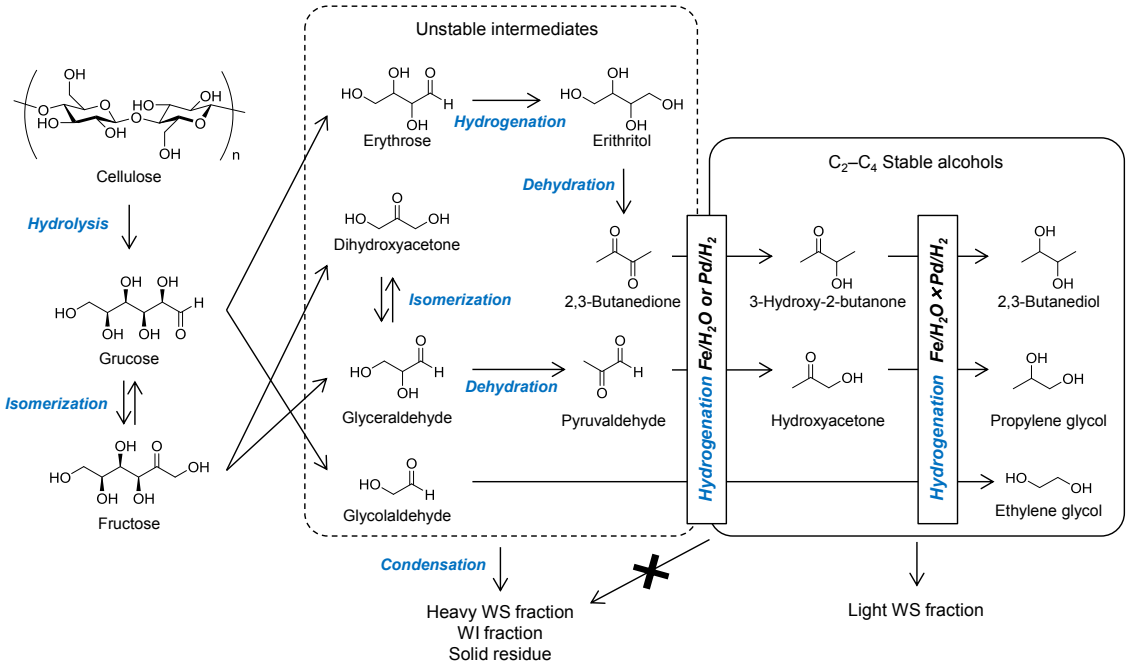

Scheme 1. Plausible mechanism for the effect of Pd catalysts on the Fe-assisted HTL of cellulose.

4.4. Conclusion

The addition of metal hydrogenation catalysts increased the yield and quality of the WS fraction formed in the Fe-assisted HTL of cellulose and facilitated the efficient conversion of this fraction into light olefins and aromatics. These catalysts increased the hydrogen-to-effective-carbon ratio and the proportion of volatile compounds in the WS fraction, and were suggested to promote the hydrogenation of unstable aldehydes into stable alcohols to increase the content of light components in the WS fraction, which contributed to the increase of catalytic cracking yield. Iron oxides generated in situ were proposed to catalyze the isomerization of glucose to fructose and the retro-aldol condensation of sugars into low-molecular-weight compounds (C_2–C_4). As a consequence, the combined use of Fe and metal hydrogenation catalysts favorably affected the overall pathway of the Fe-assisted HTL of cellulose to improve the yield and quality of the WS fraction due to synergistic acceleration by the both of an electron-transfer-type reduction by metallic Fe and hydrogenation by a metal catalyst. These results indicate the importance of increasing the yield/quality of light WS fraction components and provide a strategy for realizing economically viable biomass HTL and cracking systems.

4.5. References

1. Ragauskas, A. J.; Williams, C. K.; Davison, B. H.; Britovsek, G.; Cairney, J.; Eckert, C. A.; Frederick, W. J.; Hallett, J. P.; Leak, D. J.; Liotta, C. L.; Mielenz, J. R.; Murphy, R.; Templer, R.; Tschaplinski, T., The Path Forward for Biofuels and Biomaterials. *Science* **2006,** *311* (5760), 484–489.
2. Swain, P. K.; Das, L. M.; Naik, S. N., Biomass to Liquid: A Prospective

Challenge to Research and Development in 21st Century. *Renew. Sust. Energy Rev.* **2011,** *15* (9), 4917–4933.

3. Chu, S.; Majumdar, A., Opportunities and Challenges for a Sustainable Energy Future. *Nature* **2012,** *488* (7411), 294–303.
4. Gallezot, P., Conversion of Biomass to Selected Chemical Products. *Chem. Soc. Rev.* **2012,** *41* (4), 1538–58.
5. Sheldon, R. A., Green and Sustainable Manufacture of Chemicals from Biomass: State of the Art. *Green Chem.* **2014,** *16* (3), 950–963.
6. Akhtar, J.; Amin, N. A. S., A Review on Process Conditions for Optimum Bio-Oil Yield in Hydrothermal Liquefaction of Biomass. *Renew. Sust. Energy Rev.* **2011,** *15* (3), 1615–1624.
7. Toor, S. S.; Rosendahl, L.; Rudolf, A., Hydrothermal Liquefaction of Biomass: A Review of Subcritical Water Technologies. *Energy* **2011,** *36* (5), 2328–2342.
8. Tekin, K.; Karagöz, S.; Bektaş, S., A Review of Hydrothermal Biomass Processing. *Renew. Sust. Energy Rev.* **2014,** *40*, 673–687.
9. Elliott, D. C.; Biller, P.; Ross, A. B.; Schmidt, A. J.; Jones, S. B., Hydrothermal Liquefaction of Biomass: Developments from Batch to Continuous Process. *Bioresour. Technol.* **2015,** *178*, 147–156.
10. Cao, L.; Zhang, C.; Chen, H.; Tsang, D. C. W.; Luo, G.; Zhang, S.; Chen, J., Hydrothermal Liquefaction of Agricultural and Forestry Wastes: State-of-the-Art Review and Future Prospects. *Bioresour. Technol.* **2017,** *245*, 1184–1193.
11. Dimitriadis, A.; Bezergianni, S., Hydrothermal Liquefaction of Various Biomass and Waste Feedstocks for Biocrude Production: A State of the Art Review. *Renew. Sust. Energy Rev.* **2017,** *68*, 113–125.

12. Baloch, H. A.; Nizamuddin, S.; Siddiqui, M. T. H.; Riaz, S.; Jatoi, A. S.; Dumbre, D. K.; Mubarak, N. M.; Srinivasan, M. P.; Griffin, G. J., Recent Advances in Production and Upgrading of Bio-Oil from Biomass: A Critical Overview. *J. Environ. Chem. Eng.* **2018,** *6* (4), 5101–5118.

13. Gollakota, A. R. K.; Kishore, N.; Gu, S., A Review on Hydrothermal Liquefaction of Biomass. *Renew. Sust. Energy Rev.* **2018,** *81*, 1378–1392.

14. Kumar, M.; Olajire Oyedun, A.; Kumar, A., A Review on the Current Status of Various Hydrothermal Technologies on Biomass Feedstock. *Renew. Sust. Energy Rev.* **2018,** *81*, 1742–1770.

15. Lange, J. P., Lignocellulose Liquefaction to Biocrude: A Tutorial Review. *ChemSusChem* **2018,** *11* (6), 997–1014.

16. Zhang, B.; von Keitz, M.; Valentas, K., Thermochemical Liquefaction of High-Diversity Grassland Perennials. *J. Anal. Appl. Pyrolysis* **2009,** *84* (1), 18–24.

17. Hammerschmidt, A.; Boukis, N.; Hauer, E.; Galla, U.; Dinjus, E.; Hitzmann, B.; Larsen, T.; Nygaard, S. D., Catalytic Conversion of Waste Biomass by Hydrothermal Treatment. *Fuel* **2011,** *90* (2), 555–562.

18. Yin, S.; Tan, Z., Hydrothermal Liquefaction of Cellulose to Bio-Oil under Acidic, Neutral and Alkaline Conditions. *Appl. Energy* **2012,** *92*, 234–239.

19. Shi, W.; Li, S.; Jin, H.; Zhao, Y.; Yu, W., The Hydrothermal Liquefaction of Rice Husk to Bio-Crude Using Metallic Oxide Catalysts. *Energy Sources, Part A* **2013,** *35* (22), 2149–2155.

20. Meryemoğlu, B.; Hasanoğlu, A.; Irmak, S.; Erbatur, O., Biofuel Production by Liquefaction of Kenaf (*Hibiscus Cannabinus L.*) Biomass. *Bioresour. Technol.*

2014, *151*, 278–283.

21. Nazari, L.; Yuan, Z.; Souzanchi, S.; Ray, M. B.; Xu, C., Hydrothermal Liquefaction of Woody Biomass in Hot-Compressed Water: Catalyst Screening and Comprehensive Characterization of Bio-Crude Oils. *Fuel* **2015,** *162*, 74–83.
22. Li, N.; Wei, L.; bibi, R.; Chen, L.; Liu, J.; Zhang, L.; Zheng, Y.; Zhou, J., Catalytic Hydrogenation of Alkali Lignin into Bio-Oil Using Flower-Like Hierarchical MoS_2-Based Composite Catalysts. *Fuel* **2016,** *185*, 532–540.
23. Long, J.; Li, Y.; Zhang, X.; Tang, L.; Song, C.; Wang, F., Comparative Investigation on Hydrothermal and Alkali Catalytic Liquefaction of Bagasse: Process Efficiency and Product Properties. *Fuel* **2016,** *186*, 685–693.
24. Bi, Z.; Zhang, J.; Peterson, E.; Zhu, Z.; Xia, C.; Liang, Y.; Wiltowski, T., Biocrude from Pretreated Sorghum Bagasse through Catalytic Hydrothermal Liquefaction. *Fuel* **2017,** *188*, 112–120.
25. Cheng, S.; Wei, L.; Julson, J.; Kharel, P. R.; Cao, Y.; Gu, Z., Catalytic Liquefaction of Pine Sawdust for Biofuel Development on Bifunctional Zn/HZSM-5 Catalyst in Supercritical Ethanol. *J. Anal. Appl. Pyrolysis* **2017,** *126*, 257–266.
26. Yim, S. C.; Quitain, A. T.; Yusup, S.; Sasaki, M.; Uemura, Y.; Kida, T., Metal Oxide-Catalyzed Hydrothermal Liquefaction of Malaysian Oil Palm Biomass to Bio-Oil under Supercritical Condition. *J. Supercrit. Fluids* **2017,** *120*, 384–394.
27. Chen, D.; Ma, Q.; Wei, L.; Li, N.; Shen, Q.; Tian, W.; Zhou, J.; Long, J., Catalytic Hydroliquefaction of Rice Straw for Bio-Oil Production Using Ni/CeO_2 Catalysts. *J. Anal. Appl. Pyrolysis* **2018,** *130*, 169–180.
28. Cheng, S.; Wei, L.; Rabnawaz, M., Catalytic Liquefaction of Pine Sawdust and

in-situ Hydrogenation of Bio-Crude over Bifunctional Co-Zn/HZSM-5 Catalysts. *Fuel* **2018,** *223*, 252–260.

29. Lee, J. H.; Hwang, H.; Choi, J. W., Effects of Transition Metals on Hydrothermal Liquefaction of Empty Fruit Bunches (EFB) for Conversion to Biofuel and Valuable Chemicals. *Energy* **2018,** *162*, 1–9.

30. Ma, Q.; Chen, D.; Wei, L.; Shen, Q.; Ji, Z.; Chen, Y.; Zou, X.; Xu, C.; Zhou, J., Bio-Oil Production from Hydrogenation Liquefaction of Rice Straw over Metal (Ni, Co, Cu)-Modified CeO_2 Catalysts. *Energy Sources, Part A* **2018,** *40* (2), 200-206.

31. Madsen, R. B.; Biller, P.; Jensen, M. M.; Becker, J.; Iversen, B. B.; Glasius, M., Predicting the Chemical Composition of Aqueous Phase from Hydrothermal Liquefaction of Model Compounds and Biomasses. *Energy Fuels* **2016,** *30* (12), 10470–10483.

32. Tommaso, G.; Chen, W. T.; Li, P.; Schideman, L.; Zhang, Y., Chemical Characterization and Anaerobic Biodegradability of Hydrothermal Liquefaction Aqueous Products from Mixed-Culture Wastewater Algae. *Bioresour. Technol.* **2015,** *178*, 139–46.

33. Cherad, R.; Onwudili, J. A.; Biller, P.; Williams, P. T.; Ross, A. B., Hydrogen Production from the Catalytic Supercritical Water Gasification of Process Water Generated from Hydrothermal Liquefaction of Microalgae. *Fuel* **2016,** *166*, 24–28.

34. Wu, K.; Yang, M.; Chen, Y.; Pu, W.; Hu, H.; Wu, Y., Aqueous-Phase Ketonization of Acetic Acid over Zr/Mn Mixed Oxides. *AlChE J.* **2017,** *63* (7), 2958–2967.

35. Vispute, T. P.; Zhang, H. Y.; Sanna, A.; Xiao, R.; Huber, G. W., Renewable Chemical Commodity Feedstocks from Integrated Catalytic Processing of Pyrolysis Oils. *Science* **2010,** *330* (6008), 1222–1227.

36. Chen, N. Y.; Degnan, T. F.; Koenig, L. R., Liquid Fuel from Carbohydrates. *CHEMTECH* **1986,** *16* (8), 506–511.

37. Zhang, H.; Cheng, Y.-T.; Vispute, T. P.; Xiao, R.; Huber, G. W., Catalytic Conversion of Biomass-Derived Feedstocks into Olefins and Aromatics with ZSM-5: The Hydrogen to Carbon Effective Ratio. *Energy Environ. Sci.* **2011,** *4* (6), 2297–2307.

38. Hirano, Y.; Kasai, Y.; Sagata, K.; Kita, Y., Unique Approach for Transforming Glucose to C3 Platform Chemicals Using Metallic Iron and a Pd/C Catalyst in Water. *Bull. Chem. Soc. Jpn.* **2016,** *89* (9), 1026–1033.

39. Hirano, Y.; Sagata, K.; Kita, Y., Selective Transformation of Glucose into Propylene Glycol on Ru/C Catalysts Combined with ZnO under Low Hydrogen Pressures. *Appl. Catal., A* **2015,** *502*, 1–7.

40. Möller , M.; Nilges , P.; Harnisch, F.; Schröder, U., Subcritical Water as Reaction Environment: Fundamentals of Hydrothermal Biomass Transformation. *ChemSusChem* **2011,** *4* (5), 566–579.

41. Chen, Y.; Cao, X.; Zhu, S.; Tian, F.; Xu, Y.; Zhu, C.; Dong, L., Synergistic Hydrothermal Liquefaction of Wheat Stalk with Homogeneous and Heterogeneous Catalyst at Low Temperature. *Bioresour. Technol.* **2019,** *278*, 92–98.

42. de Caprariis, B.; Bavasso, I.; Bracciale, M. P.; Damizia, M.; De Filippis, P.; Scarsella, M., Enhanced Bio-Crude Yield and Quality by Reductive

Hydrothermal Liquefaction of Oak Wood Biomass: Effect of Iron Addition. *J. Anal. Appl. Pyrolysis* **2019,** *139*, 123–130.

General Conclusion

In this thesis, the author investigated a novel hydrothermal liquefaction (HTL) system using zero-valent Fe as renewable additive with the aim to obtain chemical feedstocks from lignocellulosic biomass. The key findings in each chapter are summarized below.

In chapter 1, zero-valent Fe was used as a reductant for upgrading bio-oil components in situ in the HTL of oil palm empty fruit bunch (EFB), a lignocellulosic biomass source, affording bio-oil containing water-soluble (WS) and water-insoluble (WI) fractions in high yields. Fe efficiently converted unstable intermediates formed from the degradation of EFB into stable compounds, resulting in reduced char formation. WS fractions were treated with the HZSM-5 zeolite, affording light olefins (C_2–C_4), as well as benzene, toluene, and xylene. This conversion was more efficient with the WS fraction obtained in the presence of Fe. The liquefaction of EFB and the conversion of WS fractions into olefins via catalytic cracking were also achieved using recycled Fe.

In chapter 2, the quantitative analysis of the WS fraction obtained from the Fe-assisted HTL of EFB was comprehensively investigated by combining various separation and analysis methods. The volatile components of the WS fraction were analyzed by gas chromatography–mass spectrometry (GC–MS) and gas chromatography–flame ionization detection (GC–FID), and they were quantified using the relative response factors estimated by the effective carbon number method. Heavy components not detectable by GC were isolated by freeze-drying, and their elemental compositions, functional groups, and molecular-weight distributions were analyzed. The results reveal that the addition of Fe during HTL alters the types of compounds present

in the WS fraction by a large extent, and increases the proportion of volatile compounds. The reactivity of the WS fraction in the zeolite-catalyzed cracking reaction was also investigated, which revealed that the volatile components of the WS fraction are efficiently converted into olefins.

In chapter 3, commercially available carbohydrates (poly- and monosaccharides) and lignin isolated by enzymatic saccharification of EFB were used as model substrates in the evaluation of the effect of Fe on HTL product composition. For carbohydrates, Fe and oxidized Fe synergistically contributed to the production of light compounds in the WS fraction by accelerating the retro-aldol condensation of sugars and suppressing the recondensation of unstable intermediates. The reactive intermediates could be stabilized by an electron-transfer-type reduction. On the other hand, Fe showed minimal effect on the HTL of enzymatic lignin, which was mainly converted to water-insoluble products. The results for the model substrates provided a picture of the overall pathway of Fe-assisted HTL of biomass.

In chapter 4, the author demonstrated that Fe-assisted HTL of cellulose in the presence of hydrogenation catalysts improved the yield and quality of the WS fraction so as to enhance the hydrocarbon yield in catalytic cracking of the WS fraction. The addition of hydrogenation catalysts led to higher hydrogen-to-effective-carbon ratios and proportion of volatile light WS fraction than those obtained by Fe-assisted HTL due to synergistic acceleration by the both of metallic Fe and hydrogenation catalysts.

In conclusion, HTL of lignocellulosic biomass using zero-valent iron was developed, and fundamental knowledge on the effect of iron in the hydrothermal reaction was obtained. The method developed here has the potential to make HTL process be economically efficient and environmentally benign.

Publication List

1. Miyata, Y.; Sagata, K.; Hirose, M.; Yamazaki, Y.; Nishimura, A.; Okuda, N.; Arita, Y.; Hirano, Y.; Kita, Y., Fe-Assisted Hydrothermal Liquefaction of Lignocellulosic Biomass For Producing High-Grade Bio-Oil. *ACS Sustain. Chem. Eng.* **2017,** *5* (4), 3562–3569.

2. Miyata, Y.; Yamazaki, Y.; Hirano, Y.; Kita, Y., Quantitative Analysis of the Aqueous Fraction from the Fe-Assisted Hydrothermal Liquefaction of Oil Palm Empty Fruit Bunches. *J. Anal. Appl. Pyrolysis* **2018,** *132*, 72–81.

3. Miyata, Y.; Sagata, K.; Yamazaki, Y.; Teramura, H.; Hirano, Y.; Ogino, C.; Kita, Y., Mechanism of the Fe-Assisted Hydrothermal Liquefaction of Lignocellulosic Biomass. *Ind. Eng. Chem. Res.* **2018,** *57* (44), 14870–14877.

4. Hirano, Y.; Miyata, Y.; Taniguchi, M.; Funakoshi, N.; Yamazaki, Y.; Ogino, C.; Kita, Y., Fe-assisted Hydrothermal Liquefaction of Cellulose: Effects of Hydrogenation Catalyst Addition on Properties of Water-Soluble Fraction. (*Submitted*)

Acknowledgement

This is a thesis submitted by the author to Kobe University for the degree of Doctor of Engineering. The studies performed here were carried out between 2012 and 2019 in a joint research chair (2012-2017, an endowed chair), “Sustainable Chemistry (NIPPON SHOKUBAI)”, Department of Chemical Science and Engineering, Graduate School of Engineering, Kobe University. These works were financially supported by Nippon Shokubai Co., Ltd.

The author would like to express his sincerest gratitude to his research adviser, Professor Chiaki Ogino for his advice and invaluable discussion during the course for his studies.

The author would like to thank Professor Satoru Nishiyama and Professor Atsunori Mori for their kindness during the reviewing and examining of this thesis and giving constructive comments.

The author would like to extend his heartfelt gratitude to his supervisor, Professor Yuichi Kita for his leadership, kind guidance, helpful suggestions, and continuous encouragement.

The author would like to express his sincere gratitude to Associate Professor Yoshiaki Hirano for his help and valuable suggestions.

The author would like to express his appreciation to Dr. Hiroshi Teramura for his technical support and valuable discussion.

The author would like to express the deepest appreciation to joint research laboratory members, Dr. Kunimasa Sagata, Ms. Mina Hirose, Ms. Yuka Kasai, Ms.

Yoshiko Yamazaki, Ms. Nami Funakoshi, Ms. Makiko Taniguchi and Ms. Kotomi Ariyoshi for their generous and persistent assistance.

The author would like to express his sincere gratitude to Mr. Yojiro Takahashi, Senior Managing Executive Officer and Mr. Kin-ya Nagasuna, Managing Executive Officer of Nippon Shokubai Co., Ltd. for giving the author an opportunity to get doctoral degree.

The author would like to express his gratitude to Mr. Kimio Ariyoshi, Mr. Tsukasa Takahashi, Mr. Yoshitaka Arita, Mr. Norimasa Okuda, Mr. Takafumi Kubo, Ms. Aki Nishimura of Nippon Shokubai Co., Ltd. for their collaboration and valuable discussion in present work.

The author would like to thank Mr. Hirokazu Ito, Ms. Takako Watanabe, Ms. Yumiko Mori, Dr. Tomoyuki Kitano, Mr. Kin-ichi Nakayama, Ms. Yasuko Karakawa, Ms. Akiko Kuriyama, the staffs of the Analysis Technology Center of Nippon Shokubai Co., Ltd., for their technical support and fruitful discussion.

The author's appreciation goes also to Mr. Yoshikazu Fujii, Mr. Yasutaka Sumida, Mr. Masahide Shima and Dr. Tsuyoshi Yamashita, the staffs of the Innovation & Business Development Division of Nippon Shokubai Co., Ltd., for their encouragement.

Finally, the author would like to thank everyone who contributed to this thesis.

Yoshinori Miyata

Department of Chemical Science and Engineering

Graduate School of Engineering

Kobe University

Doctor Thesis, Kobe University
“Study on hydrothermal liquefaction of lignocellulosic biomass using zero-valent iron”, 151 pages
Submitted on July, 16, 2019
The date of publication is printed in cover of repository version published in Kobe University Repository Kernel.